UPPSALA
UNIVERSITET

Digital Comprehensive Summaries of Uppsala Dissertations from the Faculty of Science and Technology 1606

Modelling calving and sliding of Svalbard outlet glaciers

Spatio-temporal changes and interactions

DOROTHÉE VALLOT

ACTA
UNIVERSITATIS
UPSALIENSIS
UPPSALA
2017

ISSN 1651-6214
ISBN 978-91-513-0170-9
urn:nbn:se:uu:diva-334787

Dissertation presented at Uppsala University to be publicly examined in Hambergsalen, Villavägen 16, Uppsala, Wednesday, 24 January 2018 at 09:15 for the degree of Doctor of Philosophy. The examination will be conducted in English. Faculty examiner: PhD Tómas Jóhannesson (Icelandic Meteorological Office (IMO), Iceland).

Abstract
Vallot, D. 2017. Modelling calving and sliding of Svalbard outlet glaciers. Spatio-temporal changes and interactions. *Digital Comprehensive Summaries of Uppsala Dissertations from the Faculty of Science and Technology* 1606. 82 pp. Uppsala: Acta Universitatis Upsaliensis. ISBN 978-91-513-0170-9.

Future sea level rise associated to global warming is one of the greatest societal and environmental challenges of tomorrow. A large part of the contribution comes from glaciers and ice sheets discharging ice and meltwater into the ocean and the recent worldwide increase is worrying. Future predictions of sea level rise try to encompass the complex processes of ice dynamics through glacier modelling but there are still large uncertainties due to the lack of observations or too coarse parameterisation, particularly for processes occurring at the glacier interfaces with the bed (sliding) and with the ocean (calving). This thesis focuses on modelling these processes from two marine-terminating glaciers in Svalbard, Kronebreen and Tunabreen. By inverting three years of high temporal resolution time-series of surface velocities on Kronebreen, basal properties are retrieved with the ice flow model Elmer/Ice in Paper I. Results suggest that surface melt during the summer greatly influences the dynamics of the following season and that sliding laws for such glaciers should be adapted to local and global processes changing in space and time. The subglacial drainage system, fed by the surface melt, is modelled in Paper II during two melting seasons. Results show different configurations of efficient and inefficient drainage systems between years and the importance of using a sliding law dependent on spatio-temporal changes in effective pressure. The interaction with the ocean is incorporated in Paper III by combining a series of models, including an ice flow model, a plume model and a particle model for discrete calving and compares the output with observations. Results show the importance of glacier geometry, sliding and undercutting on calving rate and location. However, more observations and analytic methods are needed. Time-lapse imagery placed in front of Tunabreen have been deployed and a method of automatic detection for iceberg calving is presented in Paper IV. Results show the influence of the rising plume in calving and the front destabilisation of the local neighbourhood.

Keywords: cryospheric science, glacier modelling, time-lapse imagery, undercutting, sliding inversion, discrete particle model, calving model, subglacial hydrology, sliding law, automatic detection method, calving events size and frequency, ocean interaction, melt water runoff, ice dynamics, ice flow model

Dorothée Vallot, Department of Earth Sciences, LUVAL, Villav. 16, Uppsala University, SE-75236 Uppsala, Sweden.

ISSN 1651-6214
ISBN 978-91-513-0170-9
urn:nbn:se:uu:diva-334787 (http://urn.kb.se/resolve?urn=urn:nbn:se:uu:diva-334787)

Dedié à l'escargot, à l'ours-pingouin
et aux ours en général.

"Nous menons une guerre contre la Nature.
Si nous la gagnons, nous sommes perdus."
– Hubert Reeves

List of papers

This thesis is based on the following papers, which are referred to in the text by their Roman numerals.

I **Vallot, D.**, Pettersson, R., Luckman, A., Benn, D. I., Zwinger, T., Van Pelt, W. J. J., Kohler, J., Schäfer, M., Claremar, B., and Hulton, N. R. J.: Basal dynamics of Kronebreen, a fast-flowing tidewater glacier in Svalbard: non-local spatio-temporal response to water input, *Journal of Glaciology*, doi: 10.1017/jog.2017.69, 2017.

II **Vallot, D.**, Gagliardini, O., Pettersson, Benn, D. I., R., Luckman, A., Van Pelt, W. J. J., Lindbäck, K.: Modelled subglacial hydrology and basal friction at Kronebreen, a tidewater glacier in Svalbard, *Manuscript*.

III **Vallot, D.**, Åström, J., Zwinger, T., Pettersson, R., Everett, A., Benn, D. I., Luckman, A., Van Pelt, W. J. J. & Nick, F.: Effects of undercutting and sliding on calving: a coupled approach applied to Kronebreen, Svalbard, *The Cryosphere Discussion*, doi:10.5194/tc-2017-166, 2017.

IV **Vallot, D.**,Adinugroho, S., Strand, R., How, P., Pettersson, R., Benn, D. I. & Hulton, N. R. J.: Automatic detection of calving events from time-lapse imagery at Tunabreen, Svalbard, *Manuscript*.

Related work

The author has also contributed to the following papers, related, but not included in this thesis.

A Lindbäck, K., Kohler, J., Pettersson, R., Myhre, P. I., Nuth, C., Langley, K., Brandt, O., Messerli, A., and **Vallot, D.**: Subglacial topography, geology and implications for future bathymetry of Kongsfjorden, northwestern Svalbard, *Journal of Geophysical Research*, in review, 2017.

B Memon, S., **Vallot, D.**, Zwinger, T., Neukirchen, H. & Riedel, M.: Coupling glaciological models using scientific workflows, *Manuscript*.

C Åström, J. A., **Vallot, D.**, Schäfer, M., Welty, E. Z., O'Neel, S., Bartholomaus, T. C., Yan Liu, Riikilä, T. I., Zwinger, T., Timonen J. & Moore, J. C.: Termini of calving glaciers as self-organized critical systems, *Nature Geoscience*, 7(12), 874–878, doi:10.1038/NGEO2290, 2014.

Contents

1. Introduction

"Où l'on comprend qu'envisager un monde nouveau nous oblige à la fois à la prudence et à l'action. Et où l'on espère en l'homme – cette force dotée à la fois d'intelligence, de capacité à travailler ensemble et de sagesse – pour explorer des chemins inconnus." – Claude Lorius in Voyage dans l'Anthropocène

1.1 Sea level contribution

Land-based ice masses are very sensitive to external changes such as climate change that we undergo today (DeConto and Pollard, 2016; Carson et al., 2016) and are the second largest contributor to sea level change (Leclercq et al., 2011; Church et al., 2013). Moreover, the contribution from land ice, and particularly glaciers, is increasing (Church et al., 2013). The environmental and socio-economic impacts associated with sea level rise have raised important questions as to prevent any coming disaster and accurate predictions of future contribution is becoming more and more needed. However, such complex systems are difficult to model and better understanding of a number of processes is still required to be able to parameterise them with accuracy. The break-off of icebergs from glaciers terminating in the ocean through calving processes is a major uncertainty, together with sliding influencing the ice dynamics, in estimating their contribution to sea-level changes (Ritz et al., 2015; Alley et al., 2015).

1.2 Land ice processes

Glaciers form when solid precipitation (snow) falls on land and, after several years of positive mass balance (accumulated snow mass greater than mass losses through ablation) and recrystallisation, transforms into ice. The ice can then deform under its own weight and by sliding at its base. Fig. 1.1 shows the different components of the glacier (or ice sheet) system. External forcing, such as precipitation, incoming radiation and energy, sea ice or ocean water, have an effect on the system, which undergoes several complex processes. The ice is flowing non-linearly under its own weight and when reaching the ocean, discrete pieces of ice are detaching through calving to create icebergs. At the surface, if the energy balance is positive, melt water is produced and finds its way to the bed through supraglacial and englacial hydrology systems

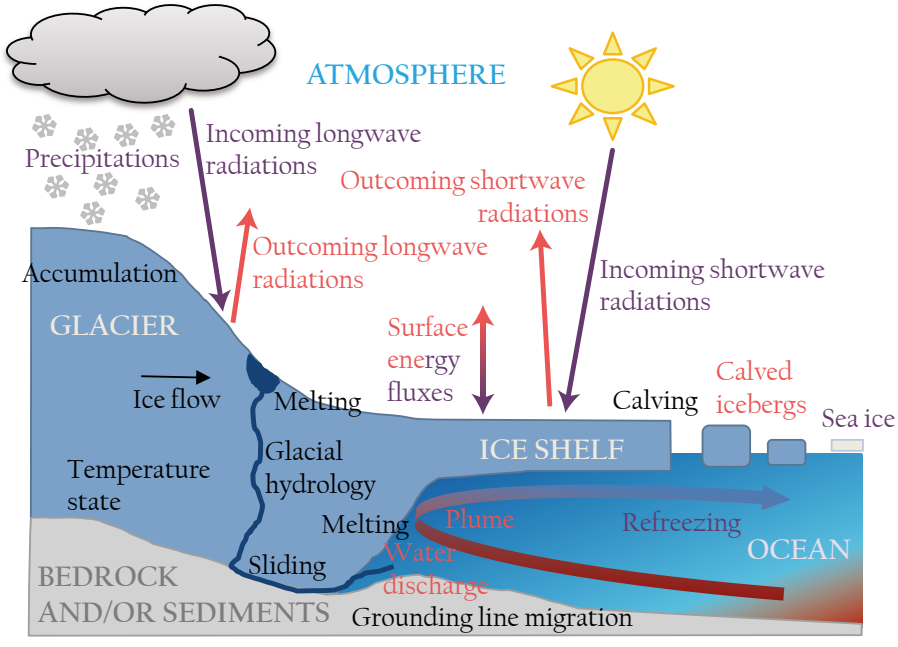

Figure 1.1. Land ice system showing the external forcing (in green), the internal processes (in black), and the influence on the outer system (in red).

to create a subglacial hydrology system also fed by melting from geothermal heat flux or friction heat provided that the glacier is temperate. Cold sections of the glacier act as barriers for the melt water. This basal water lubricates the bed and enables the ice to slide. In turn, ice masses exert an influence on the external system through outcoming radiation and energy, calved icebergs, subglacial and supraglacial water discharge. The water discharged into the ocean at the base of the glacier can mix with sea water and create a turbulent upwelling flow that enhance subglacial undercutting and facilitate calving.

This complex web of processes implies interactions and feedback between them, which one important consequence is the spatio-temporal variation of ice flow, and basal motion in particular, at different scales.

1.3 Ice velocity and spatio-temporal changes

Many studies show the importance of spatial and temporal changes in basal motion. Primarily driven by the amount of melt water reaching the bed and forming a complex subglacial network, basal sliding has consequences on the ice velocities that can be directly observed.

Surface ice velocities of alpine glaciers and Arctic glaciers have been observed to have variability at different time-scales from hours to seasons as well as interannually (Hooke et al., 1989; Vieli et al., 2004; Luckman et al.,

2006; Nick et al., 2009; Howat et al., 2010; Joughin et al., 2010). The seasonal variations can be due to different processes occurring:

- at the surface (ice-atmosphere interaction) through melt, runoff and/or supraglacial lake drainage (Zwally et al., 2002; Shepherd et al., 2009; Hoffman et al., 2011; Palmer et al., 2011; Mair et al., 2001),
- at the base through routing of surface water to the base, subglacial hydrology and basal sliding where the presence of water lubricates the bed (Jansson, 1995; Hubbard et al., 1995; Iken and Truffer, 1997; Nienow et al., 1998; Bartholomew et al., 2010; Sundal et al., 2011; Bougamont et al., 2014) and creates the paths to drain itself (Sole et al., 2011)
- or at the ice terminus (ice-ocean interaction) through calving processes, ice front position (Nick et al., 2009), fjord geometry (Carr et al., 2013), or ocean temperature changes (Christoffersen et al., 2011; Joughin et al., 2012; Straneo and Heimbach, 2013).

Moon et al. (2012) examined the seasonal velocity evolution on 55 glaciers in Greenland showing a rapid and large acceleration starting around the beginning of this century. In Moon et al. (2012), they combined velocity, terminus position, and runoff records over 5 years (2009–2013) to sort them into three different behavioral types (see Fig. 1.2):

Type 1 – Glaciers show an ice flow speed-up at the beginning of the melt season with velocities remaining high until late winter or early spring. The correlation between ice speed and front position could indicate that ice dynamics is very much influenced by the calving processes as Nick et al. (2009) suggest. This behavior is usually temporally isolated since only a few glaciers are regularly of type 1.

Type 2 – Glaciers show a strong correlation between ice motion and runoff anytime during the year. This suggests that the subglacial drainage never really becomes well-developed and efficient.

Type 3 – Glaciers exhibit an early summer speed-up but a decrease in velocity in times of high runoff particularly pronounced at the end of the summer. This might be due to a seasonal switch between inefficient and efficient subglacial drainage.

The difference between type 2 and 3 could be determined by melt water availability at the bed either due to melt water quantity and duration of melt season either due to firn aquifer storage or variation of water availability with elevation.

Sundal et al. (2011) also noticed that for some glaciers in Greenland, even if peak rates of ice flow speed-up events are correlated to surface melting, the mean summer flow rates are not. When a runoff threshold is exceeded, the glacier slows down, suggesting the development of a more efficient water drainage. By the end of the season, it became more efficient and migrates up-glacier to drain regions that could have previously been isolated from the effective drainage system (Bartholomew et al., 2011).

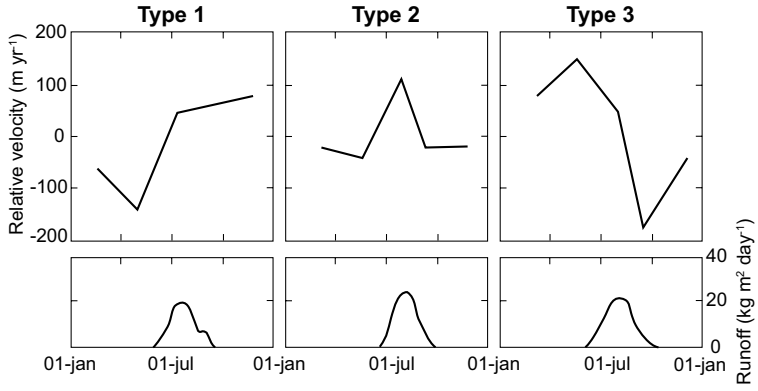

Figure 1.2. Different behavioral types of Greenland glaciers (Moon et al., 2014). Upper panel shows the mean velocity pattern and the lower panel the mean runoff during a whole year.

At the inter-annual time-scale, concerns have been recently raised about winter motion (Tedstone et al., 2015). However, Sole et al. (2013) observed no clear correlation between normalized summer melt and annual ice flow but a negative relationship between melt and winter displacement. They suggest that the influence of the melt season characteristics on the processes at the ice-bed interface determines the winter motion, reducing the inter-annual variation sensitivity. This has also been discussed by van de Wal et al. (2015) who favors a self-regulation between surface melt water production and basal motion so that melting and ice motion do not have a statistically significant relationship over long time periods. However, Tedstone et al. (2015) who suggests a significant correlation between summer melt and autumn–winter ice motion while there is no relationship between the annual melt volume and ice motion. They studied annual ice motion for three transects across an 8000 km land-terminating region of the west Greenland Ice Sheet (GIS) margin, extending to 1100 m above sea level. They found that despite an increase of surface melt water production since 2002, the region is 12 % slower in 2007–2014 than 1985–1994. This decrease in velocity cannot be explained by thinning alone and they suggest a large contribution from the basal motion changes. When the summer season has extreme melt, the subglacial drainage system will tend to become more efficient over a longer period but also further up-glacier due to melt at higher elevation (Doyle et al., 2014). Those channels would stay open, at the atmospheric pressure, longer after the melt stopped and the water pressure would increase gradually through the next winter. The unchannelised drainage regions and their connectivity to the channelised drainage system are in this case seen as governing the subsequent ice motion. However, while higher melt water productions are observed everywhere, most tidewater glaciers are accelerating suggesting that other processes becomes more important as Moon et al. (2014) showed.

2. Objectives of the thesis

The main objective of this thesis is to use observation data into modelling in order to gain better understanding in two of the most important unknown processes in glaciology, sliding and calving, their interactions with each other and other processes. These processes act at the boundary of glaciers and are difficult to study or model because of their complex interactions with other processes and the apparent singularity of a particular glacier or a group of glaciers. It is therefore not enough to either analyse observations or have a theoretical model, a combination of both is necessary.

By inverting three years of high temporal surface velocity, **Paper I** shows the spatio-temporal distribution of basal properties under Kronebreen, a tidewater glacier in Svalbard and compare the results to surface runoff. However, basal friction being intrinsically linked to basal water and pressures, modelling the subglacial hydrology system is a prerequisite to better understanding of sliding. This is the subject of **Paper II**.

While ice flow can be modelled as a continuous process, because of their timescale and behaviour calving and crevasse formation are better modelled as discrete processes. For that reason, a discrete particle model has been used to simulate calving. Moreover, the calving process is interacting with many others and particularly ice dynamics, subglacial discharge and ocean processes. Coupling different models is therefore necessary to take into account these feedbacks. In **Paper III**, an offline coupling is used to compare modelled results to observations and estimate the role of each process in calving.

Finally, to better understand calving, more observations are necessary and **Paper IV** present a method to automatically detect calving events from timelapse camera imageries. This can serve as a tool to monitor size and frequency of calving events.

3. Background

Sliding and calving are two complex processes, which have a great influence on glacier dynamics. Interactions with other processes in space and time, as well as the difficulties to acquire meaningful observations, make any parameterisation in models difficult. The known mechanisms and implications for modelling are presented here.

3.1 Sliding at the base of glaciers

3.1.1 Examples of subglacial environment observations

The subglacial environment is difficult to observe but different techniques have been used throughout the years to understand subglacial hydrology, sliding and their relation with one another.

Geomorphology of deglaciated landscapes gives the first hint on how ice, water and rock (or sediments) interact (Walder and Hallet, 1979). When the ice is present, however, these landscapes are difficult to observe. In this context, a technique to investigate the origin of the water is to measure different variables in proglacial streams associated with the runoff discharge such as electrical conductivity, suspended sediment concentration (Gurnell A., 1996; Box and Ski, 2007) or hydrochemistry (Tranter et al., 1996; Rutter et al., 2011). It is also possible to follow the route of the water from a moulin to the terminus of the glacier by injecting dye into the subglacial environment. Measuring its concentration shows the diurnal changes in efficiency of the hydraulic system (Nienow et al., 1998; Hock and Hooke, 1993) but also its extent along the glacier.

Accessing the bedrock directly can be done by exploring the englacial and subglacial tunnels (Gulley et al., 2009; Cohen et al., 2005; Lefeuvre et al., 2015) or cavities (Anderson et al., 1982). Moreover, borehole drilling, enabling different measurements. can be performed at different locations across the glacier. Water pressure, measured with pressure transducers suspended in boreholes above the bed, reflect the balance between melt water supply at the bed and the ability of the drainage system to evacuate this water supply (Hubbard and Nienow, 1997). It is also possible to measure the turbidity, the electrical properties or the geochemistry of the water in the borehole (Stone and Clarke, 1996; Hubbard et al., 1995) to estimate the sediment content and the exposition to the the subglacial environment. Borehole videos can give an

indication on the 'soft' or 'hard' state of the bed (Harper and Humphrey, 1995) and on the water movements (Fountain et al., 2005). To measure the deformation of the bed and strain rates, tiltmeters can be placed into the subglacial sediments (vertically distributed cells) while sediment mechanical properties are measured with a ploughmeter (Fischer and Clarke, 1994).

Geophysical techniques are also useful to indicate the presence of water or the shape of the drainage systems. Walter et al. (2008) measured the seismic activity of Gornergletscher, Switzerland, during the summers of 2004–2006 and recorded icequakes close to the glacier bed. They show that basal seismic activity are linked to the diurnal water pressure changes, surface lowering and glacier sliding. Röösli et al. (2014) reported glacial tremors lasting several hours, which epicentre was located at a large moulin, and showing strong correlation with the water level of this moulin. Ground penetrating radars (GPR) can be used to locate and measure the size of tunnels exploiting the different propagation velocity in the air, in the water or in the ice (e.g Moorman and Michel, 2000; Irvine-Fynn et al., 2006).

Observations of the basal environment are numerous but are often limited in time and space. Modelling becomes therefore necessary to interpret observation and understand dynamical behaviour.

3.1.2 Theoretical considerations of the subglacial drainage system

Flowers (2015) put together a review on subglacial hydrology models and she showed their evolution in time from single elements, early models adopted from groundwater hydrology models to next-generation glaciological models and multi-elements models.

Elements of the basal drainage system

To infer the physics behind the basal drainage system, information gathered by observations can be conceptualized into isolated elements.This simple approach helps to understand better the mechanisms of opening and closure, the flow state (laminar or turbulent) through the element, the relationship between water pressure and water discharge or the stability of the drainage system.

Thin film of water or water sheet – Weertman (1957) was the first to introduce the concept of thin film of water when explaining his theory on sliding around bedrock obstacles. Thickness (Weertman, 1962, 1972; Nye, 1973), stability (Walder, 1982) and partial support of the ice roof by clasts (Creyts and Schoof, 2009) have later been studied to understand its impact on glacier sliding.

Channels (or R-channels) – Channels incised into the ice are thought to permit fast and efficient drainage. Shreve (1972) established the hydraulic potential concept for glaciers where water could escape through tunnels. Large tunnels, because of their lower water pressure, have the tendency to capture

the water from smaller conduits. These tunnels are called the R-channels in reference to Röthlisberger (1972) who physically described the opening due to melting and the closure due to creep of the channel walls, recently investigated by Meyer et al. (2016). Further investigations, including time or temperature dependency (Spring and Hutter, 1981), focused on the dynamics of channel formation especially during a jökulhlaup.

Cavities – Cavities would open due to sliding and close due to viscous creep (Lliboutry, 1968) creating a network of linked cavities along the ice-bed contact surface. The water flow in this linked-cavities system behave fundamentally different from channel systems: water pressure increases with discharge and, at an equal cross-section, water flow velocity is lower than R-channels under the same hydraulic gradient. Cavity instability could be at the origin of channel formation (when creep closure cannot balance opening anymore because of water pressure) but cavities are more stable than R-channels (Kamb, 1987). Walder (1986) incorporated glacier hydraulics theory and Iken (1981) investigated numerically the relationship between cavity pressure and sliding. Lliboutry (1979) and Kamb (1987) introduced the concept of linked- cavities systems that would form from different type of cavity (step, wave and hybrid cavities). Later, Schoof (2005) produced an analytical explanation of the effect of cavitation on glacier sliding.

Canals (or N-channels) – If the ice is able to incise into the till or the bedrock, canals, called N-channels after Nye (1973), can form (Alley, 1992). According to Walder and Fowler (1994), evolution of canals is governed by till erosion and creep and the effective pressure decreases with increasing drainage. Canals are favoured over R-channels when the slope is not steep and the hydraulic potential gradient is small.

Drainage through sediments: porous flow – Water can infiltrate the sediment layer and the relative impermeability of till allows it to be saturated and a potential source of sliding (Shoemaker, 1986). Assuming porosity and aquifer compressibility, the groundwater moves according to the diffusion equation. Tulaczyk et al. (2000a) suggests that the soil behavior and failure strength depends on the effective stress history (Mohr-Coulomb criterion) and that the soil can be in two states: normally consolidated (the current effective stress is higher than any effective stress of the past) or overconsolidated (mainly elastic deformations).

Combined subglacial hydrology models

Single element studies give a good understanding of the physics behind each process but do not reproduce well what has been observed at the base of ice sheets or glaciers. It is therefore important that subglacial hydrology models should include a combination of different elements and the possibility to switch between them.

One-dimensional models are usually described for an idealised geometry with the same elements but a different implementation for a single channel

(e.g. Kingslake and Ng, 2013; Pimentel and Flowers, 2010) or for more channels (e.g. Flowers et al., 2004; Colgan et al., 2011; Hewitt, 2011). The switch between fast and slow drainage systems can be prescribed given critical cross-section, discharge, basal effective pressure and sliding speed and depends on the basal water supply (Kingslake and Ng, 2013; Hewitt and Fowler, 2008). Schoof et al. (2014); Kessler and Anderson (2004) allow the drainage system to oscillate from slow to fast depending on melt opening, opening due to sliding and creep closure.

In two-dimensions, four models have been developed up to current date. In Schoof (2010) model, each edge of the mesh represents an individual conduit element and, depending on the balance of opening and closure processes, can evolve into a cavity or an R-channel and switch between the two configurations at a critical discharge depending on the sliding velocity, the hydraulic gradient along the conduit and the bed obstacle size. The novelty brought by Hewitt (2013) and Werder et al. (2013) is that more than one cavity is allowed per grid cell describing the distributed system as a sheet. Werder et al. (2013) also introduce a term in the channel opening equation, linked to the cavity characteristics, which can create a channel even when the initial cross-section is null. The characteristic height of cavity-forming bed obstacles and their spacing control the evolution of sheet thickness. A continuity equation, including englacial storage, regulates the water flow in the sheet and channel system. Water pressures are assumed the same at the boundary between both systems. de Fleurian et al. (2014) followed a double continuum approach using porous layers to compute water heads in efficient and inefficient drainage systems. The activation of the fast drainage system establishes a transfer flux between the two systems.

3.1.3 Sliding mechanisms and laws

Sliding at the base of the glacier, on hard bedrock or on soft bed (sediments), has a large contribution on ice motion (see Fig. 3.1a) unless the base is frozen. Typically, this boundary condition experiences a relationship between the basal shear stress, τ_b, and the tangential basal velocity, u_b called the sliding law. It also depends on several other parameters such as the water pressure, the roughness, etc. Elaborate a realistic sliding law (relating the basal stress to the basal velocity) has been a subject of study for many years. Attempts have been made using empirical or mathematical theories (e.g. Weertman, 1957; Lliboutry, 1968; Iken, 1981; Fowler, 1981; Budd et al., 1984; Schoof, 2005; Gagliardini et al., 2007; Tsai et al., 2015) but are poorly tested against observations.

Weertman (1957); Lliboutry (1968) were the first to develop a theoretical framework to the construction of a sliding law, of which Fowler (2010) gives the main steps. Sliding at the base was already well know when Weertman

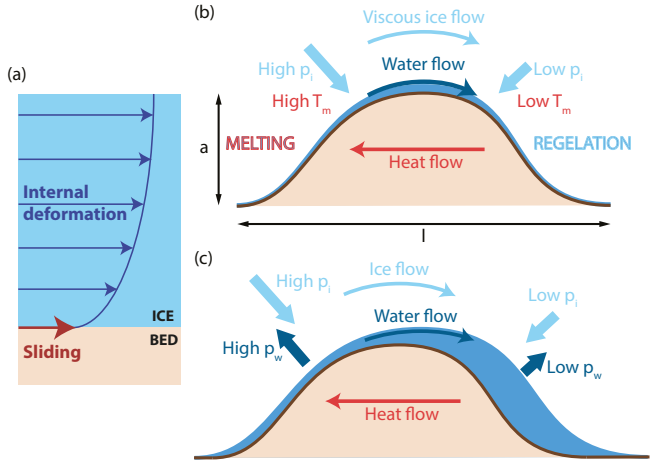

Figure 3.1. **(a)** Schematic velocity distribution in a glacier. **(b)** Combination of regelation (ice melting upstream of bump, flowing as thin water film, and ice refreezing downstream of bump) and plastic flow (increased normal stress upstream and decreased downstream). **(c)** Combination of regelation (ice melting upstream of the obstacle, flowing as thin water film, and ice refreezing downstream of bump), plastic flow (increased normal stress upstream and decreased downstream) and cavitation processes.

(1957) gave a physical explanation to it by quantifying two processes: regelation and enhanced creep or viscous flow (see Fig. 3.1b).

Regelation is the process whereby ice melts upstream of an obstacle, where the pressure is high (lower melting temperature), flows as thin water film, and refreezes downstream of the bump where the pressure is lower (higher melting temperature). Released latent heat downstream is transported upstream by the temperature gradient and on the upside of the obstacle the latent heat is used to melt the ice. The effect is that ice moves past obstacles without deformation. This process is most significant for small obstacles and very smooth beds. The regelative ice velocity can be written as

$$u_R = \left(\frac{k\gamma}{\rho_i L a} \right) \frac{\tau_b}{R^2}, \tag{3.1}$$

where ρ_i is the density of ice, k is the thermal conductivity of the bedrock, L is the latent heat, a is the obstacle dimension, l is the distance between obstacles, $R = \frac{a}{l}$ is the aspect ratio and γ is the slope of the Clapeyron curve in the Clapeyron formula.

The enhanced creep or viscous flow comes from the Glen's flow law, in which the strain rates are non-linearly related to applied stress (more details in section 6.1.1). This explains why enhanced stress upstream of an obstacle locally increases strain rates and drives the ice flow around the bump. This process is most significant for large obstacles. The velocity due to viscous

shearing past the obstacle can be written as

$$u_V = 2aA\left(\frac{\tau_b}{R^2}\right)^n. \tag{3.2}$$

Weertman (1964) added together the velocities from regelation and from viscous shearing so that the basal stress equals to

$$\tau_b = R^2\left[R_r a u_b + Rv\left(\frac{u_b}{a}\right)^{1/n}\right], \tag{3.3}$$

where $R_r = \frac{\rho_i L}{k\gamma}$ and $R_v = \left(\frac{1}{2A}\right)^{1/n}$.

At a typical controlling obstacle size, regelation and viscous stresses are comparable and for this value of a, we obtain

$$\tau_b = R^2 R u_b^{\frac{2}{n+1}}, \tag{3.4}$$

where $R = \left(\frac{\rho_i L}{2k\gamma A}\right)^{\frac{1}{n+1}}$. Nye (1969) and Kamb (1970) extended the Weertman's law using a mathematical model by solving the Stokes flow equations best known as the Nye-Kamb model.

Lliboutry (1959) introduced a third process, known as the cavitation process where water filled cavities form behind the bed obstacles and influence the ice-bed contact. This process acts in combination with the viscous flow, leading to ice separation from the bed in the lee of obstacles (see Fig. 3.1c). Basal shear stress decreases with velocity and increases with effective pressure $N = p_i - p_c$ where p_i is the ice pressure and p_c is the cavity pressure. These cavities reduce the effective roughness of the bed and make the sliding relation multi-valued. The cavities usually form downstream of a bump when the water film pressure reaches the local drainage pressure. Iken (1981) introduced a critical effective pressure $N_c > 0$ below which sliding would be unstable. Water pressure and ice velocity appear to have a strong correlation (Iken and Truffer, 1997) but not constant through time and space. Fowler (1986) suggested a sliding law of the form

$$\tau_b = Nf\left(\frac{u_b}{N}\right), \tag{3.5}$$

where f is a function increasing to a maximum, f_{max}, and then decreasing to zero for high values of u_b. Iken's separation pressure is attained when $N = \tau_b / f_{max}$. It is reached when a cavity behind an obstacle get so large that it reaches the next obstacle down stream of the obstacle causing the cavity. In other terms, when a cavity forms at the lee of an obstacle, the maximum up-slope of the bed limits the basal friction value to a maximum. The maximum possible shear stress that can be supported by the bed is called the Iken's bound.

These developments have been described for hard bedrock but early studies on till and sediment rheology suggested that the bed composition may have

an impact on the glacier dynamics. Blankenship et al. (1986) correlated high speed of Whillans Ice Stream, Antarctica, to the deformation of the underlying till layer saturated with water. Later glaciological or geophysical investigations of West Antarctica ice streams confirmed the presence of a weak till layer responsible of basal lubrication and fast sliding (Alley et al., 1986; Engelhardt et al., 1990; Kamb, 1991) at relatively low driving stresses. Describing the rheology of the glacial till, which is a granular material, helps to understand sliding on deformable bed. The first studies, based on in-situ deformation measurements (Boulton and Hindmarsh, 1987), assumed viscous or Bingham fluid deformation laws for the sediments (e.g. Alley et al., 1986; MacAyeal, 1992), but Kamb (1991) showed almost no strain rate dependence of sediment strength in a laboratory experiment and concluded that glacier sediments have a nearly plastic behaviour. Criticism followed this assumption mainly due to limitations in the experiment itself. Tulaczyk et al. (2000a) built a model based on experiments results from beneath Ice Stream B, Antarctica, and supported the use of a Coulomb-Plastic rheology by showing that the failure strength, τ_f, of the till was strongly dependent on effective normal stress, N_e, but independent of strain and strain rate. They proposed a compressible Coulomb-Plastic till model with three state variables: the shear strength, τ, the void ratio , e, and the normal effective stress, N_e. A material is said to be normally consolidated when compacted only by its own weight and overconsolidated when subjected to additional load such as shear stress or experiencing a reduction in overburden pressure. A granular material deforming at a constant strain rate first deform elastically with the strain rate up to the yield strength, s, and above it, the deformation becomes visco-plastic and irrecoverable. The shear stress continues to increase with strain until a failure strength, τ_f, and subsequently decreases to attain a constant residual or ultimate strength. If a flow law for till exists, this residual strength should increase with strain rate otherwise till would be perfectly plastic. The classical Mohr-Coulomb relation for the failure strength, τ_f, states

$$\tau_f = c + N_e tan(\phi), \tag{3.6}$$

where the cohesion, c, and the angle of internal friction, ϕ, are two physical properties of the material and the effective normal stress, $N_e = \sigma_n - p_w$ is the difference between the total normal stress, σ_n, and the pore pressure, p_w. For glacial till, the cohesion, c depends primarily on the amount and types of clay minerals present. The internal friction, ϕ depends on the granulometry of the material. The void ratio, $e = V_p/V_s$, the ratio between the volume of pores, V_p, and the volume of solids, V_s, varies with the effective pressure, N_e

$$e = e_0 - C_p log(\frac{N_e}{N_{e0}}), \tag{3.7}$$

where e_0 is the void ratio for a given effective normal stress, N_{e0}, and C_p is a dimensionless coefficient of compressibility.

3.1.4 Sliding parameterisations used in models

The different laws described in the section above have been used as parameterisation of sliding in models and are summarised below.

Weertman-type sliding law
By extension of the Weertman theory, a non-linear Weertman-type sliding law can be written

$$\tau_b = \left(\frac{u_b}{A_s}\right)^{\frac{1}{m}}, \tag{3.8}$$

where $A_s > 0$ is the sliding parameter and m is the stress exponent.

Bindschadler-Budd sliding law
Bindschadler (1983), Budd et al. (1984) and Raymond and Harrison (1987) added the effective pressure variable and discussed the parameterisation of a law of the form

$$\tau_b^m = \frac{u_b}{A_s} N^q, \tag{3.9}$$

where $m = 3$ and $q = 1$ or $q = 2$.

Schoof-Gagliardini friction law
Using a mathematical model, Schoof (2005) proposed a friction law for the case of sliding with cavitation. Gagliardini et al. (2007) generalised the law by adding a post-peak exponent, q_s, that if positive enables the friction law to be multi-valued,

$$\tau_b = CN \left(\frac{\chi}{1 + \alpha \chi^{q_s}}\right)^{\frac{1}{m}}, \tag{3.10}$$

where $\alpha = (q_s - 1)^{q_s - 1}/q_s^{q_s}$ and

$$\chi = \frac{u_b}{C^m N^m A_s}, \tag{3.11}$$

where A_s is the sliding parameter in absence of cavitation and C is the bed geometry coefficient assumed dependent on space but not on time.

Tsai sliding law
Tsai et al. (2015) proposed to fullfill the Iken's bound with a law of the type

$$\tau_b = min\left(\left(\frac{u_b}{A_s}\right)^{\frac{1}{n}}; f_{max} N\right). \tag{3.12}$$

Viscous model of till deformation

Alley et al. (1986) and MacAyeal (1992) used an intuitive constitutive relation between the strain rate, $\dot{\varepsilon}$, and the shear stress, τ, of the form

$$\dot{\varepsilon} = k_2 \frac{(\tau - \tau_c)^m}{N_e^p}, \tag{3.13}$$

where k_2 is a constant, τ_c is a critical critical shear stress below which no deformation occurs.

Compressible Coulomb-Plastic Till Model

Using Eq.3.6 and Eq.3.7, Tulaczyk et al. (2000b) obtained an empirical till deformation law of the type

$$\tau_f = ae^{-be}, \tag{3.14}$$

where a and b are two experimental constants. If we assume that the basal resistance to ice motion is determined by the till strength ($\tau_b = \tau_f$), the ice sliding is then directly dependent on the void ratio and the effective normal pressure.

Some of the sliding laws described above are compared in Fig. 3.2.

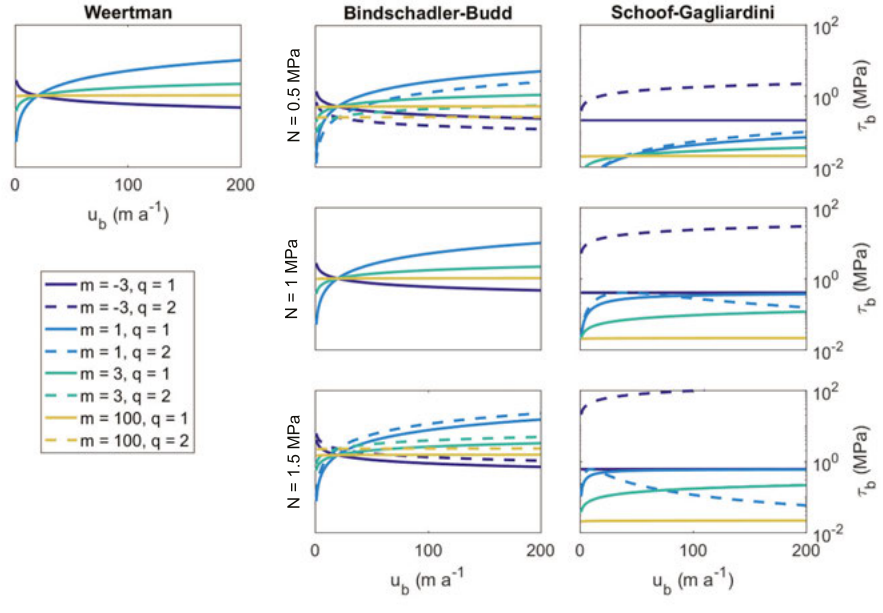

Figure 3.2. Comparison of different sliding laws for different values of N, m and q, $As = 20\,\mathrm{MPa}^{-m}\,\mathrm{a}^{-1}$ and $C = 0.4$.

3.1.5 Inverse methods and basal friction

Observations of the subglacial environment are sparse and locally constrained in time and space. To be able to understand the past glaciations or to predict the future behaviour of ice masses, models need to incorporate a valid sliding law. Ritz et al. (2015) showed that future contribution of polar ice sheets to sea level rise are highly sensitive to uncertainties in sliding parameterisation. The parameterisation of such a law can be inferred by assimilating observed data such as surface velocities and minimise the misfit between observed and modelled velocity fields (Habermann et al., 2012). In the glaciology literature, such inverse methods have been used to determine bed topography (Morlighem et al., 2011; Van Pelt et al., 2013; Michel-Griesser et al., 2014), basal friction (Joughin et al., 2004; Gudmundsson and Raymond, 2008; Morlighem et al., 2010; Jay-Allemand et al., 2011; Goldberg and Sergienko, 2011; Gillet-Chaulet et al., 2012; Schäfer et al., 2012; Brinkerhoff and Johnson, 2013; Sergienko and Hindmarsh, 2013; Minchew et al., 2016; Shapero et al., 2016) or both (Gudmundsson, 2003; Thorsteinsson et al., 2003; Raymond and Gudmundsson, 2009), basal friction and mass balance (Larour et al., 2004), ice viscosity (Rommelaere and Macayeal, 1997; Larour et al., 2005; Arthern and Gudmundsson, 2010), transient ice flow (Larour et al., 2014) and accumulation rates and patterns (Waddington et al., 2007; Eisen, 2008; Steen-Larsen et al., 2010; Van Pelt et al., 2014).

Most ice flow models use a linear or non-linear Weertman-type sliding law with an optimized but temporarily and spatially fixed parameter (e.g. Joughin et al., 2004; Gudmundsson and Raymond, 2008; Morlighem et al., 2010; Gillet-Chaulet et al., 2012; Van Pelt et al., 2012). However, from the observed highly variable dynamic behavior of glaciers, it is clear that basal parameters in models should vary over both time and space depending on current conditions at the bed (Iken and Truffer, 1997; Schoof, 2010; Sole et al., 2011). Jay-Allemand et al. (2011) inverted ten years of surface velocity prior to and during the surge of Variegated glacier, Alaska, fitted a Schoof-Gagliardini type sliding law and showed the long-term varying spatio-temporal pattern of basal properties on a flow line but to date, no seasonal inversion had been performed. Gillet-Chaulet et al. (2016) inverted five years of surface velocity of Pine Island Glacier, Antarctica, assuming temporally fixed but spatially variable sliding coefficient with a non-linear Weertman-type sliding law and find a best fit for $m = 20$. But this wouldn't hold for fast-flowing glaciers in areas of surface melt water influence. Minchew et al. (2016) assimilated surface velocity observations at three dates for Hofsjökull Ice Cap, Iceland, and noticed a weakening of the bed during the melting season. Shapero et al. (2016) also found low resistance of the bed for three glaciers in Greenland with isolated patches of high basal resistivity. Habermann et al. (2013) correlated changes in basal stress of Jakobshavn Isbrae, Greenland, between 1985 and 2008 with

changes in height above flotation and used a Mohr-Coulomb type sliding law to parameterise τ_b.

Inversions are usually made with a linear Weertman-type sliding law in order to retrieve a spatial map of A_s, which becomes an effective sliding coefficient, and other sliding laws can then be fitted. Minchew et al. (2016) confirmed that using a linear or a non-linear sliding law for the inversion result in a similar basal shear stress pattern (within a few percent). Because of its construction, the most common value of m in Eq. 3.8 is the ice flow law exponent, $n = 3$ but it is possible to change the value in order to simulate different behaviours. If $m < n$, it could represent viscous deformation of the subglacial till at large scales (Hindmarsh, 1997) and if $m \gg n$, on the contrary, it could represent plastic till rheology (Tulaczyk, 2006) or ice flowing over a rigid bed with cavities (Schoof, 2005) as presented in section 3.1.3. Most studies would use a positive stress exponent, m, but it has been suggested that it could be negative implying a rate weakening behaviour (Scholz, 2002) that could mimic the multi-valued relation described by Lliboutry (1959). In the case of hard beds, where cavities can grow in the lee of bumps, Schoof (2005) discuss it theoretically, as a base for his cavitation theory, Gagliardini et al. (2007) proposed to add a post-peak exponent, and Zoet and Iverson (2016) shows it experimentally in a confined glacier sliding experiment. In the case of soft beds, this velocity weakening mechanism has been observed (e.g. Rousselot and Fischer, 2005) and Thomason and Iverson (2008) discuss the role of particle ploughing and pore-pressure feedback. However, good knowledge of bed properties are needed in order to choose the exponent m and it is not very often available. In a nutshell, sliding laws need to be tested in a larger spatial and temporal scale than previously done.

3.2 Calving at the front of glaciers

Calving involves a series of different processes, which may have important impacts on the glacier dynamics. Calving models try to encompass them but still more observations are needed.

3.2.1 Processes leading to calving

Calving is a component of the mass balance process for tidewater (or marine-terminating) glaciers and it consists of the mechanical loss of land ice into the ocean. It occurs when tensile stresses are large enough to propagate fractures through the glacier ice. The calving process depends on a number of external factors and some of them are shown in Fig. 3.3.

Benn et al. (2007) listed different mechanisms leading to calving and sorted them into four categories. First, surface velocity gradients can lead to stretching of the ice and formation of crevasses. Calving can subsequently occur

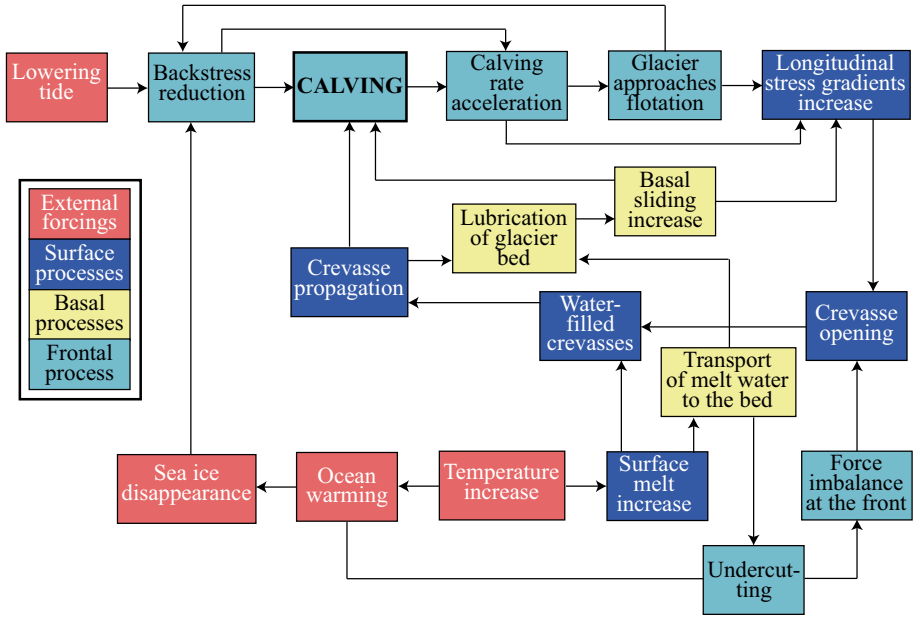

Figure 3.3. Diagram of different processes leading to calving. Adapted from Wainwright (2014).

following these lines of weakness. The strain rate pattern is therefore a good measure of preferential calving and it particularly increases near the terminus as the glacier approaches flotation. Crevasses also propagate because of hydro-fracturing due to water filling them (Scambos et al., 2000). Uneven stress patterns at the base of the glacier, together with the presence of subglacial water can also lead to the formation of basal crevasses (Benn et al., 2007). Second, calving can occur when a force imbalance exists at the terminal cliff due to uneven cryospheric pressure and water pressure exerted by the ocean (Reeh, 1968). Third, undercutting at or below the water line and formed when melt rates are greater than aerial melt rates at these locations, can have an influence on the stability of the frontal ice. Recently, a number of studies have pointed out the role of melt undercutting in calving (e.g. Holland et al., 2008; Motyka et al., 2013; Luckman et al., 2015; Rignot et al., 2015; Fried et al., 2015; Truffer and Motyka, 2016). Undercutting at the front are formed when subglacial glacier water discharged in the ocean is mixed with warm sea water entraining buoyant melt water plumes upwards and melting the ice front (Jenkins, 2011). Forced by oceanic properties, plume models are used to study the effect of melting on the glacier front (e.g. Kimura et al., 2013; Carroll et al., 2015; Stevens et al., 2016; Slater et al., 2015, 2016, 2017a,b) and can estimate melt rates. Increased rates of submarine melt may be attributed to two different mechanisms, the temperature increase of a thicker ocean layer in the fjord or an increase of subglacial discharge (Straneo and Heimbach, 2013).

Fourth, calving can occur because of buoyancy-driven forces created by hydrostatic disequilibrium leading to the detachment and overturning of tabular blocks, particularly in Greenland (e.g. James et al., 2014; Murray et al., 2015; Medrzycka et al., 2016).

3.2.2 Calving laws and models

Calving laws try to describe the calving process and make it possible to incorporate it into ice flow models. They either solve the calving rate (frontal ablation) or the frontal position. The frontal ablation rate at the water margin at time t_i, $\dot{a}_c(t_i)$, is the difference between the ice velocity at the front, $u_w(t_i)$ and the rate of change of the frontal position, $\partial L/\partial t$ integrated over the terminus domain Γ_w as defined in McNabb et al. (2015). This yields

$$\dot{a}_c(t_i) = \int_{\Gamma_w} u_w(t_i) - \frac{\partial L}{\partial t}\, \mathrm{d}\Gamma_w, \tag{3.15}$$

with

$$\int_{\Gamma_w} \frac{\partial L}{\partial t}\, \mathrm{d}\Gamma_w = \frac{\Delta A(t_i)}{t_i - t_{i-1}} \int_{z_{\Gamma_w}} \mathrm{d}z, \tag{3.16}$$

where $\Delta A(t_i)$ is the area change at the terminus over the time $t_i - t_{i-1}$.

The water depth criterion (Brown et al., 1982; Warren, 1992) simply relates the water depth, D_w, to the calving rate based on observations in a linear fashion ($\dot{a}_c = a + bD_w$). However, no single law is evident for all glaciers.

Vieli et al. (2001) and van der Veen (2002) introduced a flotation criterion, from observations in Columbia glacier, Alaska, to determine an effective ice thickness at the front, H_{ice}, based on a flotation height, $H_f = D_w(\rho_w/\rho_i)$ where ρ_w and ρ_i are the water and ice densities, respectively. But such a criterion does not allow any ice shelf to form. Amundson and Truffer (2010) claimed that the terminus thickness, H_1, after a calving event is larger than the terminus thickness, H_0, before the event and proposed a calving framework. Calving events are triggered when terminus thickness decreases to some critical value, H_0 and when initiated, the terminus retreats to a location where the terminus thickness equals another critical value, H_1. However, it is very difficult to determinate these thresholds in general.

The crevasse-depth criterion is based on the assumption that calving occurs when crevasses reach a critical depth, either the water line (Benn et al., 2007) or the full depth (Nick et al., 2010). Crevasses, in turn, are assumed to open by longitudinal stretching or water filling them (van der Veen, 2007). Krug et al. (2014) combined damage and fracture mechanics to propagate crevasses until the critical depth is reached. A number of other studies use this crevasse-depth criterion (e.g. Otero et al., 2010; Cook et al., 2014; Lea et al., 2014; Todd and Christoffersen, 2014; Pollard et al., 2015). However, such a criterion, even if more theoretically based than the former laws, lacks the incorporation

of other factors contributing to calving. Moreover, these models are based on one-dimensional flow line and vertical flow band models. Alternatively, Morlighem et al. (2016) use the level set method to move a two-dimensional boundary and empirically tune a strain rate or a stress criteria adapted from a von-Mises yield criterion to predict calving rates. Nevertheless, to be more accurate, models need calving laws that are based on calving processes and take into account associated feedbacks from ice and ocean dynamics (Vieli and Nick, 2011; Nick et al., 2013; O'Leary and Christoffersen, 2013; Luckman et al., 2015; Joughin et al., 2012; Benn et al., 2017).

Traditionally, glaciers and ice masses are considered to flow as a non-linear, incompressible and isotropic viscous fluid and continuum models, such as Elmer/Ice, are extensively used. However, when it comes to fractures, crevasses formation or calving processes, ice can be viewed as a solid and deformation described as a discrete process. In such models, ice is represented by discrete particles linked together by weak beams that are able to break when the elastic load is greater than a fracture threshold. The Helsinki Discrete Element Model, HiDEM, (Åström et al., 2013), together with other discrete particle models (Bassis and Jacobs, 2013), are leading the way to another approach to model the calving process and understand its links with external forcing, glacier geometry as well as ice and ocean dynamics. A new approach to calving modelling, using the benefits from both continuum and discrete models, is starting the emerge. Such a coupling is described in **Paper B** and deployed as a workflow in UNICORE (Streit et al., 2010), a middleware abstraction for job submission and management on different kind of job scheduling systems. Benn et al. (2017) have developed a new strategy to formulate calving laws using HiDEM to model fractures and calving and Elmer/Ice to identify critical stress states. They found that (i) location and orientation of preexisting cracks favor low magnitude calving events, (ii) large enough undercuts, as a calving multiplier effect (O'Leary and Christoffersen, 2013), enable calving events of larger magnitude, and (iii) the development of super-buoyant conditions is related to ice flowing into deepening water or to dynamic thinning. However, such a coupling needs to be confronted to observations in order to be validated as well as include models simulating interactions with the ocean.

3.2.3 Size and frequency of calving events

In **Paper C**, calving glaciers are identified as self-organised critical systems (Jensen, 1998) and specifically as the simplest form of them, the Abelian sandpile model. The size distribution of 'avalanches' (sand grains or calving events) is a scale-invariant power law. Another example in nature is the Gutenberg-Richter law for earthquakes. No event should be considered as exceptional. They are in fact just following this law and the system always try to be at a critical point. They can fluctuate between subcritical advance

and supercritical retreat states that are close to the critical point (as a sandpile is building mass and catastrophically collapses when grains are added) in response to changes in climate and in geometric conditions. However, when the supercritical state is favoured, because of changing conditions, the glacier front will experience rapid collapse and disintegration.

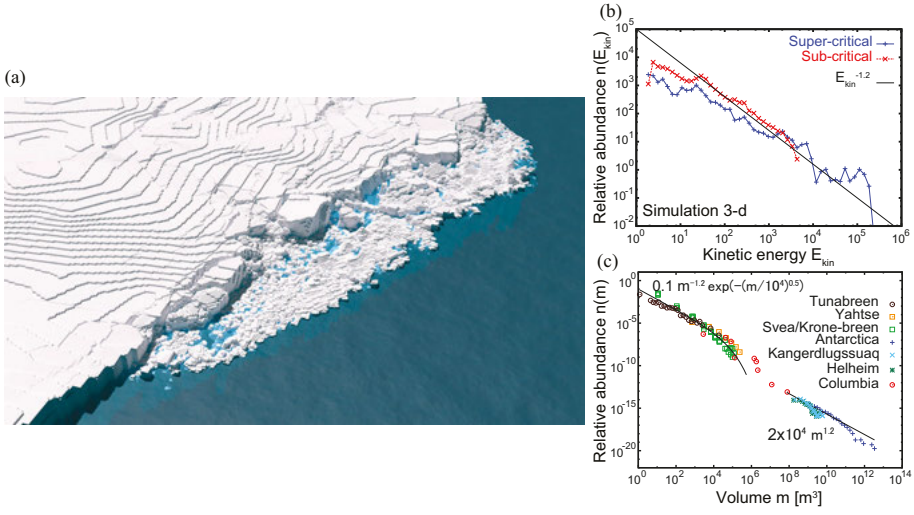

Figure 3.4. **(a)** Modelisation of the front of Kronebreen, Svalbard, using the Helsinki Discrete Element Model(HiDEM). **(b)** Calving event size distribution of a simulated glacier. **(c)** Calving event size distribution of different glaciers including Tunabreen. Reproduced from **Paper C**.

The paper showed that by pairing a discrete particle-based model, HiDEM, (see Fig. 3.4a–b) with observations of calving events spanning 12 orders of magnitude in size (see Fig. 3.4c), calving belongs to a generic class of brittle fragmentation and the crack propagation triggers calving 'avalanches' that have size and frequency distributions with a striking resemblance to the so-called Abelian sandpile model. To assess the future stability and calving rates of marine-terminating glaciers, more observations are needed to constrain the external forcing and initial conditions to feed the model. Observations of size and frequency of calving events can help to understand calving processes better.

The most obvious way to gather such information is to visually monitor the front and qualitatively assess the size, the shape and the frequency of calving events. O'Neel et al. (2007) visually determined the magnitude and frequency of glacier calving by watching the terminus of Columbia glacier, Alaska, during 16 days (excluding night times) in June 2005. Event sizes were estimated in a 1–10 magnitude scale ranging from small ice slabs flaking off the terminus to the breaking off of the whole terminus at once. To convert the qualitative magnitude to a quantitative volume, they photographed 20 events and pho-

togrammetrically scaled a three-dimensional perspective bounding box of the calved ice by the local height of the terminus. Submarine event volumes were extended using the local depth of the sea bed (Åström et al., 2014). Chapuis and Tetzlaff (2014) used a similar method over 16 days (including night times) for two glaciers in Svalbard, Kronebreen and Sveabreen, in August 2009. In June 2010, Bartholomaus et al. (2012) also visually surveyed the terminus of Yahtse glacier, Alaska. By deploying a broadband seismic network around the margins of the glacier, they calibrated a statistical relationship between iceberg sizes and icequake properties using visual observations and were able to reconstruct 18 months of calving volumes. With the same idea, Köhler et al. (2016) calibrated a 15 years of seismic record with seven years of satellite-derived frontal ablation measurements of Kronebreen, Svalbard, from FORMOSAT-2 satellite optical imagery (2 m resolution) at 2–5 week intervals during the Arctic summer. Satellite imagery has also been used to determinate the terminus position, hence calving size, of Helheim and Kangerdlugssuaq, Greenland Schild and Hamilton (2013) using MODIS satellite (250 m resolution) in intervals of 24 h at best during nine years. It is also possible to use time lapse cameras placed in front of a glacier and this has been done for Columbia glacier, Alaska (Walter et al., 2010), Tunabreen and Paierlbreen, Svalbard (**Paper C**), Tunabreen, Svalbard (Westrin, 2015) or Rink Isbræ, West Greenland (Medrzycka et al., 2016).

4. Study areas

Two tidewater glaciers, both situated in Svalbard, are studied in this thesis: Kronebreen (**Paper I–III** and **Paper A**) and Tunabreen (**Paper IV** and **Paper B–C**).

4.1 Kronebreen, Svalbard

Kronebreen is a grounded tidewater glacier, south-east of Ny-Ålesund situated in North-West Svalbard (Fig. 4.1a) terminating in Kongsfjorden. Two accumulation basins, Holtedahlfonna and the smaller Infantfonna, feed a fast flowing terminal tongue over the lowermost ten kilometers (Nuth et al., 2012) bounded to the north by a nunatak, Collethøgda, and to the south by Kongsvegen, as shown in Fig. 4.1b. Below roughly 500 m a.s.l, the glacier is highly crevassed (see Fig. 4.1c) and passes through three major ice falls.

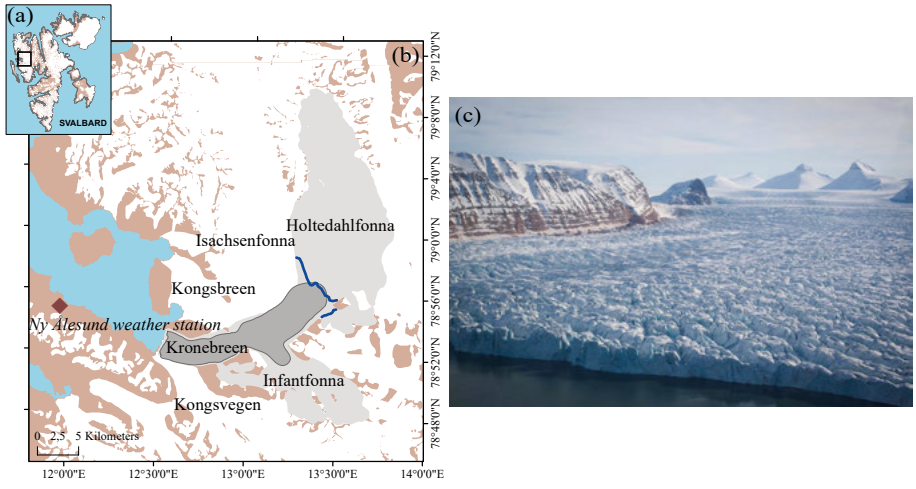

Figure 4.1. **(a)** Map of Svalbard glacier area. **(b)** The Kongsfjord region (König et al., 2013) with the Kronebreen glacier system in light gray and model domain in dark gray. The equilibrium line at 610 m a.s.l. for the period 1961–2012 (Van Pelt and Kohler, 2015) is shown in thick black. Reproduced from **Paper I**. **(c)** Picture taken in May 2014 from a helicopter at the front of Kronebreen showing the crevasse field.

The maximum elevation of the catchment is 1400 m a.s.l. The equilibrium line altitude was approximately at 610 m a.s.l. for the period 1961–2012 and during

the last decade, the firn line has retreated (Van Pelt and Kohler, 2015). Despite a slightly positive surface mass balance (SMB), around 0.13 m w.e. a^{-1}, for the period 1961–2012, melt rates have increased 21 % between the periods 1961–1999 and 2000–2012 (Van Pelt and Kohler, 2015) and the mass loss has accelerated since 1990 (Nuth et al., 2012). After a relatively stable period, the front of Kronebreen has started retreating since 2011 (overall net retreat of ∼2 km between 2011 and 2015) with seasonal oscillations (Schellenberger et al., 2015; Luckman et al., 2015; Köhler et al., 2016). Velocities at the front can reach 5 m d^{-1} in the summer and Schellenberger et al. (2015) showed that for the period 2007–2013, ice-flow variations during the melt season are closely linked to surface melt through changes of the subglacial hydrology system and the basal sliding. The observed winter velocities of 2012–2013 were particularly high compared to previous years and they speculated that a retreat of the terminus position, associated with a reduction in backstress, could be the cause of persistently high winter velocities.

Luckman et al. (2015) showed that calving rates are strongly correlated with subsurface fjord temperatures, which could indicate that the dominant control on calving is melt undercutting. During the summer, significant influx of warm water masses enters Kongsfjorden (Cottier et al., 2005; Nahrgang et al., 2014) and the temperature of the fjord is experiencing seasonal variations with maximum values for the upper 100 m toward the end of the season (Nahrgang et al., 2014). From fjord bathymetry (Howe et al., 2003; Aliani et al., 2016) and bed topography (**Paper A**), the actual terminus height is roughly 150 m with 100 m below sea level. Two sediment plumes have been observed in the fjord in the summer (Trusel et al., 2010; Kehrl et al., 2011; Darlington, 2015; How et al., 2017; Schild et al., 2017). The plume situated in the north is generally more active and extended than the southern one (see Fig. 4.2).

Figure 4.2. Picture of the front of Kronebreen taken in September 2014 where the plumes are visible.

4.2 Tunabreen, Svalbard

Tunabreen is an outlet glacier of the Lomonosovfonna ice cap situated at the head of Templefjorden in central Svalbard (see Fig. 4.3a-b). The glacier is approximately 27 km long with a terminus 3 km wide and 70 m thick (grounded in 40 m deep water) and its drainage area is roughly 174 km^2 (Nuth et al., 2013). Tunabreen has a surging history (1930, 1970 and lately 2002-2005) and the series of advances and retreats left remarkable submarine footprints (Forwick et al., 2010; Flink et al., 2015). After a recent maximum extension in 2004, it retreated until 2016. Size and frequency of calving events have been monitored manually during 4 days in 2012 with a time-lapse camera and studied in **Paper C**. A typical calving event is shown in Fig 4.3c. A main sediment plume, plume 1, has been described in detailed by Schild et al. (2017) and another one, smaller, plume 2, is also present on some of the time-lapse images used in **Paper IV**. Both plumes are shown in Fig 4.3b.

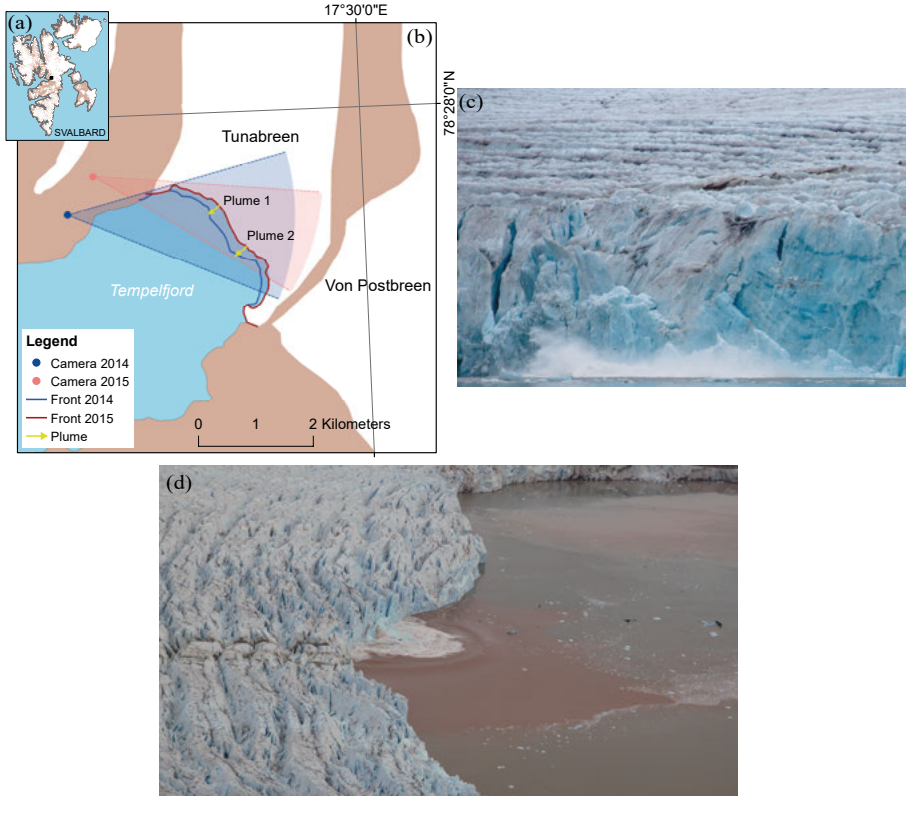

Figure 4.3. **(a)** Map of Svalbard glacier area. **(b)** Map of Tunabreen, Svalbard with terminal position as to August 2014 (in blue) and August 2015 (in red). The subglacial drainage portal is shown by the yellow arrow. **(c)** Picture of a calving event at the front of Tunabreen. **(d)** Picture of the front of Tunabreen taken in August 2014 where the plumes are visible.

5. Data

5.1 Data for Kronebreen

The dataset for Kronebreen includes surface velocity acquired by satellite imagery, frontal positions, surface and bed topographies as well as surface mass balance for the period 2013–2015.

5.1.1 Surface runoff

The SMB and surface runoff are calculated using a coupled surface energy balance-snow model (Van Pelt et al., 2012; Van Pelt and Kohler, 2015) forced with meteorological input of temperature, precipitation, cloud cover and relative humidity. More details are given in **Paper I**.

5.1.2 Surface and bed topographies

The initial surface topography is a combination of a SPOT SPIRIT DEM from 2009, a DRL TanDEM-X IDEM DEM product from 2011, and points measured from a helicopter radar survey in 2014. More details are given in **Paper I**. More details on the surface evolution are given in section 6.1.1.

Bed topography required for the modeling was obtained by a compilation of common-offset radio-echo sounding profiles distributed over Kronebreen conducted in 2009, 2010 and 2014. More details are given in **Paper A** and **Paper I**.

5.1.3 Surface ice velocities and frontal positions

Surface velocity data are derived by feature tracking from TerraSAR-X satellite images from December 2012 to November 2015, using the method of Luckman et al. (2015), with each successive image generally separated by 11 days. The surface horizontal velocity fields contain some anomalies such as magnitudes or directions that differ widely from neighbouring values so we applied a filter. Frontal positions have been manually digitised by Luckman et al. (2015). More details are given in **Paper I**. Observed velocity maps averages over different seasons (see Table 5.1) is shown in Fig. 5.1.

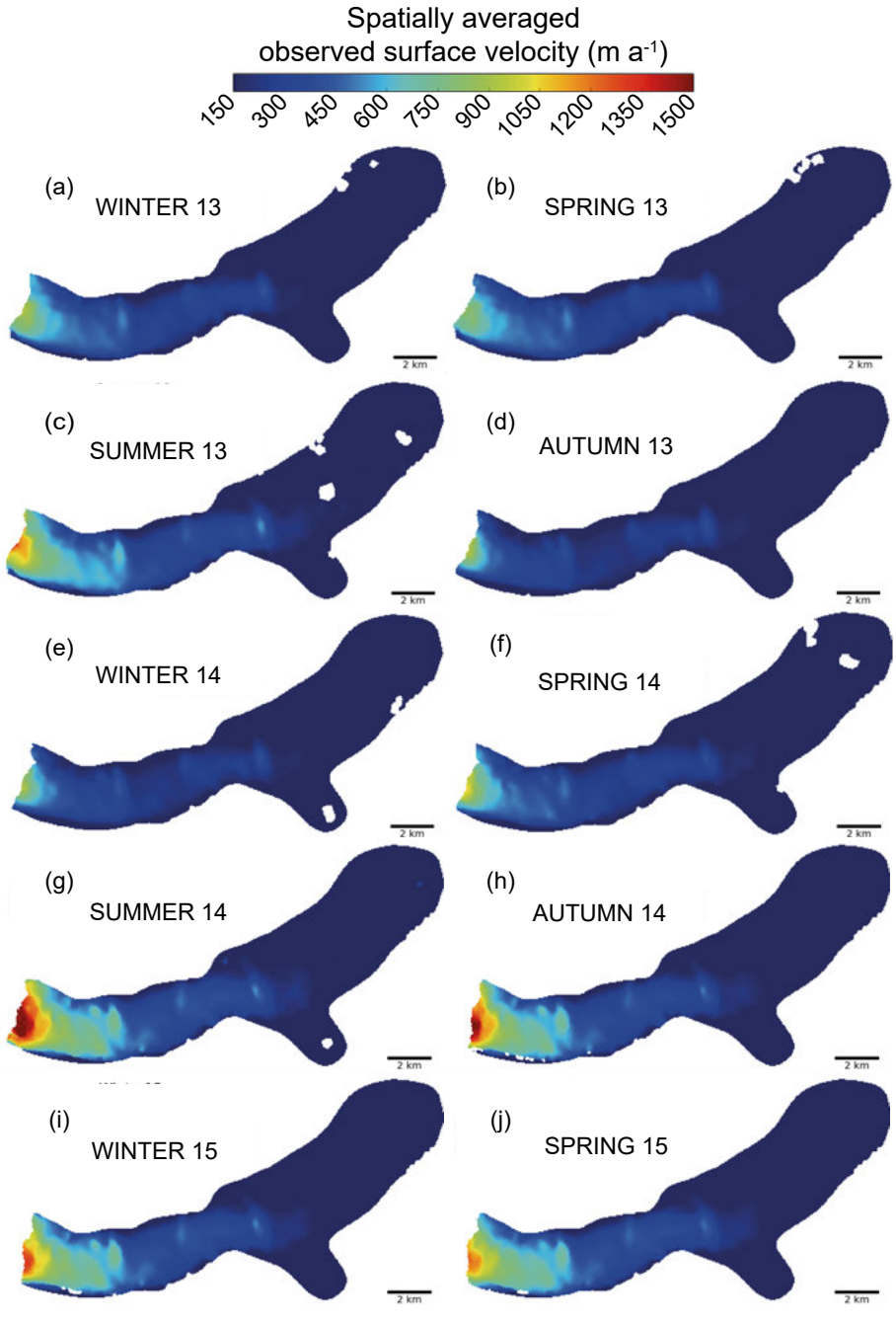

Figure 5.1. Seasonally averaged observed velocity maps ($\mathrm{m\,a^{-1}}$).

5.1.4 Spatio-temporal partitionning

Each year can be divided in four time periods (not necessarily related to actual seasons):

- Winter (January–March) when the front position is advancing,
- Spring (March–June) when the front position is more or less stable,
- Summer (June–October) when water is produced at the surface, velocities are the highest of the year with strong variability and the front is retreating,
- Autumn (October–December) when velocities are decreased but the front continues to retreat.

The start and end dates of each season is shown in Table 5.1.

Table 5.1. *Start and end dates of seasons.*

Season	Start date	End date
Winter 2013	30 December 2012	17 Mars 2013
Spring 2013	17 Mars 2013	2 June 2013
Summer 2013	2 June 2013	16 October 2013
Autumn 2013	16 October 2013	12 January 2014
Winter 2014	12 January 2014	30 Mars 2014
Spring 2014	30 Mars 2014	4 June 2014
Summer 2014	4 June 2014	25 October 2014
Autumn 2014	25 October 2014	19 December 2014
Winter 2015	19 December 2014	13 Mars 2015
Spring 2015	13 Mars 2015	9 June 2015
Summer 2015	9 June 2015	19 October 2015

As shown in **Paper I**, the glacier topography presents three major surface ice falls 1, 2 and 3 (5, 8 and 12 km from the front respectively) as indicated in Fig. 5.2. Given the velocity pattern along the flow line, the glacier has also been divided in different zones as indicated in Fig. 5.2.

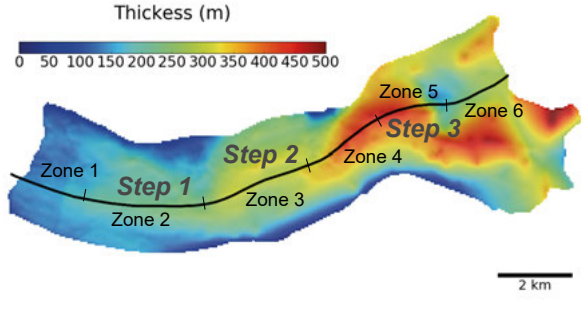

Figure 5.2. Glacier thickness for elevations below 500 m a.s.l. and flow line in black. The different zones and steps are indicated.

Fig. 5.3 shows the surface and bed topographies along the flow line (see Fig. 5.2) for each season (see Table 5.1).

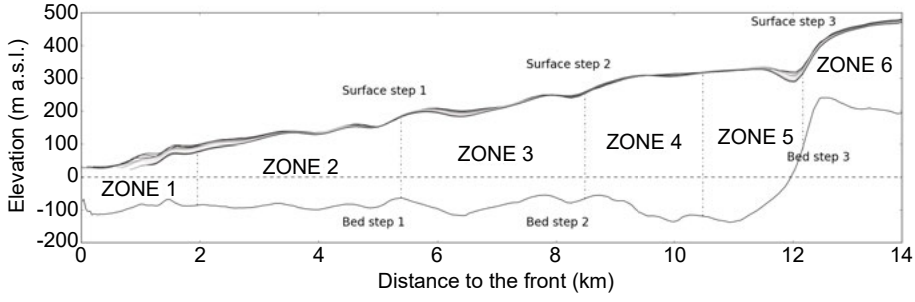

Figure 5.3. Surface and bed elevations along the flow line for each season.

5.2 Data for Tunabreen

Time-lapse cameras have been placed in front of Tunabreen during summer 2014 (Fig. 5.4a) and summer 2015 (Fig. 5.4b) at two different locations . The position of the front is manually digitised from georeferenced satellite images from several Landsat 8 OLI/TIRS C1 Level-1 downloaded from USGS EROS (ten images from July–September 2014 and one image from August 2015). More details are given in **Paper IV**.

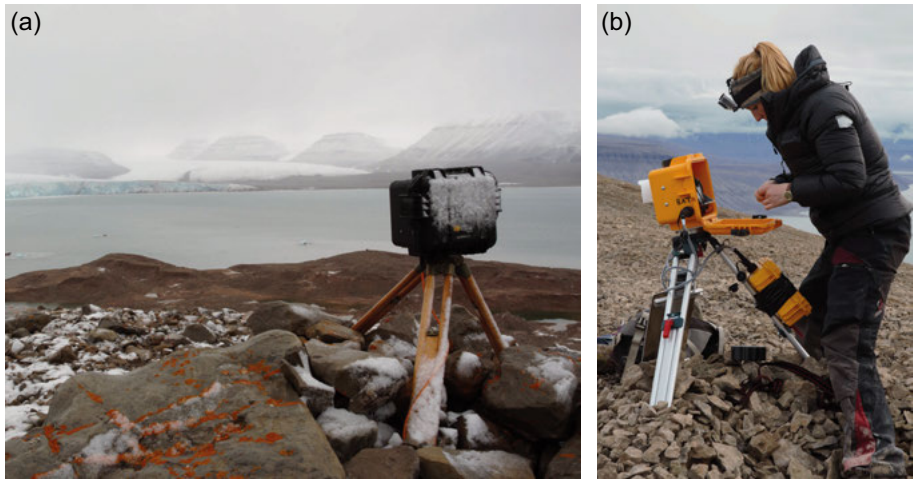

Figure 5.4. Time-lapse cameras placed in front of Tunabreen **(a)** in 2014 (photo taken in September 2014), and **(b)** in 2015 (photo taken in August 2015).

6. Methods

6.1 Ice modelling

Depending on the timescale, the spatial scale and the process of interest, ice can be viewed either as a fluid, ice flow is then modelled as a continuum process, or as a solid, ice flow is then modelled as a discrete process.

6.1.1 Ice is a fluid: full Stokes model

A fluid is a substance that, under continuous applied stress, deforms continuously and the rate of deformation is a function of the stress. Ice can be modelled as a non-Newtonian, incompressible viscous fluid that flows slowly, so that the acceleration terms and inertia are neglected in the momentum equation. The parameter values described below are summarised in Table 6.1.

Table 6.1. *Parameters and physical constants used in the model.*

Parameter	Symbol	Value
Gravitational acceleration	g	$9.81\,\mathrm{m\,s^{-2}}$
Density of ice	ρ_i	$910\,\mathrm{kg\,m^{-3}}$
Density of water	ρ_w	$1025\,\mathrm{kg\,m^{-3}}$
Glen's flow law exponent	n	3
Enhancement factor	E	1
Glen's flow law prefactor	A_*	$\begin{cases} 2.4\times10^{-24}\,\mathrm{Pa^{-3}\,s^{-1}} & \text{if } T \geq -10^\circ C \\ 3.5\times10^{-25}\,\mathrm{Pa^{-3}\,s^{-1}} & \text{if } T < -10^\circ C \end{cases}$
Activation energy	Q	$\begin{cases} 115\,\mathrm{kJ\,mol^{-1}} & \text{if T} \geq -10^\circ C \\ 60\,\mathrm{kJ\,mol^{-1}} & \text{if T} < -10^\circ C \end{cases}$
Universal gas constant	R	$8.314\,\mathrm{J\,mol^{-1}\,K^{-1}}$
Geothermal heat flux	G	$63\,\mathrm{mW\,m^{-2}}$
Thermal conductivity	k	$2.2\,\mathrm{W\,m^{-1}\,K^{-1}}$

Conservation Equations

The Stokes equations can be solved over the ice volume Ω such as

$$\boldsymbol{\nabla}\cdot\boldsymbol{\sigma}+\rho_i\mathbf{g}=\boldsymbol{\nabla}\cdot(\boldsymbol{\tau}-p\mathbf{I})+\rho_i\mathbf{g}=\mathbf{0}. \tag{6.1}$$

We also assume conservation of mass and incompressibility of the ice so that

$$\boldsymbol{\nabla}\cdot\mathbf{u}=tr(\dot{\boldsymbol{\varepsilon}})=0, \tag{6.2}$$

where $\boldsymbol{\sigma} = \boldsymbol{\tau} - p\mathbf{I}$ is the Cauchy stress tensor, $p = -\frac{1}{3}tr(\boldsymbol{\sigma})$ is the isotropic pressure, $\boldsymbol{\tau}$ is the deviatoric stress tensor, $\mathbf{I}$ is the identity matrix, ρ_i is the density of ice, $\mathbf{g} = (0,0,-g)$ is the gravitational acceleration vector, $\dot{\boldsymbol{\varepsilon}}$ is the strain rate and $\mathbf{u} = (u_x, u_y, u_z)$ is the velocity vector. The strain rate tensor is defined as

$$\dot{\boldsymbol{\varepsilon}} = \frac{1}{2}(\boldsymbol{\nabla}\mathbf{u} + \boldsymbol{\nabla}\mathbf{u}^{\mathbf{T}}). \tag{6.3}$$

Rheology of the Ice

Ice rheology is modeled using Glen's flow law, which assumes the ice is flowing as a non-linear isotropic viscous fluid. It relates the deviatoric stress tensor to the strain rate tensor, and thus the velocities, as

$$\boldsymbol{\tau} = 2\eta\dot{\boldsymbol{\varepsilon}}, \tag{6.4}$$

where the effective viscosity, η, is defined as

$$\eta = \frac{1}{2}(EA)^{-\frac{1}{n}}\,\dot{\varepsilon}_e^{\frac{1-n}{n}}, \tag{6.5}$$

where $\dot{\varepsilon}_e^2 = tr(\dot{\boldsymbol{\varepsilon}}^2)/2$ the square of the second invariant of the strain rate, E is the enhancement factor supposed to account for anisotropic effects, $n = 3$ is an empirically determined constant and

$$A = A(T') = A_*\, e^{-\frac{Q}{R}\left[\frac{1}{T'} - \frac{1}{T_*}\right]} \tag{6.6}$$

is a rheological parameter which depends on the ice temperature relative to the pressure-melting point temperature, T', given the pressure, via an Arrhenius law with A_* the pre-factor, Q the activation energy, and R the gas constant (Cuffey and Paterson, 2010).

Given Eq. 6.3, we therefore can rewrite the Stokes equations (Eqs. 6.1 and 6.2) in function of the velocity, $\mathbf{u}$

$$\boldsymbol{\nabla}\cdot\left(\eta(\boldsymbol{\nabla}\mathbf{u} + \nabla\mathbf{u}^{\mathbf{T}}) - p\mathbf{I}\right) + \rho_i\mathbf{g} = \mathbf{0}, \tag{6.7a}$$

$$\boldsymbol{\nabla}\cdot\mathbf{u} = 0. \tag{6.7b}$$

Boundary conditions

Surface boundary condition (ice/atmosphere)

The upper surface, Γ_s, or $z = z_s(x,y)$, in contact with the atmosphere, is defined as a stress-free surface so that a Neumann boundary condition is applied

$$\boldsymbol{\sigma}\cdot\mathbf{n_s} = \mathbf{0}, \tag{6.8}$$

where $\mathbf{n_s}$ is the normal unit vector to the free surface (pointing outward).

The surface elevation of the glacier is able to evolve as a consequence of ice flow forced by a net surface mass balance rate $\dot{a}_c(t) = \dot{a}_c(x,y,t)$ following an advection equation. Basal ice mass loss or gain (melting, refreezing) is neglected. The evolution of the upper surface is given by

$$\frac{\partial z_s}{\partial t} + u_x(z_s)\frac{\partial z_s}{\partial x} + u_y(z_s)\frac{\partial z_s}{\partial y} - u_z(z_s) = \dot{a}_c(t). \tag{6.9}$$

Lower Boundary Condition (ice/bed)
On the lower boundary, Γ_b or $z = z_b(x,y) = b$, in contact with the bed, we assume a no-penetration condition with no basal melting nor accumulation ($\mathbf{u} \cdot \mathbf{n_b} = 0$, with $\mathbf{n_b}$ the normal unit vector to the bed) and a linear friction law (Weertman type sliding law) defined as a Robin boundary condition (linear combination of Dirichlet – velocities – and Neumann – stress – boundary conditions),

$$\mathbf{t_{i,b}} \cdot (\boldsymbol{\sigma} \cdot \mathbf{n_b}) + \beta\ \mathbf{u} \cdot \mathbf{t_{i,b}} = 0, \tag{6.10}$$

where $\mathbf{t_{i,b}}$ $(i = 1,2)$ are the basal tangent unit vectors in two directions aligned with the Cartesian axes and β is a basal friction parameter.

Lateral Boundary Conditions
Lateral boundary conditions can be of different types depending on the physical conditions at the glacier margins. The domain used in this thesis has three different lateral boundary conditions: ice/ocean interface for the front, ice/rock interface where the ice flow is constrained by a nunatak and ice/ice interface where a tributary glacier is confluent with the main body for the spatial treatment of the lateral boundary conditions (see Fig. 6.1).

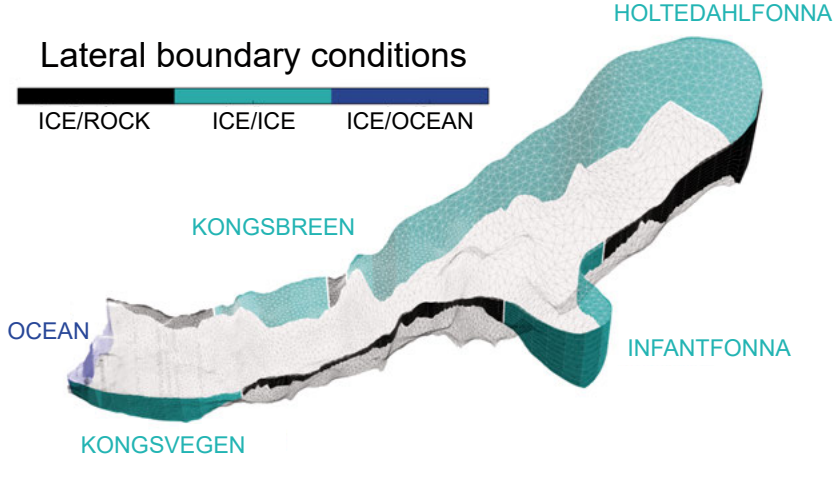

Figure 6.1. Treatment of the boundary conditions for Kronebreen model shown on a 3D-plot. The surface and lower boundary conditions are represented by the mesh.

At the front of the glacier (interface ice/ocean), Γ_w, the normal component of the stress vector is equal to the hydrostatic water pressure exerted by the ocean where ice is below sea level

$$\begin{cases} \mathbf{n_c} \cdot (\boldsymbol{\sigma} \cdot \mathbf{n_c}) = f_w, \\ \mathbf{t_{i,c}} \cdot (\boldsymbol{\sigma} \cdot \mathbf{n_c}) = 0, \end{cases} \tag{6.11}$$

with $f_w = -\max[\rho_w g(l_w - z), 0]$ where ρ_w is the sea water density, l_w the sea level, $\mathbf{n_c}$ the normal unit vector assumed to point out of the ice and $\mathbf{t_{i,c}}$ the unit tangent vectors.

For the lateral of ice/rock interface, Γ_r, a minimum ice thickness is prescribed to 10 m. The boundary condition is the same as at the bedrock (Eq. 6.10) with a friction parameter being equal to the basal friction parameter prior, β_p at $z = z_b$. With $\mathbf{n_r}$ and $\mathbf{t_{i,r}}$ the normal and tangential vectors, we have

$$\begin{aligned} \mathbf{t_{i,r}} \cdot (\boldsymbol{\sigma} \cdot \mathbf{n_r}) + \beta_p \, \mathbf{u} \cdot \mathbf{t_{i,r}} &= 0, \\ \mathbf{u} \cdot \mathbf{n_r} &= 0. \end{aligned} \tag{6.12}$$

The basal friction parameter prior, β_p, is calculated from the shallow ice approximation equations

$$\beta_p = \frac{\rho_i g (z_s - z_b) \, \|\mathbf{grad}(\mathbf{z_s})\|}{\|\mathbf{u^{obs}}(z_s)\|}, \tag{6.13}$$

where $\|\mathbf{grad}(z_s)\| = \left(\left(\frac{\partial z_s}{\partial x} \right)^2 + \left(\frac{\partial z_s}{\partial y} \right)^2 \right)^{\frac{1}{2}}$ is the Euclidean norm of the surface gradient and $\left\|\mathbf{u^{obs}}(z_s)\right\| = \left(u_x^{obs}(z_s)^2 + u_y^{obs}(z_s)^2\right)^{\frac{1}{2}}$ is the Euclidean norm of the observed surface velocity.

For the ice/ice interface, Γ_g, we impose a Dirichlet boundary condition using the observed velocity field.

Ice flow model Elmer/Ice

To solve the above equations for my simulations in the thesis, I use the software package Elmer, an open-source finite element software designed for multiphysical and multiscale problems and developed at the CSC-IT Center for Science based in Espoo, Finland. It is divided into different executables including the solver of Elmer (ElmerSolver) and a mesh manipulable tool (ElmerGrid). ElmerSolver can solve general advection-diffusion problems, steady-state or transient, and supports parallelism. Elmer/Ice is built on Elmer and is dedicated to glaciological problems. More information can be found at `www.elmerice.elmerfem.org`. More details on the finite element method are given in the appendix 10.4.

6.1.2 Ice is a solid: particle model

A solid body deforms under applied stress until an equilibrium is reached and the deformation is a function of the stress. There are two modes of deformation: elastic (reversible) and plastic (irreversible) and the material can fail above a certain threshold.

Governing equations

The main difference of the discrete particle model with the continuum treatment of ice is that each particle, i, of a certain diameter, is bound to another by an elastic massless beam which can break if stretched, sheared or bent beyond elastic threshold limits. The elastic deformation of the beam is

$$\boldsymbol{\sigma} = \mathbf{K}\boldsymbol{\varepsilon} \tag{6.14}$$

where $\boldsymbol{\sigma}$, $\mathbf{K}$ and $\boldsymbol{\varepsilon}$ are the stress, the stiffness and the strain tensors, respectively. The fracture threshold can be based either on a stress or on a strain criterion. A general elliptic criterion (Zhang and Eckert, 2005) reads

$$\frac{\sigma_I^2}{\sigma_0^2} + \frac{\sigma_{II}^2}{\tau_0^2} \geq 1 \tag{6.15}$$

where σ_I is the normal stress determined by the first invariant of the stress tensor, σ_{II} is the shear stress determined by the second invariant and σ_0, τ_0 are material dependent constants. Once the beam is broken, particles are able collide. The collision is inelastic and releases kinetic energy. The equation of motion for the particle i typically is

$$\mathbf{M}\ddot{\mathbf{r}}_i + \mathbf{C}\dot{\mathbf{r}}_i + \sum_j \gamma_{ij}\mathbf{C}'\dot{\mathbf{r}}_{ij} + \sum_j \gamma'_{ij}\mathbf{K}\mathbf{r}_{ij} = F_i \tag{6.16}$$

where $\mathbf{M}$ is the diagonal mass matrix with masses ($\rho_i \times V$ where V is the volume) and moments of inertia ($\rho_i \int r^2 dV$) of the particles, $\mathbf{C}$ is the diagonal damping matrix for drag ($1/2\rho_i v^2 c_D S$ where v is the velocity, S is the cross sectional area of the object to which the drag is applied and c_D is the Reynolds number dependent drag coefficient), and $\mathbf{C}'$ is the damping matrix for inelastic collisions. The position of the particle i is $\mathbf{r}_i$ and the relative position of particles i and j is $\mathbf{r}_{ij}$. The parameters γ_{ij} and γ'_{ij} are zero for particles not in contact/colliding and unity for particles in contact/colliding. The sum of other forces acting on particle i is F_i (gravitation, buoyancy, atmospheric and hydrodynamic/static force, etc).

The viscous cohesion of ice is modelled by 'melting-refreezing probability', which means that the probability for a stretched or bent elastic beam to break is non-zero and that particles, close to each other but without connecting beam, are allowed to connect. The probability is adjusted to satisfy the Glen's flow law (Eq. 6.4). This approach is benchmarked against Elmer/Ice results in Åström et al. (2013).

Discrete particle model HiDEM
The Helsinki Discrete Element Model (HiDEM) is developped at CSC-IT Center for Science and is based on the equations presented above. It is written in Fortran and C++ and can be parallelised. The time step length is limited to $\sim 10^4$ s because of the rapid timescale of the brittle failure events. More details are given in Åström et al. (2013) and **Paper C**.

6.2 Solving the interface problems

6.2.1 Inverse method

In glaciology, there are still some inherently important data that are not, or hardly, observed while others are more straight forward to obtain. Typically, it is possible to collect information on the glacier surface such as surface velocity through satellite or in-situ measurements while basal conditions are far more difficult or even impossible to gather at a larger scale. However, knowing a certain number of observed data, $\mathbf{d^{obs}}$, and assuming a certain behaviour of the system by a forward model operator, G, describing the physics of it, it is possible to retrieve a set of model parameters, $\mathbf{m}$, using an inverse method. Habermann et al. (2012) gave an overview and a comparison between iterative methods used to reconstruct basal properties in glaciology such as the Gauss-Newton, the steepest descent and non-linear conjugate gradient methods.

Let's assume a well-posed forward problem (see appendix 10.3) such as $G(\mathbf{m}) = \mathbf{d^{mod}}$ where $\mathbf{d^{mod}}$ is the data vector computed. We then need to inverse G and determine the model parameters that minimise the misfit between observed and modelled data. The misfit function, $J(\mathbf{m})$, is usually given by a suitably defined norm $\|.\|$ such as $J(\mathbf{m}) = \|\mathbf{d^{obs}} - \mathbf{d^{mod}}\|$.

We choose to use the L^2-norm denoted $\|.\|$. The forward Stokes problem presented above is summarised as

$$\boldsymbol{\nabla} \cdot \big(\eta(\boldsymbol{\nabla}\mathbf{u} + \nabla\mathbf{u}^{\mathbf{T}}) - p\mathbf{I}\big) + \rho_i \mathbf{g} = \mathbf{0} \quad in\ \Omega, \tag{6.17a}$$

$$\boldsymbol{\nabla} \cdot \mathbf{u} = 0 \quad in\ \Omega, \tag{6.17b}$$

$$\big[\eta(\boldsymbol{\nabla}\mathbf{u} + \boldsymbol{\nabla}\mathbf{u}^{\mathbf{T}}) - p\mathbf{I}\big] \cdot \mathbf{n_s} = 0 \quad on\ \Gamma_s, \tag{6.17c}$$

$$\mathbf{t_{i,b}} \cdot \big[\big(\eta(\boldsymbol{\nabla}\mathbf{u} + \boldsymbol{\nabla}\mathbf{u}^{\mathbf{T}}) - p\mathbf{I}\big) \cdot \mathbf{n_b}\big] + \beta\ \mathbf{u} \cdot \mathbf{t_{i,b}} = 0 \quad on\ \Gamma_b, \tag{6.17d}$$

$$\mathbf{u} \cdot \mathbf{n_b} = 0 \quad on\ \Gamma_b, \tag{6.17e}$$

$$\mathbf{n_c} \cdot \big[(\eta(\boldsymbol{\nabla}\mathbf{u} + \boldsymbol{\nabla}\mathbf{u}^{\mathbf{T}}) - p\mathbf{I}) \cdot \mathbf{n_c}\big] - f_w = 0 \quad on\ \Gamma_w, \tag{6.17f}$$

$$\mathbf{t_{i,c}} \cdot \big[(\eta(\boldsymbol{\nabla}\mathbf{u} + \boldsymbol{\nabla}\mathbf{u}^{\mathbf{T}}) - p\mathbf{I}) \cdot \mathbf{n_c}\big] = 0 \quad on\ \Gamma_w, \tag{6.17g}$$

$$\mathbf{t_{i,r}} \cdot \big[(\eta(\boldsymbol{\nabla}\mathbf{u} + \boldsymbol{\nabla}\mathbf{u}^{\mathbf{T}}) - p\mathbf{I}) \cdot \mathbf{n_r}\big] + \beta_p\ \mathbf{u} \cdot \mathbf{t_{i,r}} = 0 \quad on\ \Gamma_r, \tag{6.17h}$$

$$\mathbf{u} \cdot \mathbf{n_r} = 0 \quad on\ \Gamma_r, \tag{6.17i}$$

$$e_z \cdot \big[(\eta(\boldsymbol{\nabla}\mathbf{u} + \boldsymbol{\nabla}\mathbf{u}^{\mathbf{T}}) \cdot \mathbf{n}\big] - \beta_p \mathbf{u^{obs}} \cdot \mathbf{n} = \mathbf{0} \quad on\ \Gamma_g, \tag{6.17j}$$

$$\mathbf{n} \cdot \big[(\eta(\boldsymbol{\nabla}\mathbf{u} + \boldsymbol{\nabla}\mathbf{u}^{\mathbf{T}}) - p\mathbf{I}) \cdot \mathbf{n}\big] + \rho_i g(z - z_s) = 0 \quad on\ \Gamma_g. \tag{6.17k}$$

Solving these equations leads to an expression of the modelled velocity, $\mathbf{u}^{\mathbf{mod}}$, in function of the friction coefficient, β, so that $\mathbf{G_u}(\beta) = \mathbf{0}$ defined in the whole glacier, Ω, with $\mathbf{G_u}(\beta)$ composed of Eq. 6.17a and Eq. 6.17b. The model parameter that we would like to tune is the friction parameter, β, as defined in Eq. 6.10 and we would like to minimize the mismatch between the observed horizontal surface velocity, $\mathbf{u}^{\mathbf{obs}}$, and the horizontal modelled surface velocity, $\mathbf{u}^{\mathbf{mod}}$. We then define the misfit function as the following non-linear least-squares minimisation problem

$$J_0(\beta) = \frac{1}{2}\int_{\Gamma_s} |\mathbf{u}^{\mathbf{obs}} - \mathbf{u}^{\mathbf{mod}}(\beta)|^2 \, d\Gamma. \tag{6.18}$$

This non-linear problem (because of the rheology of ice) has to be solved using iterative inverse methods to minimise the misfit function. Starting with an initial estimate, β^p, of the friction coefficient (Eq. 6.13), each iteration k determines a search direction δ_k and performs an inexact line search to find a scalar $\alpha_k > 0$ so that $J(\beta_k + \alpha_k \delta_k)$ is approximately minimised. The next value of the friction parameter β_{k+1} is then updated to $\beta_{k+1} = \beta_k + \alpha_k \delta_k$.

However, G is usually non-linear and the inverse problem is non-unique (multiple minima of varying heights) and unstable (small changes in $\mathbf{d}^{\mathbf{mod}}$ can lead to large changes in $\mathbf{m}$), which leads to an ill-posed problem. To restore well-posedness, it is necessary to apply a regularisation technique that imposes additional constraints and stabilize the inversion (Calvetti et al., 2000). It also limits over- and under-fitting (due to a premature termination of a too slow iterative method). Here we use a Tikhonov regularisation penalising the first spatial derivatives of β

$$J_{reg}(\beta) = \frac{1}{2}\int_{\Gamma_b} \left(\frac{\partial \beta}{\partial x}\right)^2 + \left(\frac{\partial \beta}{\partial y}\right)^2 + \left(\frac{\partial \beta}{\partial z}\right)^2 \, d\Gamma. \tag{6.19}$$

The cost function to minimise becomes

$$J(\beta) = J_0 + \lambda J_{reg}, \tag{6.20}$$

where $\lambda > 0$ is determined by the L-curve method (Hansen, 2001). The role of this coefficient is to find a compromise between smoothing and fitting of the solution.

Using the method of Lagrange multipliers (see appendix 10.2), β is minimizing J if and only if it exists $\mathbf{v}$ and q so that

$$\frac{\partial J}{\partial \beta}(\beta) = \int_{\Gamma_b} \mathbf{ut_{i,b}} : \mathbf{vt_{i,b}} \, d\Gamma_b. \tag{6.21}$$

More details on the minimisation are given in appendix 10.5.

In a nutshell, we use a complete adjoint model and the Tikhonov regularisation with a conjugate gradient method for the minimisation (Gillet-Chaulet et al., 2012; Morlighem et al., 2010; Goldberg and Sergienko, 2011). This method is directly implemented in Elmer/Ice (Gagliardini et al., 2013).

6.2.2 Subglacial hydrology model

In **Paper II**, we use the two-dimensional Glacier Drainage System model – GlaDS (Werder et al., 2013), that couples distributed (represented as a continuous water sheet of variable thickness, h) and channelised (represented through Röthlisberger channels) subglacial water flow.

6.2.3 Schoof-Gagliardini friction law

The Schoof-Gagliardini friction law has been described in section 3.1.4 and in Eq. 3.10. In **Paper II**, the effective pressure, N, is inferred in space and time from the subglacial hydrology model described in section 6.2.2, C is a scaled map of the logarithm of the roughness described in **Paper A** and for different configurations of m and q_s, the sliding parameter without cavitation, A_s, is calculated with the winter velocity, $\mathbf{u_{b,w}}$, basal shear stress, $\tau_{\mathbf{b,w}}$, and effective pressure, N_w, by solving

$$A_s^{q_s} - \frac{\mathbf{u_{b,w}}}{{\tau_{\mathbf{b,w}}}^m} A_s^{q_s - 1} + \alpha \left(\frac{\mathbf{u_{b,w}}}{C^m N_w^m} \right)^{q_s} = 0. \tag{6.22}$$

More details are given in **Paper II**.

6.2.4 Subglacial discharge, plume and undercutting model

To model the amount of undercutting created by subglacial discharge, four models have been used in **Paper III**. The flow path of the melt-water towards the glacier front is determined from the hydraulic potential surface of integrated daily surface runoff assumed to be directly transferred down to the glacier bed. The subglacial discharge at the front is determined by the amount and location of the flow path at the terminus. A plume model, solving the Navier-Stokes equations on a fully unstructured three-dimensional finite element mesh and using Kronebreen terminus geometry and oceanic properties, estimates the melt rates associated with the subglacial discharge. Finally, an undercutting model projects the melt rates to the front of Kronebreen. More details are given in **Paper III**.

6.3 Automatic and manual calving detection

In order to gain more understanding on calving behaviour, quantitative and qualitative analysis of observations is necessary. Acquiring time-lapse images of the front is a way to monitor the frequency and size of calving events. The time-lapse images are analysed with an automatic calving detection method and compared to a manual method for validation. The automatic method, detailed in **Paper IV**, is based on four steps:

1. Feature-based image registration,
2. Segmentation using region-based active contour,
3. Region-based change detection using image texture,
4. Change mask recognition using the α-shape method,
5. Size calculation.

6.4 Simulations

6.4.1 Inversion for basal friction and elevation change

These simulations are done in **Paper I** and used in **Paper II** and **Paper III**. The aim is to inverse each observed velocity map (see section 5.1.3) to retrieve the basal friction coefficient described in Eq. 6.10 given initial topographies and using Eq. 6.17a–k. After each iteration, the surface evolution is relaxed using Eq. 6.9.

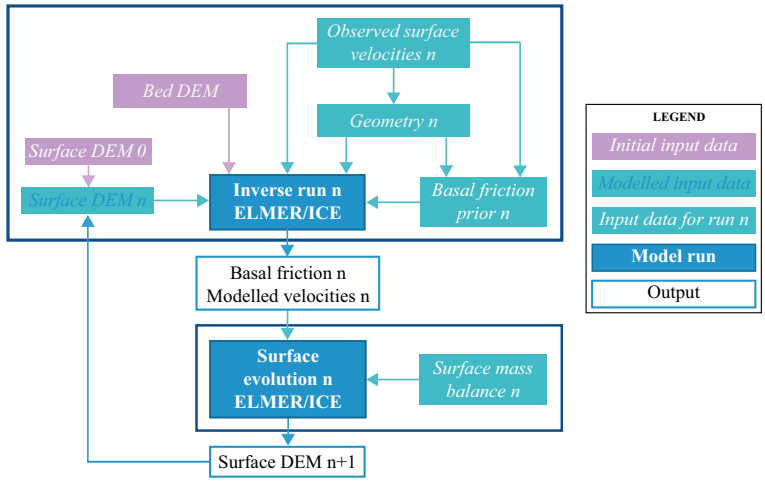

Figure 6.2. Different steps and input data for each inversion.

6.4.2 Offline coupling

The offline coupling approach, detailed in **Paper III**, is divided into three parts using six models (see Fig. 6.3):

- computing sliding and geometry (from the inversion method described in section 6.2.1) with Elmer/Ice, described in section 6.1.1,
- estimating undercutting with an energy balance model for the surface runoff, a subglacial hydrology model, a plume model and an undercutting model, described in section 6.2.4,
- computing calving with HiDEM, described in section 6.1.2.

The geometry is updated from observations at each time steps and is not coupled to the last iteration. That is why it is called offline coupling.

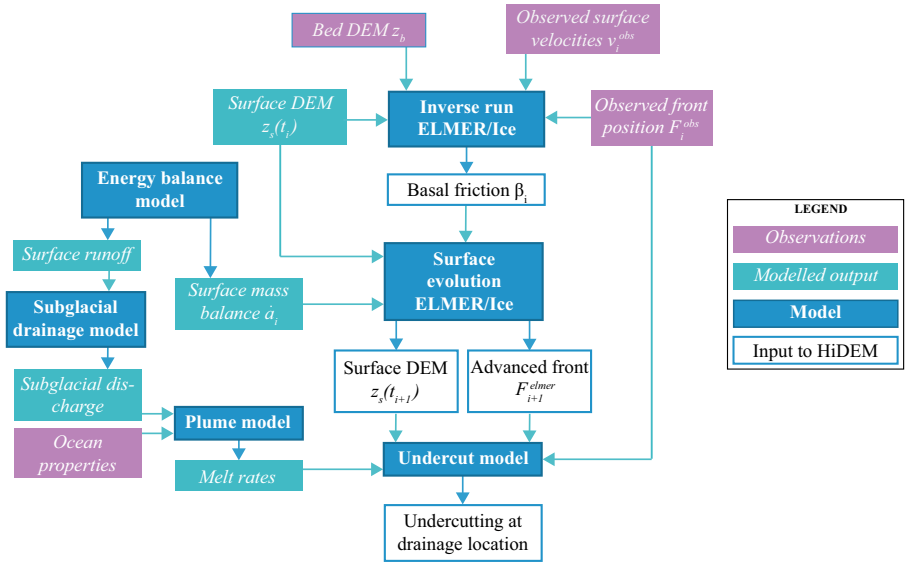

Figure 6.3. Model scheme presenting the calculation of the sliding and geometry (Elmer/Ice) as well as the undercutting at the subglacial discharge as input to the glacier calving from the HiDEM. Reproduced from **Paper III**.

6.4.3 Coupling Elmer/Ice and HiDEM

The next step is to fully couple the models using a sliding law instead of inversion results. In **Paper B**, we use an infrastructure ready workflow management system called UNICORE (Streit et al., 2010) which supports different kind of HPC resources to implement the coupling. The steps, are as follows:

Step 0 – Shared Preprocessing to facilitate the involved applications with required input data sets and prepare output directories,

Step 1 – Generation of the mesh for Elmer/Ice based on the general contour and the modelled front position,

Step 2 – Transient advance with Elmer/Ice using a sliding law and the surface evolution equation described in Eq. 6.9,

Step 3 – Translation from Elmer/ICE domain to HiDEM domain,

Step 4 – Calving with HiDEM to retrieve a new front position,

Step 5 – Translation from HiDEM domain to Elmer/Ice domain.

7. Summary of papers

Paper I

Vallot, D., Pettersson, R., Luckman, A., Benn, D. I., Zwinger, T., Van Pelt, W. J. J., Kohler, J., Schäfer, M., Claremar, B., and Hulton, N. R. J.: Basal dynamics of Kronebreen, a fast-flowing tidewater glacier in Svalbard: non-local spatio-temporal response to water input, *Journal of Glaciology*, doi: 10.1017/jog.2017.69, 2017.

This paper uses a full-Stokes model (Elmer/Ice) to invert three years, from 2013 to 2015, of high temporal resolution surface velocity data (derived from TerraSAR-X products) to evaluate the spatio-temporal variability of the basal properties of Kronebreen, a fast-flowing tidewater glacier in northwestern Svalbard, which is subjected to seasonal surface melting that may largely vary interannually in space and time. The results suggest that: (i) the basal properties of Kronebreen are strongly influenced by the amount and pattern of surface meltwater input during the melt season, (ii) that a single (spatially and temporally static) basal friction field is inadequate to simulate the short timescale (seasonal to interannual) behavior of the glacier, (iii) that in the absence of substantial meltwater inputs that result in the creation of an efficient (presumably primarily channelized) basal drainage system, glacier geometry (in this case ongoing calving and changes in calving front geometry) may influence basal properties, (iv) that large portions of the driving stress may be supported by small portions of the bed and/or lateral boundaries, (v) that Weertman-style laws are likely insufficient to properly simulate basal shear stress over a range of timescales, and (vi) that an effective pressure based basal sliding law and/or modeling of discrete basal hydrologic features may be necessary to simulate short timescale variability in basal conditions and ice flow.

Contribution: DV designed of the study, the simulations, the analysis and wrote the paper. RP contributed to the design of the study. TZ and MS contributed to the Elmer/Ice set-up. DB, NH and AL provided the observed surface velocity maps. WVP developed the coupled energy balance - snow modelling approach. BC provided the surface temperatures. JK provided the interpolated bed map. All authors contributed to the writing of the paper and the analysis.

Paper II

Vallot, D., Gagliardini, O., Pettersson, Benn, D. I., R., Luckman, A., Van Pelt, W. J. J., Lindbäck, K.: Modelled subglacial hydrology and basal friction at Kronebreen, a tidewater glacier in Svalbard, *Manuscript*.

This paper presents a simulation of the subglacial hydrology system under Kronebreen, a tidewater glacier in Svalbard during the melt seasons 2013 and 2014. The two-dimensional Glacier Drainage System model (GlaDS) couples an inefficient drainage system composed of a continuous water sheet of variable thickness, to an efficient drainage system composed of a channel network. Input variables include basal ice velocity and stress that are retrieved by inverting observed surface velocity. Water input to the subglacial system is provided by a coupled energy balance-snow modelling approach and the estimated surface runoff is routed through the glacier surface to spatially distributed moulins. A steady-state is reached, before the melting season, using winter averaged variables, and is used as an initial condition to the melting season simulation. Results show that the spatio-temporal changes in water input play an important role in the subglacial drainage system organisation. Between years, the transition from inefficient to efficient system presents different characteristics and influences the ice dynamics during and after the melting season. Furthermore, the modelled effective pressure is used as a variable to the Schoof-Gagliardini friction law, a non-linear friction law between basal shear stress and velocity, which is also dependent on a post-peak exponent (enabling the basal shear stress to decrease with the velocity after a certain peak), a sliding exponent, basal roughness and a sliding parameter fixed in time. Relative errors between this calculated basal shear stress and the modelled basal shear stress show how good the model performs spatially during the melting season. Results show that: (i) the post-peak exponent need to be > 1 in order to give low errors, (ii) relative errors are low in most of the domain below 500 m a.s.l. surface elevation if the sliding exponent varies in space and the sliding parameter is calibrated with the former winter variables, (iii) errors are very large if the sliding parameter is calibrated on the winter from the year before with the spatially fixed sliding exponent from the year before, and (iv) errors are low in most of the domain below 500 m a.s.l. surface elevation but high in some regions if the sliding parameter is calibrated on the winter from the year before.

Contribution: DV designed the study, ran all the simulations and wrote the manuscript. OG developed the GlaDS model on Elmer/Ice. RP developed the surface routing model on Matlab. OG and RP provided help to design the study. WVP developed the coupled energy balance-snow modelling approach. DB and AL provided the observed surface velocity maps and KL the roughness map.

Paper III

Vallot, D., Åström, J., Zwinger, T., Pettersson, R., Everett, A., Benn, D. I., Luckman, A., Van Pelt, W. J. J. Nick, F. & J. Kohler: Effects of undercutting and sliding on calving: a global approach applied to Kronebreen, Svalbard, *The Cryosphere Discussion*, doi: 10.5194/tc-2017-166, 2017.

This paper presents a new perspective on the role of ice dynamics and ocean interaction in glacier calving process applied to Kronebreen, a tidewater glacier in Svalbard. A new coupled modelling approach has been developed including ice flow modelling, undercutting estimation by a combination of glacier energy balance and plume modelling as well as calving by a discrete particle model. Here we combine observations (surface velocity, frontal positions, atmospheric and oceanographic characteristics) and modelling in an offline coupling approach to assess the contribution of different processes to calving. The ice flow is modelled by Elmer/Ice as a continuous process while calving and fracturing is modelled by the Helsinki Discrete Element Model (HiDEM) as a discrete process. The sliding velocity is modelled by inverting high temporal resolution surface velocity data (derived from satellite imagery) during the melting season of 2013. The amount of melt water discharged at the front is calculated with a simple hydrology model and a plume model estimates the melt rates associated given oceanic and glaciologic characteristics. From these melt rates, we estimated the undercutting between each time step. By comparing modelling and observations for different time steps and cases, we show that (i) modelling undercutting is necessary to simulate the same order of magnitude of observed retreat in the vicinity of high discharge locations, and (ii) calving rates are also influenced by basal friction, through its effects on near-terminus strain rates and ice velocity.

Contribution: DV contributed to the design of the study, the offline coupling, the development of the undercut model, the Elmer/Ice and HiDEM set-ups and the writing of the manuscript. DB edited the manuscript. All other authors provided comments to the manuscript. JÅ developed the HiDEM model and used Kronebreen as test and development case. AE developed the plume model. TZ contributed to the Elmer/Ice set-up. RP calculated the water discharge. DB and AL provided the observed surface velocity maps. WVP developed the coupled energy balance - snow modelling approach. JK provided the interpolated bed map.

Paper IV

Vallot, D., Adinugroho, S., Strand, R., How, P., Pettersson, R., Benn, D. I. & Hulton, N. R. J.: Automatic detection of calving events from time-lapse imagery at Tunabreen, Svalbard, *Manuscript*.

This paper presents a novel method to quantify the sizes and frequency of calving events from time-lapse camera imageries. The calving front of a tide-water glacier experiences different episodes of iceberg deliveries that can be captured by a time-lapse camera situated in front of the glacier. An automatic way of detecting calving events is presented here and follows different steps: (i) feature-based image registration, (ii) segmentation using region-based active contour, (iii) region-based change detection from one image to another using image texture, (iv) change mask recognition using the α-shape method, and (v) size calculation given the position of the camera and the position of the front. We use two time-series from two cameras placed at two different locations to monitor the front of Tunabreen, Svalbard, during the melt seasons of 2014 and 2015 to test the method and we compare the results with a manual (visual) detection method. In general, the automatic method performs well with normal weather conditions but poorly when the fog is too dense or the image is too illuminated. From both years, it appears that the largest calving events are triggered where the most extended plume is rising. Large events are also triggered at another plume location and minor events are simultaneously happening at the most extended plume location. In general where a large event is triggered and if another smaller event is triggered, it occurs adjacent to the large one.

Contribution: DV and RP have designed and constructed the time-lapse cameras for 2014. PH and NH have designed the time-lapse camera for 2015. DV, RP, NH, DB and PH have co-ordinated the camera deployment and collected the memory cards. SA, RS and DV have developed the automatic detection and DV the manual detection. DV manually detected calving events from the 2015 record. DV has written the main part of the article and all authors have contributed.

8. Results and discussion

8.1 Spatio-temporal variations and influence of surface water input on basal motion

By using high spatio-temporal resolution observations during three consecutive years (2013–2015) for a fast-flowing tidewater glacier in Svalbard, Kronebreen, **Paper I** aimed at solving the sliding parameter by inverting the surface velocities over three years (2013–2015) using the ice flow model Elmer/Ice. The observed dynamical patterns are strikingly different between the years 2013 and 2014 and particularly during and after the melt season (see Fig. 4–5 in **Paper I** and Fig. 1 in **Paper II**). The results show high spatio-temporal resolution of the basal friction under the glacier (see Fig. 9 in **Paper I**) and non-linear response of the subglacial hydrology system to melt water input (see Fig. 4 in **Paper II**).

Summer 2013 exhibits three peaks of velocity coinciding with peaks of surface runoff. The first peak, in the end of June, was the highest, suggesting that the subglacial hydrology system was not able to accommodate the incoming water, suddenly increasing the water pressure (as shown in **Paper II**), decoupling the bed and increasing basal sliding (as shown in **Paper I**). Thereafter a series of high runoff peaks leads to higher water pressures in the distributed drainage system and the formation of the first channels. The following runoff peaks are accompanied with a decrease of velocity and water pressure and at that time most the melt water is evacuated through the channel network. This suggest an adaptation of the subglacial hydrology system from inefficient to efficient described in **Paper II**. Surface water input decreases drastically in mid-August, leading to a closing up of the drainage system immediately followed by a second peak. Water pressure increases and the drainage system has to accommodate the water again. Basal sliding increases as a consequence but the channelised system is certainly still well developed to be reactivated and evacuate most of input melt water. After the melt-season, the glacier velocity decreases rapidly and higher sliding is concentrated close to the front.

In summer 2014, surface melt is less extended in space, in time and in quantity than in 2013. The first surface melt occurs in the end of June and is increasing more gradually than in 2013, so that the water pressure builds up slower, postponing the opening of drainage channels and constricting the water in the less efficient distributed system. A few days separate the first runoff peak from the second one and the efficient drainage system didn't develop enough to accommodate this new input of water so that water pressure increase

again as well as basal sliding. Channels start to form but the input of water is not sustained long enough to maintain high flux in the channels so that the drainage system is constantly trying to adapt. Also, by the end of the season, the velocity remains high compared to 2013, despite local fluctuations, particularly in the first kilometers from the front and downflow of steps 1 and 2, until spring 2015. The basal sliding is higher than in 2013 and highest values are found over the entire front region. Moreover, during that time, the ice front was retreating faster suggesting a relationship between ice dynamics and calving.

In 2013, the region where the main sediment plume has been observed, and a channel is probably discharging water, had higher friction than the other parts of the front. This was not the case in 2014. Moreover, while the frontal discharge in 2013 is concentrated at two main subglacial portals most of the season, it is more spread out in 2014. This suggest that water was not as well evacuated in 2014 as in 2013.

Despite a dominant temporal variability during summer 2013, before and after the summer, in 2013, there is more spatial than temporal variation. The magnitude of the variability is different in each zone but remains in the same order within a zone. However, in 2014, spatial variation is higher than temporal variation during the summer. This suggests that high temporal variations or spatial variations in time are conditioned by changes in subglacial hydrology, surface gradient or in ice thickness while spatial variations constant in time are connected to inherent properties of the glacier (basal topography, basal roughness, bed gradient). The analysis of these two years is in line with the conclusions of Sole et al. (2013) and Tedstone et al. (2015) that autumn-winter ice motion was correlated to summer runoff. However, longer time-series would be needed to draw a general conclusion on Kronebreen.

8.2 Towards a sliding law

In **Paper I**, the modelled basal shear stress, τ_b, and basal velocity, u_b are compared in space and time in order to determine a potential sliding law candidate of the form discussed in the background (section 3.1.4). When an optimized basal friction coefficient, spatially variable but temporally fixed, is used in forward modelling, the results show non-negligible discrepancy between the observed and modelled velocities and particularly during the melting season (see Fig. 12 in **Paper I**). This suggests that both spatial and temporal changes in basal conditions need to be taken into account when modelling sliding at the base of such glaciers.

The basal shear stress varies in an inverse fashion with the basal velocity (see Fig. 10 in **Paper I**) and particularly in zones 5 and 6 (far from the front), where the velocity is $< 300\,\mathrm{m\,a^{-1}}$ for a basal shear stress varying from 20 to 200 kPa and the ratio between basal shear stress and driving stress is > 0.6.

Close to the front, in zone 1, u_b is spreading from 600 to 1600 m a^{-1} and τ_b is consistently < 20 kPa and the ratio with the driving stress is ~ 0.3. The situation is similar in zone 2 with u_b spreading from 300 to 1000 m a^{-1} and τ_b between 20 and 30 kPa. In these regions, the driving stress must be supported non-locally by other regions.

The spatio-temporal variability and the non-local influence of certain regions explain why a non-linear Weertman sliding law is not adequate as shown in the results of **Paper I**. Furthermore, the inverse relationship between τ_b and u_b, in most regions, can only be modelled with a negative value of the stress exponent, which is usually not the case as described in background (section 3.1.5). Whether the Weertman parameters are fixed or variable in space and time, the law fails to describe the sliding process. Instead, the sliding law should take into account the variable characteristics of the glacier in space and time such as bed properties, surface gradient change, thickness change, subglacial hydrology.

In **Paper II**, the effective pressure modelled by the subglacial hydrology model GlaDS has been used to constrain the Schoof-Gagliardini sliding law presented in Eq. 3.10 in order to take into account the temporal variations of the subglacial system during the melting season. The spatial variations are incorporated with the spectral roughness of the bed through the temporally fixed parameter C in Eq. 3.10. This choice is discutable as the spatial scale, over which the spectral roughness is calculated, is much higher than the cavity scale and it should be investigated further. There are three other parameters, which need to be assessed, the temporally fixed sliding parameter, A_s, the post-peak exponent, q_s and the sliding exponent, m. The post-peak exponent, q_s, is particularly important as it allows the friction law to be multi-valued so that after at a certain value of the basal velocity, the basal shear stress reaches a peak and decreases afterwards. Gagliardini et al. (2007) showed that for larger values of q_s the post-peak basal shear stress decreases faster and the peak is much lower than predicted by the Iken's bound. The sliding parameter, A_s, is calculated from averaged winter variables and is maintained constant in time. If the sliding exponent, m, is fixed in space and in time, and q_s is allowed to vary in space, the relative error between basal shear stress inverted from observed velocity and basal shear stress calculated from Eq. eq:cavit:fric is spatially dependent on the choice of m and q_s is generally equal to 2 (see Fig. 8 in **Paper II**). The fact that $q_s > 1$ is not surprising with regard to the results of **Paper I** showing a decrease of the basal shear stress with the basal velocity. If the sliding exponent, m, is fixed not fixed in space and q_s is, errors using the temporal median of best m at each point, m_{med}, errors are low in most of the domain apart from some cluster of points and higher than 500 m a.s.l. surface elevation (see Fig. 9 in **Paper II**). However, the spatial distribution of m_{med} is different between years. If A_s and m_{med} optimised from 2013 are used in 2014, errors are larger than 100 % in some clusters but still reasonable in most of the domain below 500 m a.s.l. surface elevation (see Fig. 10 in **Paper II**).

However, if A_s from 2013 is used but m is equal to the temporal median of best m at each point, m_{med}, errors are low in most of the domain below 500 m a.s.l. surface elevation with the same spatial pattern as if A_s was optimised for 2014 (see Fig. 11 in **Paper II**). This suggests that the sliding law is less sensitive to the choice of A_s than the choice of m, which is dependent on the melting season. The next step is therefore to quantify how the sliding parameter is influenced by other variables during the melting season and couple the ice flow model to the subglacial hydrology model.

This study is done on a tidewater glacier experiencing high seasonal variations in melt water input and is applied on a relatively short time-scale. Other type of ice masses, such as ice streams in Antarctica, may have a complete different different behaviour.

8.3 Influence of subglacial hydrology on calving

The subglacial hydrology do not only have an influence on sliding but is also contributing to calving at the front of the glacier. In **Paper III**, the outputs from the ice flow modelling (sliding and ice thickness), modelled in **Paper I** have been used as boundary conditions for the discrete particle model HiDEM. As presented in the background (section 3.2.2), the calving process is more of a discrete than a continuous type. The interaction with the ocean is simulated using a subglacial hydrology model based on hydraulic potential, a plume model and an undercutting model. We tested different configurations of geometry, sliding and undercutting and compare the results with observations (see Fig. 9 in **Paper III**). The two sediment plumes detected at the surface of the ocean water close to the glacier front are simulated to apply undercutting. At high subglacial discharge, maximum melt on the calving front is concentrated just below the ocean water surface while at low discharge, it is more spread to the lower part of the front. Simulations with and without undercutting, associated with geometry, subglacial drainage, and ocean properties, show that, during the melting season, undercutting plays a role in the calving process at these locations.

Results should, however, be taken with care since they are limited by the availability of observations and the number of cases studied. The time-span between two observations is 11 days or larger so that ice is advancing and the amount of undercutting is accumulating during this time period. Calving modelled by the HiDEM may therefore be biased towards larger events. More systematic analysis on shorter time-spans should be performed in order to validate the findings.

In **Paper IV**, the effect of the plume on calving is also indirectly assessed at another tidewater glacier in Svalbard, Tunabreen. Time-lapse cameras have been placed in front of the glacier during the melt seasons of 2014 and 2015 and the images have been analysed with an automatic detection method for

calving events. The results have been compared with detection of calving events using a manual detection method on the same images. Results show that calving is more intense in front sections where a plume has been observed than other sections. There is one main plume, plume 1, constantly bringing up subglacial melt water on the pictures, and a secondary plume, plume 2, intermittently visible and less extended. Furthermore, when a large calving event happen close to plume 2 location and if a smaller event is detected at the same time (within the time-lapse between two consecutive images), this smaller event is most often detected close to plume 1 location. This could be due to subglacial drainage activity happening simultaneously at the two discharge points. In addition, when several calving events happen a the same time, it is more likely that they will be close to each others and particularly close to the plume zone. Another important result is the fact that the the relative abundance of sizes estimated by the automatic detection method is following a power law of the same form as discussed in **Paper C** and characteristic of a SOC system as described in the background (section 3.2.3).

However, there are some limitations associated with the detection method that prevent a full analysis of the data. The time between two consecutive images has an impact on the size of the calving events. A cascade of several smaller events close to each others within the lapse of time between two imagesmay be detected as one single large event. Also if a piece of ice, attached to the front is about to be detached and moves between two images, the method will detect a change and label it as a calving. Moreover, weather conditions have an important impact on the method. Cases of dense fog or high illumination have to be removed because the method fails to detect changes properly. Further work on fog removal or fog detection need therefore to be investigated.

9. Conclusion and future work

"On ne fait jamais attention à ce qui a été fait; on ne voit que ce qui reste à faire." – Marie Skłodowska Curie

9.1 Summary of the thesis

In this thesis, the complex behaviour of an Arctic tidewater glacier, Kronebreen, has been analysed in the light of calving and sliding processes. Basal sliding coefficients have been inferred by inverting observed surface velocities acquired at a high spatial and temporal resolution ($\sim$ 11 days between images). The spatio-temporal complex behaviour of this sliding parameter appears to be associated with subglacial hydrology development, which is developing very differently from one year to another, mainly due to melt water input differences, but also with calving processes. Furthermore, applying a simple fixed parameterisation in space and time or even a non-linear Weertman-type sliding law at the lower boundary are shown not to be good choices in forward modelling. Basal sliding for this glacier appeared not only to be linked to local processes but also by processes acting on larger distance and longer time period such as ice-thickness changes, subglacial hydrology organisation during the melting season or changes in calving front geometry. A sliding law of Schoof-Gagliardini-type, which takes into account the effective pressure variations in space and time during the melting season is therefore a better choice for glaciers such as Kronebreen but the choice of parameters is not straightforward and required further studies.

The development of the subglacial hydrology system and its organisation is not only sensitive to sliding but also to calving as subglacial water, discharged at the front, mixes with the ocean water. In this thesis, calving front observations have been compared to results from an offline coupling between different models, which simulates the behaviour of ice dynamics, the surface and subglacial hydrology, the rising plume of subglacial melt water into the fjord, the melted undercutting of the front and the calving process. The ice dynamics are modelled by a continuous ice flow model, Elmer/Ice, while the calving and fracturing processes are modelled by a discrete particle model, HiDEM. The rising plume of melt water from subglacial discharge at the front melts the frontal ice and results show the importance of modelling this undercutting to simulate calving front position at the discharge location. Frontal geometry and basal siding are also shown to have an impact on the calving rate.

The size and frequency of calving events have been analysed at another Arctic tidewater glacier, Tunabreen. Time-lapse cameras have been placed in front of the terminus for two consecutive years. An automatic detection of calving events method has been developed and compared to a manual method to assess long time series. Results show that the detected calving events are more likely occurring in the region where the subglacial water plume is rising. However, weather conditions should be assessed in a more accurate way for the method to perform better. Also, further studies on the relationship between calving events and environmental controls can help to constrain processes interacting with calving.

9.2 Future work: towards a full coupling

The papers included in this thesis are describing models characterising different processes in interaction with each others. In **Paper III**, the series of models are only used in an offline coupling but it is a first attempt to take into account the interactions between sliding and calving. At the front, the ice is in contact with the ocean and the water discharged from subglacial drainage systems, together with the ocean processes, may be at the origin of the formation of a rising plume that is able to melt the front of the glacier, creating an undercutting and influencing calving. At the bed, the ice is in contact with bedrock or sediments and, because of the presence of water, is able to slide, which changes the dynamics of the glacier. These processes are complex, non linear and linked to one another. A full coupling would need to solve the sliding law problem in connection with the subglacial hydrology in line with the results of **Paper II**. Ice dynamics and subglacial drainage can be coupled and modelled by an ice flow model such as Elmer/Ice. The melt water produced at the surface and the surface mass balance can be modelled by a surface energy model. The water discharged at the front can then be used as input to a plume model, which estimates melt rates at the submarine part of the calving front and is able to create an undercutting at the front of the glacier. The plume model should encompass the variable ocean properties of the glacier fjord and the changing geometry of the glacier front. Finally, a discrete particle model such as the HiDEM can be used to model calving and the new geometry sent as input to the ice flow model for a new iteration. Technically, the coupling of Elmer/Ice and HiDEM has been put together in a workflow as described in **Paper B** and more models can be added to the workflow in the future. However, there are some issues to solve before being able to perform such a coupling and multiple sensitivity tests have to be done in order to determine the sets of parameters and time-steps to use.

Finally, the interaction between sliding and calving has been touched upon in this thesis and a study in this direction should be performed in a more systematic way.

10. Appendix

10.1 Integration by parts

Let Ω be a an open bounded subset of $\mathbb{R}^n$ with a piecewise smooth boundary Γ. If $\mathbf{u}$ and $\mathbf{v}$ are two continuously differentiable functions on the closure of Ω, then the formulae for integration by parts are

$$\int_\Omega \boldsymbol{\nabla}\mathbf{u}\cdot\mathbf{v}\,d\Omega = \int_\Gamma \mathbf{u}(\mathbf{v}\cdot\mathbf{n})\,d\Gamma - \int_\Omega \mathbf{u}\boldsymbol{\nabla}\cdot\mathbf{v}\,d\Omega, \tag{10.1a}$$

$$\int_\Omega (\boldsymbol{\nabla}\cdot\mathbf{A})\cdot\mathbf{v}\,d\Omega = \int_\Gamma \mathbf{A}\cdot(\mathbf{v}\cdot\mathbf{n})\,d\Gamma - \int_\Omega \mathbf{A}:\boldsymbol{\nabla}\mathbf{v}\,d\Omega, \tag{10.1b}$$

where $\mathbf{n}$ is the outward unit surface normal to Γ.

10.2 Lagrange multipliers method

The Lagrange multipliers method is used to find extrema of a function given a certain set of constraints. Let a function $\phi : \mathscr{E} \to \mathbb{R}$ and a vector of m functions $\boldsymbol{\psi} = (\psi_j : \mathbb{E} \to \mathbb{R})_{j\in[|1,m|]} \in \mathscr{F}$ (with $dim(\mathscr{F} < dim(\mathscr{E})$ have continuous first partial derivatives. We are looking for the vector $\mathbf{x_0} \in \mathbb{E}$ that minimises ϕ given the constraint $G = \left\{\mathbf{x} \in \mathscr{E},\ \forall j \in [|1,m|],\ \psi_j(\mathbf{x}) = 0\right\}$ We consider the function $L : \mathscr{E}x\mathscr{F} \to \mathbb{R}$ called the Lagrangian defined so that

$$\forall \mathbf{x} \in \mathbb{R}^n,\ \forall \boldsymbol{\lambda} \in \mathbb{R}^m,\ L(\mathbf{x},\boldsymbol{\lambda}) = \phi(\mathbf{x}) + \boldsymbol{\lambda}\cdot\psi(\mathbf{x}). \tag{10.2}$$

$\mathbf{x_0}$ is minimising ϕ if and only if it exists $(\boldsymbol{\lambda}_0) \in \mathscr{F}$ called the Lagrange multipliers so that $DL(\mathbf{x_0},\boldsymbol{\lambda}_0) = 0$. This implies that $\exists\boldsymbol{\lambda}_0) \in \mathscr{F}, D\phi(\mathbf{x_0}) + D(\boldsymbol{\lambda}_0 \cdot \boldsymbol{\psi}(x_0)) = 0$

Example
If we are in the coordinate system ($\mathscr{E} = \mathbb{R}^n$ and $\mathscr{F} = \mathbb{R}^m$ with $(n,m) \in \mathbb{N}^2$ and $m < n$). $\forall(x_i) \in \mathbb{R}^n,\ \forall(\lambda_j) \in \mathbb{R}^m,\ L(x_1,\ldots,x_n,\lambda_1,\ldots,\lambda_n) = \phi(x_1,\ldots,x_n) + \sum_{j=0}^m \lambda_j\psi(x_1,\ldots,x_n)$. $(a_i)_{i\in[|1,n|]}$ is minimising ϕ if and only if it exists $(\alpha_j)_{j\in[|1,m|]}$ called the Lagrange multipliers so that $\forall i \in [|1,n|],\ \frac{\partial L}{\partial x_i} = 0$. This implies that $\forall i \in [|1,n|],\ \frac{\partial\phi}{\partial x_i}(a_1,\ldots,a_n) + \sum_{j=0}^m \alpha_j \frac{\partial\phi}{\partial x_i}(a_1,\ldots,a_n) = 0$.

10.3 Well-posedness

Let X and Y be normed spaces, $K : X \to Y$ a (linear or nonlinear) mapping. The equation $Kx = y$ is called properly-posed or well-posed if the following holds:

1. Existence: For every $y \in Y$ there is (at least one) $x \in X$ such that $Kx = y$,
2. Uniqueness: For every $y \in Y$ there is at most one $x \in X$ with $Kx = y$,
3. Stability: The solution x depends continuously on y; that is, for every sequence $(x_n) \subset X$ with $Kx_n \underset{n\to\infty}{\longrightarrow} Kx$, it follows that $x_n \underset{n\to\infty}{\longrightarrow} x$.

Equations for which (at least) one of these properties does not hold are called improperly-posed or ill-posed.

10.4 The finite element method

The finite element approximation is based on the variational formulation and its discretisation. Here we want to approximate Eq. 6.7. To derive a variational formulation of Stokes problem we multiply Eq. 6.1 by a function $\mathbf{v} \in V$ assumed to vanish at the boundaries to simplify the problem (no slip condition, no lateral BC), where $V := \left\{\mathbf{v} \in [H^1(\Omega)]^3 : v_{\Gamma_b} = \mathbf{0}\right\}$ and integrate using Green's formula or integration by parts (see appendix 10.1). find $\mathbf{u} \in V$ and $p \in Q$, where $Q := \left\{q \in L^2(\Omega)\right\}$, such that

$$A(\mathbf{u},\mathbf{v}) + B(\mathbf{v},p) = F(\mathbf{v}) \;\; \forall \mathbf{v} \in V, \tag{10.3a}$$

$$B(\mathbf{u},q) = 0 \qquad \forall q \in Q. \tag{10.3b}$$

Here, we have

$$A(\mathbf{u},\mathbf{v}) = \int_\Omega \eta(\boldsymbol{\nabla}\mathbf{u} + \boldsymbol{\nabla}\mathbf{u}^\mathbf{T}) : \boldsymbol{\nabla}\mathbf{v} d\Omega, \tag{10.4a}$$

$$B(\mathbf{v},p) = \int_\Omega p\boldsymbol{\nabla}\cdot\mathbf{v} d\Omega, \tag{10.4b}$$

$$F(\mathbf{v}) = -\int_\Omega \rho\mathbf{g}\cdot\mathbf{v} d\Omega. \tag{10.4c}$$

Let $\mathscr{K}$ be a triangulation of Ω, let V_h and Q_h be the space of continuous piecewise linears on $\mathscr{K}$ and let $V_{h,0} \subset V_h$ be the subset $V_{h,0} := \left\{\mathbf{v} \in V_h : v_{\Gamma_b} = \mathbf{0}\right\}$. Each function of Eq. 10.4 is uniquely defined by their values at each node of the the finite element mesh. Using the Galerkin discretisation method, the finite element method reads: find $\mathbf{u_h} \in V_{h,0}$ and $p \in Q_h$ such that

$$A(\mathbf{u_h},\mathbf{v_h}) + B(\mathbf{v_h},p_h) = F(\mathbf{v_h}) \;\; \forall \mathbf{v_h} \in V_h, \tag{10.5a}$$

$$B(\mathbf{u_h},q_h) = 0 \qquad \forall q_h \in Q_h. \tag{10.5b}$$

and can be written

$$\begin{pmatrix} \mathbf{A} & B^T \\ B & \mathbf{0} \end{pmatrix} \begin{pmatrix} \mathbf{u} \\ p \end{pmatrix} = \begin{pmatrix} \mathbf{u} \\ -\rho\mathbf{g} \end{pmatrix}. \tag{10.6}$$

10.5 Adjoint method to minimise the cost function Eq. 6.20

To minimize a function, one can use the method of Lagrange multipliers, a mathematical optimization strategy presented above. Thus we introduce the Lagrangian function $L(\mathbf{u}(\beta), p, \mathbf{v}, q)$ where $\mathbf{v}$ and q are the Lagrangian multipliers with the constraints being Eq. 6.17a and Eq. 6.17b.

$$\begin{aligned} L(\mathbf{u}(\beta), p, \mathbf{v}, q) = J(\beta) + \int_\Omega \mathbf{v} \cdot \left[\boldsymbol{\nabla} \cdot \left(\eta (\boldsymbol{\nabla}\mathbf{u} + \boldsymbol{\nabla}\mathbf{u}^\mathbf{T}) - p\mathbf{I} \right) + \rho \mathbf{g} \right] \, d\Omega \\ + \int_\Omega q (\boldsymbol{\nabla} \cdot \mathbf{u}) d\Omega. \end{aligned} \tag{10.7}$$

We can then integrate by parts the second term on right side of Eq. 10.7 given Eq. 6.7

$$\begin{aligned} \int_\Omega \mathbf{v} \cdot \boldsymbol{\nabla} \cdot (2\eta \dot{\varepsilon}_u - p\mathbf{I}) \, d\Omega = \int_\mathbf{\Gamma} \mathbf{v} \cdot \left[(2\eta \dot{\varepsilon}_u - p\mathbf{I}) \cdot \mathbf{n} \right] \, d\Gamma \\ - \int_\Omega \boldsymbol{\nabla} v : 2\eta \dot{\varepsilon}_u \, d\Omega + \int_\Omega p \nabla \cdot \mathbf{v} \, d\Omega, \end{aligned} \tag{10.8}$$

where $\mathbf{\Gamma} = (\Gamma_s, \Gamma_b, \Gamma_w, \Gamma_r, \Gamma_g)$, $\dot{\varepsilon}_u = \frac{1}{2}(\boldsymbol{\nabla}\mathbf{u} + \boldsymbol{\nabla}\mathbf{u}^\mathbf{T})$ and : is the scalar product (or double inner product) of two tensors. For the first term on the right side of Eq. 10.8, we know that it is equal to zero on Γ_s because of Eq. 6.17c.

Since $\mathbf{v} = (\mathbf{v} \cdot \mathbf{t_1})\mathbf{t_1} + (\mathbf{v} \cdot \mathbf{t_2})\mathbf{t_2} + (\mathbf{v} \cdot \mathbf{n})\mathbf{n}$, we can deduce that

$$\int_{\Gamma_b} \mathbf{v} \cdot ((2\eta \dot{\varepsilon}_u - p\mathbf{I}) \cdot \mathbf{n}) \, d\Gamma_b = \int_{\Gamma_b} -\beta \, \mathbf{ut_{i,b}} : \mathbf{vt_{i,b}} \, d\Gamma_b, \tag{10.9a}$$

$$\int_{\Gamma_w} \mathbf{v} \cdot ((2\eta \dot{\varepsilon}_u - p\mathbf{I}) \cdot \mathbf{n}) \, d\Gamma_w = \int_{\Gamma_w} f_w \mathbf{v} \cdot \mathbf{n} \, d\Gamma_w, \tag{10.9b}$$

$$\int_{\Gamma_r} \mathbf{v} \cdot ((2\eta \dot{\varepsilon}_u - p\mathbf{I}) \cdot \mathbf{n}) \, d\Gamma_r = \int_{\Gamma_r} -\beta_p \, \mathbf{ut_{i,r}} : \mathbf{vt_{i,r}} \, d\Gamma_r, \tag{10.9c}$$

$$\int_{\Gamma_g} \mathbf{v} \cdot ((2\eta \dot{\varepsilon}_u - p\mathbf{I}) \cdot \mathbf{n}) \, d\Gamma_g = \int_{\Gamma_g} (z - z_s) \left(\frac{1}{H(-\beta_p - \gamma_{z_s} H^n)} v_z \mathbf{u^{obs}} - \rho g \mathbf{v} \right) \cdot \mathbf{n} \, d\Gamma_g. \tag{10.9d}$$

Since $\boldsymbol{\nabla}\mathbf{v} = (\boldsymbol{\nabla}\mathbf{v} + \boldsymbol{\nabla}\mathbf{v}^\mathbf{T}) - \boldsymbol{\nabla}\mathbf{v}^\mathbf{T} = 2\dot{\varepsilon}_v - \boldsymbol{\nabla}\mathbf{v}^\mathbf{T}$, the second term on the right side of Eq. 10.8 can be decomposed as follows

$$\int_\Omega \boldsymbol{\nabla} v : 2\eta \dot{\varepsilon}_u \, d\Omega = \int_\Omega 4\eta \dot{\varepsilon}_v : \dot{\varepsilon}_u \, d\Omega - \int_\Omega \boldsymbol{\nabla} v^T : 2\eta \dot{\varepsilon}_u \, d\Omega. \tag{10.10}$$

We know that $\dot{\varepsilon}_u$ is symmetric, thus $\boldsymbol{\nabla} v^T : 2\eta \dot{\varepsilon}_u = \boldsymbol{\nabla} v : 2\eta \dot{\varepsilon}_u$. This leads to

$$\int_\Omega \boldsymbol{\nabla} v : 2\eta \dot{\varepsilon}_u \, d\Omega = \int_\Omega 2\dot{\varepsilon}_v : \dot{\varepsilon}_u \, d\Omega = \int_\Omega 2\dot{\varepsilon}_u : \dot{\varepsilon}_v \, d\Omega. \tag{10.11}$$

Finally, we obtain

$$\begin{aligned} L(\mathbf{u}(\beta),p,\mathbf{v},q) = J(\beta) &+ \int_{\Gamma_w} f_w \mathbf{v}\cdot\mathbf{n}\, d\Gamma_w \\ &- \int_{\Gamma_b} \beta\ \mathbf{ut_{i,b}} : \mathbf{vt_{i,b}}\, d\Gamma_b - \int_{\Gamma_r} \beta_p\ \mathbf{ut_{i,r}} : \mathbf{vt_{i,r}}\, d\Gamma_r \\ &+ \int_{\Gamma_g} (z-z_s)\left(\frac{1}{H(-\beta_p-\gamma_{z_s}H^n)} v_z \mathbf{u^{obs}} - \rho g \mathbf{v}\right)\cdot\mathbf{n}\, d\Gamma_g \\ &- \int_\Omega 2\dot{\varepsilon}_u : \dot{\varepsilon}_v\, d\Omega + \int_\Omega p\nabla\cdot\mathbf{v}\, d\Omega + \int_\Omega q\nabla\cdot\mathbf{u}\, d\Omega. \end{aligned} \tag{10.12}$$

Using the method of Lagrange multipliers, β is minimizing J if and only if it exists $\mathbf{v}$ and q so that

$$\frac{\partial J}{\partial \beta}(\beta) = \int_{\Gamma_b} \mathbf{ut_{i,b}} : \mathbf{vt_{i,b}}\, d\Gamma_b. \tag{10.13}$$

11. Sammanfattning på svenska

En av morgondagens största utmaningar för samhället och ett hot mot miljön är höjningen av havsnivån kopplat till den globala uppvärmningen. Ett stort bidrag till havsyteförändringarna kommer från smältande glaciärer eller från istäcken och deras bidrag förutspås öka i framtiden med ett varmare klimat. Olyckligtvis finns stora osäkerheter i dagens uppskattningar av glaciärers bidrag främst på grund av brist på direkta observationer och luckor i vår kunskap om de komplexa glaciala processer som bidrar till tillförsel av glaciäris och smältvatten till haven. Fysikaliska isflödesmodeller som simulerar isens flöde och dess dynamik är ett viktigt verktyg för att öka förståelsen av deras beteende och transport av vatten till haven. Två av de största osäkerheterna i dagens modeller är hur glaciärerna glider över sitt underlag samt hur isberg bryts loss när glaciären når havet, en process som kallas kalvning.

Bottenglidningen spelar en roll i isdynamiken genom att påverka hastigheten på isens rörelse. För glaciärer som har stora variationer i inflödet av smältvatten kan bottenglidningen förändras år från år, speciellt under smältsäsongen. Det finns många observationer av glaciärers bottenmiljöer men de är ofta begränsade i tid och rum. Modellering blir därför nödvändigt för att tolka observationerna och förstå de dynamiska processerna. Vanligtvis finns det ett samband mellan bottenskjuvspänning och bottenglidning, detta samband kallas glidlag.

Kalvning är en del av massbalansprocessen för tidvattenglaciärer (glaciärer som flödar ut i havet) och innebär att delar av landisen bryts loss och hamnar i havet. Detta sker när dragspänningar är tillräckligt stora för att skapa och sprida sprickor i isen. Kalvningen beror på flera olika externa faktorer och involverar en rad olika processer som kan ha en viktig påverkan på glaciärens dynamik. Kalvningsmodeller försöker inkludera dessa faktorer och processer men det finns fortfarande ett behov av mer observationer för att kunna förbättra modellerna och förstå kalvning bättre.

Den här avhandlingen är inriktad mot modellering av bottenglidnings- och kalvningsprocesser i syfte att dels förstå två glaciärers komplexa beteende och dels förbättra parameteriseringen i modellerna. Att förstå glidning och kalvning bättre är en viktig nyckel för att kunna modellera glaciärers beteenden och deras påverkan på havsnivåhöjningen.

Beroende på tidsskalan, rumsskalan och den process man är intresserad av kan is betraktas antingen som en fluid (isens beteende modelleras då som en kontinuerlig process) eller som ett ämne i fast form (isens beteende modelleras då som en diskret process). En fluid är ett ämne som vid en kontinuerligt applicerad spänning deformeras kontinuerligt. Hastigheten på deformationen

är då en funktion av den applicerade spänningen. Is kan modelleras som en icke-Newtonsk, icke kompressibel viskös fluid som flödar långsamt. På så sätt kan accelerationstermen och trögheten försummas i Navier-Stokes ekvationer. När isflöden och bottenglidning modelleras i denna avhandling betraktas isen som en fluid och flödesmodellen Elmer/Ice har använts. Ett ämne i fast form deformeras när det utsätts för spänning tills ett jämviktstillstånd uppnås. Deformationen beror på den applicerade spänningen. Det finns två typer av deformering, elastisk (reversibel) och plastisk (irreversibel), och efter en viss tröskelspänning bryts materialet sönder. När man modellerar kalvning och sprickbildning kan man se isen som ett ämne i fast form, i dessa fall har "Helsinki Discrete Element Model" (HiDEM) använts.

Kronebreen och Tunabreen är två tidvattensglacärer på Svalbard som båda flödar med hög hastighet, vilket indikerar aktiv bottenglidning, och når ned till havet där kalvning sker. Genom att justera isflödesmodellen Elmer/Ice till att efterlikna observationer av isrörelser över tre år med 11-dagars intervall har bottenglidningen bestämts. I uppsats I jämförs ytsmältning på glaciären med bottenglidningen och resultaten visar att under sommaren påverkas isens rörelse starkt av smältvatten, men detta vatten påverkar även glaciärens rörelse nästkommande år. Jämförelsen visar också att parameteriseringen av bottenglidningen i modellen inte enbart bör anpassas till lokala processer utan även globala. Det subglaciala dräneringssystemet modelleras i Uppsats II och jämförs med den ytsmältning som sker under de tre åren. Resultaten visar att olika konfigurationer av effektiva och icke effektiva dräneringssystem utvecklas mellan år och vikten av att använda en parameterisering av bottenglidningen som beror på förändringar av effektivt vattentryck vid botten av glaciären och dess variation i tid och rum. Genom att anpassa olika parametrar hos en befintlig glidlag och använda det effektiva trycket, vilket varierar över tid, kan man få mindre fel än om man använder en tidsoberoende glidlag.

Kalvningsprocesserna är studerade i Uppsats III genom att kombinera en rad modeller så som en isflödesmodell, en havscirkulationsmodell och en modell för diskret kalvning. Resultaten visar på betydelsen av geometri av glaciärens front i kontakt med havet, och underminering genom smältning under havsnivån för kalvningens hastighet och plats. Mer observationer och analytiska metoder behövs dock. Kameror för regelbunden fotografering har monterats framför Tunabreen och en automatisk metod för detektering av kalvning presenteras i Uppsats IV. Resultaten visar på betydelsen av den stigande smältvattenplymen och destabiliseringen av den lokala front-miljön.

Framtida arbete bör fokusera på att identifiera en glidlag som fungerar bra såväl inom som utanför smältsäsongen. På så sätt kan isflödesmodellen kopplas med den subglaciala hydrologimodellen. En full sammankoppling med kalvningsmodellen blir då möjlig vilket kan bidra till att förutspå beteendet hos tidvattenglaciärer i ett förändrande klimat.

12. Acknowledgement

"Alone I go faster but together we go further." – African wisdom

My involvement in research in general and in glaciology in particular is somehow the product of different factors but mostly luck! After my MSc in structural engineering, I worked in a design office in Paris, France, building bridges and tunnels, but I rapidly felt the need of something else to be complete in my working life, something closer to the nature and the environment. Through a combination of circumstances, I quit my job and I ended up working for two years at the scientific department of the French Embassy in Sweden in charge of environmental research. I happened to organise a French-Swedish summer-school in Abisko in the north of Sweden on sub-polar environments in June 2010. This is where everything started: my interest for research and for Arctic related issues! Therefore, I would like to thank the French Embassy in Sweden that let me start the first chapter of this journey. My first inspirations came from Ninis Rosqvist for glaciology, Erik Lundin for fieldwork and the Swedish Polar Secretariat for communication and logistics. After these two years, I was determined and I dedicated my time to acquire better knowledge in both glaciology and research. At the department of Geography in Stockholm University, I followed the glaciology lectures and I thank Peter Jansson for his trust as well as Patrick Applegate and Nina Kirchner, who I worked for in my first glacier modelling project. I would also like to thank the Tarfala Research Station, where I had the opportunity to work in summer 2012 and met wonderful people, particularly my co-workers Baptiste Gombert, Stefan Richter and Joakim Robygd. This same summer, I was going for the first time in Svalbard for a course at UNIS (University Centre in Svalbard). Together, with Heidi Sevestre, we placed a first camera, for four days, in front of Tunabreen, which started my interest in calving and time-lapse cameras. During that time, I also met Doug Benn, who, since then, always encouraged me to go further and showed real enthusiasm in my work and my motivations.

A new chapter, when the dream comes true, finally began with my involvement in PhD studies in February 2013 at the University of Uppsala. For that, I would like to warmly thank my supervisors Rickard Pettersson, Veijo Pohjola and Ken Mattsson. I particularly thank Rickard Pettersson, my main supervisor for his involvement. During these years, I have learnt a lot at different levels. First on a scientific level, my knowledge in glaciology (theories, modelling, fieldwork) but also in scientific methods or presentations have broaden and I feel much safer in a research environment today than when I started.

Once again, I would like to thank Doug Benn who gave me the opportunity to work on a fantastic glacier in Svalbard, Kronebreen. The data I had access to were exactly what I needed to get started! But it would have been very difficult to continue without the great help of the Elmer/Ice community and particularly Thomas Zwinger, Martina Schäfer, Fabien Gillet-Chaulet and Olivier Gagliardini, who taught me a lot on glacier modelling. In the modelling section, I would also like to thank Jan Åström who shared his discrete particle model and has always helped me when needed. But glaciology is not only about modelling and I have been lucky to see the other face of the coin by joining several fieldwork projects. For that, I would like to thank Veijo Pohjola, Sergey Marchenko, Rickard Pettersson, Ward Van Pelt, Katrin Lindbäck and Christian Zdanowicz for great adventures on Nordenskiöldsbreen, Jack Kohler on Kronebreen and Penny How, Doug Benn, Nick Hulton, Chris Borstad and Anne Flink on Tunabreen. I also had my own fieldwork with the time-lapse camera and I would like to thank Heidi Sevestre, Rickard Pettersson, Doug Benn, Penny How, Sergey Marchenko, Elena Marchenko, Pontus Westrin, Silje Smith-Johnsen as well as the UNIS logistics for their help. I also learned so much through the different courses, meetings, conferences and workshops I had the chance to participate to thanks to my involvement in the Nordic Center of Excellence SVALI (Stability and Variations of Arctic Land Ice). It enabled me to broaden my knowledge and meet the right persons at the right moment. This brings me to the second level, the collaboration. It has been thrilling to confirm that alone we go faster but together we go further. I enjoyed all scientific collaborations I happened to be part of through the writing of my articles. I would therefore like to thank all my co-authors and students I had the pleasure to supervise. And since I am here, I would also like to thank the editors and the anonymous referees, who did a wonderful job in questioning and criticising our work! Finally, I learned how important the role of the scientific community is in a research career. It is necessary, in my opinion, in order to create a healthy research environment both scientifically and socially. I am therefore very grateful to the SVALI community who welcomed me as a member and I must say that the links, which have been created there, are very strong thanks to the project leaders and the PhDs/postdocs. I would like to thank a few who have been particularly important for me and who I didn't mention before: Jon-Ove Hagen, Tómas Jóhannesson , Andreas Ahlstrøm, Guðfinna Aðalgeirsdóttir, Anna Sinisalo, Bergur Einarsson, Charalampos Charalampidis (Babis), Pierre-Marie Lefeuvre (PiM), Ágúst Gunnlaugsson, Ilona Välisuo, Signe Hillerup Larsen, Solveig Havstad Winsvold, Yongmei Gong, Eyolfur Magnusson, Johan Nilsson, Thomas Schellenberger and Alexandra Messerli. The discussion I had in Uppsala with my colleagues at LUVAL, in geocentrum, were also very important for my development. I would like to particularly thank Sergey Marchenko and Eduardo Reynolds, my office-mates, but also Ward van Pelt, Benoît Dessirier, Joachim Place, Saba Joodaki, Jean-Marc Mayotte, Marc Girons, Bea Quesada,

Nino Amvrosiadi, Carmen Vega, Audrey Campeau, Adam Dingwell, Nina Svensson, Lebing Gong, Kristina Konrady, Kaycee Okoli, Agnes Soto, Diana Fuentes, Antonin Berlet-Vanide, Reinert Huseby Karlsen, Thomas Stevens, Korbinian Jakob, Lichuan Wu, Liang Tian, Chiara Danchremileotti and those I forget... I also want to thank Eva Borgert and Fatima Ryttare-Okorie, from the administration, who helped me a lot. I must also mention the interesting meetings I had with the ice people at the IT-department and I would like to thank Cheng Gong, Per Lötstedt, Josefin Ahlkrona, Lina von Sydow and Eef van Dongen.

But what would have been my life during these years without the support I received from my friends and family? Would I have been through these years as happily as I had? Probably not... There is no word to describe how grateful I am to my parents and my sister, who regularly came to visit me and were always available when I needed them. How lucky I am! I would also like to thank my Stockholm family (Ylva, Linda, Caroline, Jonas, Philip, Isak, Robin, Fred, Elin, Fredrik, Romain, David, Axel, Nuria, Juan, Antoine & co, Bertrand & co, Julius, Andreas, Magi, Antoine, Cindy) without who life would have been much less fun in Stockholm! And I certainly do not forget my Uppsala family, Colin & Jon. It was so great to live with you and share so much good memories. Jon, you know you are the best! Thank you also Ingrid and Erland for your support. Further away but close to my heart, I would finally want to thank all my friends who came in Sweden for a visit (Tiphaine, Antoine, Mathilde, Julia, Morgane, Guillaume, Stephanie, Yann, Isabelle, Elise, Arnaud, Guillaume, Céline, Paul, Joe, Mathilde, Thibaud, Clara who promised to come, Bea, Coline, Stéphanie, Thomas, Mathieu, Zeinab, Julie, Séverin). I really thank you all for being who you are!

The PhD chapter is finally coming to an end but not the dream! A new chapter is waiting to be opened and I hope it will be full of new discoveries and challenges...

13. Funding and support

This thesis was supported by the Greenland Analogue Project (GAP) and Uppsala University. The Nordic Centre of Excellence SVALI supported my computer resource allocation at the CSC-IT Center for Science Ltd in Finland. Acquisition of the TerraSAR-X imagery and the time-lapse camera deployment in 2015 was funded by the ConocoPhillips Northern Area Program, via the CRIOS project (Calving Rates and Impact on Sea Level). I received an Arctic Field Grant from the Svalbard Science Forum to acquire radar lines for the basal topography in 2014. Fieldwork support came from Ymer-80, the Swedish Society for Anthropology and Geography (SSAG) and the Wallenberg foundation. Travels were also funded by the Nordic Centre of Excellence SVALI, Heino and Sigrid Jänes foundation, the Liljevalch foundation and Magrit Althins foundation.

References

Aliani, S., Sciascia, R., Conese, I., D'Angelo, A., Del Bianco, F., Giglio, F., Langone, L., and Miserocchi, S.: Characterization of seawater properties and ocean heat content in Kongsfjorden, Svalbard Archipelago, Rendiconti Lincei, 27, 155–162, doi:10.1007/s12210-016-0544-4, 2016.

Alley, R. B.: How can low-pressure channels and defortning tills coexist subglacially?, Journal of Glaciology, 38, doi:10.1017/S0022143000009734, 1992.

Alley, R. B., Blankenship, D. D., Bentley, C. R., and Rooney, S.: Deformation of till beneath ice stream B, West Antarctica, Nature, 322, 57–59, doi:10.1038/322057a0, 1986.

Alley, R. B., Anandakrishnan, S., Christianson, K., Horgan, H. J., Muto, A., Parizek, B. R., Pollard, D., and Walker, R. T.: Oceanic forcing of ice-sheet retreat: West Antarctica and more, Annual Review of Earth and Planetary Sciences, 43, 207–231, doi:10.1146/annurev-earth-060614-105344, 2015.

Amundson, J. M. and Truffer, M.: A unifying framework for iceberg-calving models, Journal of Glaciology, 56, 822–830, doi:10.3189/002214310794457173, 2010.

Anderson, R. S., Hallet, B., Walder, J., and Aubry, B. F.: Observations in a cavity beneath Grinnell glacier, Earth Surface Processes and Landforms, 7, 63–70, doi:10.1002/esp.3290070108, 1982.

Arthern, R. J. and Gudmundsson, G. H.: Initialization of ice-sheet forecasts viewed as an inverse Robin problem, Journal of Glaciology, 56, 527–533, doi:10.3189/002214310792447699, 2010.

Åström, J. A., Riikilä, T. I., Tallinen, T., Zwinger, T., Benn, D., Moore, J. C., and Timonen, J.: A particle based simulation model for glacier dynamics, Cryosphere, 7, 1591–1602, doi:10.5194/tc-7-1591-2013, 2013.

Åström, J. A., Vallot, D., Schäfer, M., Welty, E. Z., O'Neel, S., Bartholomaus, T., Liu, Y., Riikilä, T., Zwinger, T., Timonen, J., and Moore, J.: Termini of calving glaciers as self-organized critical systems, Nature Geoscience, 7, 874–878, doi:10.1038/NGEO2290, 2014.

Bartholomaus, T. C., Larsen, C. F., O'Neel, S., and West, M. E.: Calving seismicity from iceberg-sea surface interactions, Journal of Geophysical Research: Earth Surface, 117, doi:10.1029/2012JF002513, f04029, 2012.

Bartholomew, I., Nienow, P., Mair, D., Hubbard, A., King, M. A., and Sole, A.: Seasonal evolution of subglacial drainage and acceleration in a Greenland outlet glacier, Nature Geoscience, 3, 408–411, doi:10.1038/ngeo863, 2010.

Bartholomew, I., Nienow, P., Sole, A., Mair, D., Cowton, T., King, M., and Palmer, S.: Seasonal variations in Greenland Ice Sheet motion: Inland extent and behaviour at higher elevations, Earth and Planetary Science Letters, 307, 271–278, doi:10.1016/j.epsl.2011.04.014, 2011.

Bassis, J. and Jacobs, S.: Diverse calving patterns linked to glacier geometry, Nature Geoscience, 6, 833, doi:10.1038/ngeo1887, 2013.

Benn, D. I., Warren, C. R., and Mottram, R. H.: Calving processes and the dynamics of calving glaciers, Earth-Science Reviews, 82, 143–179, doi:10.1016/j.earscirev.2007.02.002, 2007.

Benn, D. I., Åström, J., Zwinger, T., Todd, J., Nick, F. M., Cook, S., Hulton, N. R., and Luckman, A.: Melt-under-cutting and buoyancy-driven calving from tidewater glaciers: new insights from discrete element and continuum model simulations, Journal of Glaciology, pp. 1–12, doi:10.1017/jog.2017.41, 2017.

Bindschadler, R.: The importance of pressurized subglacial water in separation and sliding at the glacier bed, Journal of Glaciology, 29, 3–19, doi:10.1017/S0022143000005104, 1983.

Blankenship, D. D., Bentley, C. R., Rooney, S., and Alley, R. B.: Seismic measurements reveal a saturated porous layer beneath an active Antarctic ice stream, Nature, 322, 54–57, doi:10.1038/322054a0, 1986.

Bougamont, M., Christoffersen, P., Hubbard, A. L., Fitzpatrick, A. A., Doyle, S. H., and Carter, S. P.: Sensitive response of the Greenland Ice Sheet to surface melt drainage over a soft bed, Nature Communications, 5, doi:10.1038/ncomms6052, 2014.

Boulton, G. S. and Hindmarsh, R. C. A.: Sediment deformation beneath glaciers: Rheology and geological consequences, Journal of Geophysical Research: Solid Earth, 92, 9059–9082, doi:10.1029/JB092iB09p09059, 1987.

Box, J. E. and Ski, K.: Remote sounding of Greenland supraglacial melt lakes: implications for subglacial hydraulics, Journal of Glaciology, 53, 257–265, doi:10.3189/172756507782202883, 2007.

Brinkerhoff, D. J. and Johnson, J.: Data assimilation and prognostic whole ice sheet modelling with the variationally derived, higher order, open source, and fully parallel ice sheet model VarGlaS, The Cryosphere, 7, 1161, doi:10.5194/tc-7-1161-2013, 2013.

Brown, C. S., Meier, M. F., and Post, A.: Calving speed of Alaska tidewater glaciers, with application to Columbia Glacier, 1982.

Budd, W., Jenssen, D., and Smith, I.: A three-dimensional time-dependent model of the West Antarctic ice sheet, Annals of Glaciology, 5, 29–36, doi:10.1007/BF00207423, 1984.

Calvetti, D., Morigi, S., Reichel, L., and Sgallari, F.: Tikhonov regularization and the L-curve for large discrete ill-posed problems, Journal of Computational and Applied Mathematics, 123, 423 – 446, doi:10.1016/S0377-0427(00)00414-3, Numerical Analysis 2000. Vol. III: Linear Algebra, 2000.

Carr, J. R., Vieli, A., and Stokes, C.: Influence of sea ice decline, atmospheric warming, and glacier width on marine-terminating outlet glacier behavior in northwest Greenland at seasonal to interannual timescales, Journal of Geophysical Research: Earth Surface, 118, 1210–1226, doi:10.1002/jgrf.20088, 2013.

Carroll, D., Sutherland, D. A., Shroyer, E. L., Nash, J. D., Catania, G. A., and Stearns, L. A.: Modeling turbulent subglacial meltwater plumes: Implications for fjord-scale buoyancy-driven circulation, Journal of Physical Oceanography, 45, 2169–2185, doi:10.1175/JPO-D-15-0033.1, 2015.

Carson, M., Köhl, A., Stammer, D., A. Slangen, A. B., Katsman, C. A., W. van de Wal, R. S., Church, J., and White, N.: Coastal sea level changes, observed and projected during the 20th and 21st century, Climatic Change, 134, 269–281, doi:

10.1007/s10584-015-1520-1, 2016.
Chapuis, A. and Tetzlaff, T.: The variability of tidewater-glacier calving: origin of event-size and interval distributions, Journal of glaciology, 60, 622–634, doi:10.3189/2014JoG13J215, 2014.
Christoffersen, P., Mugford, R. I., Heywood, K. J., Joughin, I., Dowdeswell, J. A., Syvitski, J. P. M., Luckman, A., and Benham, T. J.: Warming of waters in an East Greenland fjord prior to glacier retreat: mechanisms and connection to large-scale atmospheric conditions, The Cryosphere, 5, 701–714, doi:10.5194/tc-5-701-2011, 2011.
Church, J., Clark, P., Cazenave, A., Gregory, J., Jevrejeva, S., Levermann, A., Merrifield, M., Milne, G., Nerem, R., Nunn, P., Payne, A., Pfeffer, W., Stammer, D., and Unnikrishnan, A.: Sea Level Change, book section 13, pp. 1137–1216, Cambridge University Press, Cambridge, United Kingdom and New York, NY, USA, doi:10.1017/CBO9781107415324.026, 2013.
Claremar, B., Obleitner, F., Reijmer, C., Pohjola, V., Waxegard, A., Karner, F., and Rutgersson, A.: Applying a Mesoscale Atmospheric Model to Svalbard Glaciers, Advances in Meteorology, 2012, doi:10.1155/2012/321649, 2012.
Cohen, D., Iverson, N. R., Hooyer, T. S., Fischer, U. H., Jackson, M., and Moore, P. L.: Debris-bed friction of hard-bedded glaciers, Journal of Geophysical Research: Earth Surface, 110, doi:10.1029/2004JF000228, f02007, 2005.
Colgan, W., Rajaram, H., Anderson, R., Steffen, K., Phillips, T., Joughin, I., Zwally, H. J., and Abdalati, W.: The annual glaciohydrology cycle in the ablation zone of the Greenland ice sheet: Part 1. Hydrology model, Journal of Glaciology, 57, 697–709, doi:10.3189/002214311797409668, 2011.
Cook, S., Rutt, I., Murray, T., Luckman, A., Zwinger, T., Selmes, N., Goldsack, A., and James, T.: Modelling environmental influences on calving at Helheim Glacier in eastern Greenland, The Cryosphere, 8, 827–841, doi:10.5194/tc-8-827-2014, 2014.
Cottier, F., Tverberg, V., Inall, M., Svendsen, H., Nilsen, F., and Griffiths, C.: Water mass modification in an Arctic fjord through cross-shelf exchange: The seasonal hydrography of Kongsfjorden, Svalbard, Journal of Geophysical Research: Oceans, 110, doi:10.1029/2004JC002757, 2005.
Creyts, T. T. and Schoof, C. G.: Drainage through subglacial water sheets, Journal of Geophysical Research: Earth Surface, 114, doi:10.1029/2008JF001215, f04008, 2009.
Cuffey, K. M. and Paterson, W. S. B.: The physics of glaciers, Butterworth-Heinemann, 2010.
Darlington, E. F.: Meltwater delivery from the tidewater glacier Kronebreen to Kongsfjorden, Svalbard; insights from in-situ and remote-sensing analyses of sediment plumes, Ph.D. thesis, © Eleanor Darlington, 2015.
de Fleurian, B., Gagliardini, O., Zwinger, T., Durand, G., Le Meur, E., Mair, D., and Råback, P.: A double continuum hydrological model for glacier applications, The Cryosplere, 8, doi:10.5194/tc-8-137-2014, 2014.
DeConto, R. M. and Pollard, D.: Contribution of Antarctica to past and future sea-level rise, Nature, 531, 591–597, doi:10.1038/nature17145, 2016.
Doyle, S. H., Hubbard, A., Fitzpatrick, A. A. W., van As, D., Mikkelsen, A. B., Pettersson, R., and Hubbard, B.: Persistent flow acceleration within the interior of the Greenland ice sheet, Geophysical Research Letters, 41, 899–905, doi:

10.1002/2013GL058933, 2014.
Eisen, O.: Inference of velocity pattern from isochronous layers in firn, using an inverse method, Journal of Glaciology, 54, 613–630, doi:10.3189/002214308786570818, 2008.
Engelhardt, H., Humphrey, N., Kamb, B., and Fahnestock, M.: Physical conditions at the base of a fast moving Antarctic ice stream, Science, 248, 57–60, doi:10.1126/science.248.4951.57, 1990.
Fischer, U. H. and Clarke, G. K. C.: Ploughing of subglacial sediment, Journal of Glaciology, 40, 97–106, doi:10.1017/S0022143000003853, 1994.
Flink, A. E., Noormets, R., Kirchner, N., Benn, D. I., Luckman, A., and Lovell, H.: The evolution of a submarine landform record following recent and multiple surges of Tunabreen glacier, Svalbard, Quaternary Science Reviews, 108, 37 – 50, doi:10.1016/j.quascirev.2014.11.006, 2015.
Flowers, G. E.: Modelling water flow under glaciers and ice sheets, Proceedings of the Royal Society of London A: Mathematical, Physical and Engineering Sciences, 471, doi:10.1098/rspa.2014.0907, 2015.
Flowers, G. E., Björnsson, H., Pálsson, F., and Clarke, G. K. C.: A coupled sheet-conduit mechanism for jökulhlaup propagation, Geophysical Research Letters, 31, doi:10.1029/2003GL019088, l05401, 2004.
Forwick, M., Vorren, T. O., Hald, M., Korsun, S., Roh, Y., Vogt, C., and Yoo, K.-C.: Spatial and temporal influence of glaciers and rivers on the sedimentary environment in Sassenfjorden and Tempelfjorden, Spitsbergen, Geological Society, London, Special Publications, 344, 163–193, doi:10.1144/SP344.13, 2010.
Fountain, A. G. and Walder, J. S.: Water flow through temperate glaciers, Reviews of Geophysics, 36, 299–328, doi:10.1029/97RG03579, 1998.
Fountain, A. G., Jacobel, R. W., Schlichting, R., and Jansson, P.: Fractures as the main pathways of water flow in temperate glaciers, Nature, 433, 618–621, doi:10.1038/nature03296, 2005.
Fowler, A.: A theoretical treatment of the sliding of glaciers in the absense of cavitation, Philosophical Transactions of the Royal Society of London A: Mathematical, Physical and Engineering Sciences, 298, 637–681, doi:10.1098/rsta.1981.0003, 1981.
Fowler, A.: A sliding law for glaciers of constant viscosity in the presence of subglacial cavitation, Proceedings of the Royal Society of London, 407, doi:10.1098/rspa.1986.0090, 1986.
Fowler, A.: Weertman, Lliboutry and the development of sliding theory, Journal of Glaciology, 56, 965–972, doi:10.3189/002214311796406112, 2010.
Fried, M., Catania, G., Bartholomaus, T., Duncan, D., Davis, M., Stearns, L., Nash, J., Shroyer, E., and Sutherland, D.: Distributed subglacial discharge drives significant submarine melt at a Greenland tidewater glacier, Geophysical Research Letters, 42, 9328–9336, doi:10.1002/2015GL065806, 2015.
Gagliardini, O., Cohen, D., Råback, P., and Zwinger, T.: Finite-element modeling of subglacial cavities and related friction law, Journal of Geophysical Research-Earth Surface, 112, doi:10.1029/2006JF000576, 2007.
Gagliardini, O., Zwinger, T., Gillet-Chaulet, F., Durand, G., Favier, L., de Fleurian, B., Greve, R., Malinen, M., Martín, C., Råback, P., Ruokolainen, J., Sacchettini, M., Schäfer, M., Seddik, H., and Thies, J.: Capabilities and performance of Elmer/Ice, a

new-generation ice sheet model, Geoscientific Model Development, 6, 1299–1318, doi:10.5194/gmd-6-1299-2013, 2013.

Gillet-Chaulet, F., Gagliardini, O., Seddik, H., Nodet, M., Durand, G., Ritz, C., Zwinger, T., Greve, R., and Vaughan, D. G.: Greenland ice sheet contribution to sea-level rise from a new-generation ice-sheet model, Cryosphere, 6, 1561–1576, doi:10.5194/tcd-6-2789-2012, 2012.

Gillet-Chaulet, F., Durand, G., Gagliardini, O., Mosbeux, C., Mouginot, J., Rémy, F., and Ritz, C.: Assimilation of surface velocities acquired between 1996 and 2010 to constrain the form of the basal friction law under Pine Island Glacier, Geophysical Research Letters, 43, 10,311–10,321, doi:10.1002/2016GL069937, 2016.

Gladstone, R., Schäfer, M., Zwinger, T., Gong, Y., Strozzi, T., Mottram, R., Boberg, F., and Moore, J. C.: Importance of basal processes in simulations of a surging Svalbard outlet glacier, The Cryosphere, 8, 1393–1405, doi:10.5194/tc-8-1393-2014, 2014.

Goldberg, D. N. and Sergienko, O. V.: Data assimilation using a hybrid ice flow model, The Cryosphere, 5, 315–327, doi:10.5194/tc-5-315-2011, 2011.

Gudmundsson, G. H.: Transmission of basal variability to a glacier surface, Journal of Geophysical Research: Solid Earth, 108, 1978–2012, doi:10.1029/2002JB002107, 2003.

Gudmundsson, G. H. and Raymond, M.: On the limit to resolution and information on basal properties obtainable from surface data on ice streams, The Cryosphere Discussions, 2, 413–445, doi:10.5194/tcd-2-413-2008, 2008.

Gulley, J., Benn, D., Screaton, E., and Martin, J.: Mechanisms of englacial conduit formation and their implications for subglacial recharge, Quaternary Science Reviews, 28, 1984–1999, doi:10.1016/j.quascirev.2009.04.002, 2009.

Gurnell A., Hannah D., L. D.: Suspended sediment yield from glacier basins, vol. 25, IAHS Publ., 1996.

Habermann, M., Maxwell, D., and Truffer, M.: Reconstruction of basal properties in ice sheets using iterative inverse methods, Journal of Glaciology, 58, 795–807, doi:10.3189/2012JoG11J168, 2012.

Habermann, M., Truffer, M., and Maxwell, D.: Changing basal conditions during the speed-up of Jakobshavn Isbræ, Greenland, The Cryosphere, 7, 1679–1692, doi:10.5194/tc-7-1679-2013, 2013.

Hansen, P. C.: The L-Curve and its Use in the Numerical Treatment of Inverse Problems, in: Computational Inverse Problems in Electrocardiology, pp. 119–142, WIT Press, 2001.

Harper, J. T. and Humphrey, N. F.: Borehole video analysis of a temperate glacier's englacial and subglacial structure: Implications for glacier flow models, Geology, 23, 901–904, doi:10.1130/0091-7613(1995)023<0901:BVAOAT>2.3.CO;2, 1995.

Hewitt, I. J.: Modelling distributed and channelized subglacial drainage: the spacing of channels, Journal of Glaciology, 57, 302–314, doi:10.3189/002214311796405951, 2011.

Hewitt, I. J.: Seasonal changes in ice sheet motion due to melt water lubrication, Earth and Planetary Science Letters, 371–372, 16, doi:10.1016/j.epsl.2013.04.022, 2013.

Hewitt, I. J. and Fowler, A. C.: Seasonal waves on glaciers, Hydrological Processes, 22, 3919–3930, doi:10.1002/hyp.7029, 2008.

Hindmarsh, R.: Deforming beds: Viscous and plastic scales of deformation, Quaternary Science Reviews, 16, 1039 – 1056, doi:10.1016/S0277-3791(97)00035-8,

1997.

Hock, R. and Hooke, R. L.: Evolution of the internal drainage system in the lower part of the ablation area of Storglaciären, Sweden, Geological Society of America Bulletin, 105, 537–546, doi:10.1130/0016-7606(1993)105\<0537:EOTIDS\>2.3.CO;2, 1993.

Hoffman, M. J., Catania, G. A., Neumann, T. A., Andrews, L. C., and Rumrill, J. A.: Links between acceleration, melting, and supraglacial lake drainage of the western Greenland Ice Sheet, Journal of Geophysical Research: Earth Surface, 116, doi:10.1029/2010JF001934, f04035, 2011.

Holland, D. M., Thomas, R. H., De Young, B., Ribergaard, M. H., and Lyberth, B.: Acceleration of Jakobshavn Isbrae triggered by warm subsurface ocean waters, Nature geoscience, 1, 659–664, doi:10.1038/ngeo316, 2008.

Hooke, R. L.: Englacial and Subglacial Hydrology: A Qualitative Review, Arctic and Alpine Research, 21, 221–233, doi:10.2307/1551561, 1989.

Hooke, R. L., Calla, P., Holmlund, P., Nilsson, M., and Stroeven, A.: A 3 year record of seasonal variations in surface velocity, Storglaciären, Sweden, Journal of Glaciology, 35, 235–247, doi:10.1017/S0022143000004561, 1989.

How, P., Benn, D. I., Hulton, N. R. J., Hubbard, B., Luckman, A., Sevestre, H., Van Pelt, W. J. J., Lïndback, K., Kohler, J., and Boot, W.: Rapidly-changing subglacial hydrology pathways at a tidewater glacier revealed through simultaneous observations of water pressure, supraglacial lakes, meltwater plumes and surface velocities, The Cryosphere Discussions, 2017, 1–29, doi:10.5194/tc-2017-74, 2017.

Howat, I. M., Box, J. E., Ahn, Y., Herrington, A., and McFadden, E. M.: Seasonal variability in the dynamics of marine-terminating outlet glaciers in Greenland, Journal of Glaciology, 56, 601–613, doi:10.3189/002214310793146232, 2010.

Howe, J. A., Moreton, S. G., Morri, C., and Morris, P.: Multibeam bathymetry and the depositional environments of Kongsfjorden and Krossfjorden, western Spitsbergen, Svalbard, Polar Research, 22, 301–316, doi:10.1111/j.1751-8369.2003.tb00114.x, 2003.

Hubbard, B. and Nienow, P.: Alpine subglacial hydrology, Quaternary Science Reviews, 16, 939–955, doi:10.1016/S0277-3791(97)00031-0, 1997.

Hubbard, B., Sharp, M., Willis, I., Nielsen, M. t., and Smart, C.: Borehole water-level variations and the structure of the subglacial hydrological system of Haut Glacier d'Arolla, Valais, Switzerland, Journal of Glaciology, 41, 572–583, doi:10.3198/1995JoG41-139-572-583, 1995.

Iken, A.: The Effect of the Subglacial Water-Pressure on the Sliding Velocity of a Glacier in an Idealized Numerical-Model, Journal of Glaciology, 27, 407–421, doi:10.3198/1981JoG27-97-407-421, 1981.

Iken, A. and Truffer, M.: The relationship between subglacial water pressure and velocity of Findelengletscher, Switzerland, during its advance and retreat, Journal of Glaciology, 43, 328–338, doi:10.1017/S0022143000003282, 1997.

Irvine-Fynn, T., Moorman, B., Williams, J., and Walter, F.: Seasonal changes in ground-penetrating radar signature observed at a polythermal glacier, Bylot Island, Canada, Earth Surface Processes and Landforms, 31, 892–909, doi:10.1002/esp.1299, 2006.

Irvine-Fynn, T. D. L., Hodson, A. J., Moorman, B. J., Vatne, G., and Hubbard, A. L.: Polythermal glacier hydrology: a review, Reviews of Geophysics, 49, doi:10.1029/

2010RG000350, rG4002, 2011.
James, T. D., Murray, T., Selmes, N., Scharrer, K., and O'Leary, M.: Buoyant flexure and basal crevassing in dynamic mass loss at Helheim Glacier, Nature Geoscience, 7, 593, doi:10.1038/ngeo2204, 2014.
Jansson, P.: Water pressure and basal sliding on Storglaciären, northern Sweden, Journal of Glaciology, 41, 232–240, doi:10.1017/S0022143000016130, 1995.
Jay-Allemand, M., Gillet-Chaulet, F., Gagliardini, O., and Nodet, M.: Investigating changes in basal conditions of Variegated Glacier prior to and during its 1982–1983 surge, The Cryosphere, 5, 659–672, doi:10.5194/tc-5-659-2011, 2011.
Jenkins, A.: Convection-driven melting near the grounding lines of ice shelves and tidewater glaciers, Journal of Physical Oceanography, 41, 2279–2294, doi:10.1175/JPO-D-11-03.1, 2011.
Jensen, H. J.: Self-organized criticality: Emergent complex behavior in physical and biological systems, vol. 10, Cambridge university press, 1998.
Joughin, I., MacAyeal, D. R., and Tulaczyk, S.: Basal shear stress of the Ross ice streams from control method inversions, Journal of Geophysical Research: Solid Earth, 109, doi:10.1029/2003JB002960, 2004.
Joughin, I., Smith, B. E., Howat, I. M., Scambos, T., and Moon, T.: Greenland flow variability from ice-sheet-wide velocity mapping, Journal of Glaciology, 56, 415–430, doi:doi:10.3189/002214310792447734, 2010.
Joughin, I., Alley, R. B., and Holland, D. M.: Ice-Sheet Response to Oceanic Forcing, Science, 338, 1172–1176, doi:10.1126/science.1226481, 2012.
Kamb, B.: Sliding motion of glaciers: theory and observation, Reviews of Geophysics, 8, 673–728, doi:10.1029/RG008i004p00673, 1970.
Kamb, B.: Glacier surge mechanism based on linked cavity configuration of the basal water conduit system, Journal of Geophysical Research: Solid Earth, 92, 9083–9100, doi:10.1029/JB092iB09p09083, 1987.
Kamb, B.: Rheological Nonlinearity and Flow Instability in the Deforming Bed Mechanism of Ice Stream Motion, Journal of Geophysical Research-Solid Earth, 96, 16 585–16 595, doi:10.1029/91JB00946, 1991.
Kehrl, L. M., Hawley, R. L., Powell, R. D., and Brigham-Grette, J.: Glacimarine sedimentation processes at Kronebreen and Kongsvegen, Svalbard, Journal of Glaciology, 57, 841–847, doi:10.3189/002214311798043708, 2011.
Kessler, M. A. and Anderson, R. S.: Testing a numerical glacial hydrological model using spring speed-up events and outburst floods, Geophysical Research Letters, 31, doi:10.1029/2004GL020622, l18503, 2004.
Kimura, S., Candy, A. S., Holland, P. R., Piggott, M. D., and Jenkins, A.: Adaptation of an unstructured-mesh, finite-element ocean model to the simulation of ocean circulation beneath ice shelves, Ocean Modelling, 67, 39–51, doi:10.1016/j.ocemod.2013.03.004, 2013.
Kingslake, J. and Ng, F.: Modelling the coupling of flood discharge with glacier flow during jökulhlaups, Annals of Glaciology, 54, 25–31, doi:10.3189/2013AoG63A331, 2013.
Köhler, A., Nuth, C., Kohler, J., Berthier, E., Weidle, C., and Schweitzer, J.: A 15 year record of frontal glacier ablation rates estimated from seismic data, Geophysical Research Letters, 43, 12,155–12,164, doi:10.1002/2016GL070589, 2016GL070589, 2016.

König, M., Kohler, J., and Nuth, C.: Glacier Area Outlines - Svalbard, Tech. rep., Norwegian Polar Institute, Tromsø, Norway, 2013.

Krug, J., Weiss, J., Gagliardini, O., and Durand, G.: Combining damage and fracture mechanics to model calving, The Cryosphere, 8, 2101–2117, doi:10.5194/tcd-8-1631-2014, 2014.

Larour, E., Rignot, E., and Aubry, D.: Modelling of rift propagation on Ronne Ice Shelf, Antarctica, and sensitivity to climate change, Geophysical research letters, 31, doi:10.1029/2004GL020077, 2004.

Larour, E., Rignot, E., Joughin, I., and Aubry, D.: Rheology of the Ronne Ice Shelf, Antarctica, inferred from satellite radar interferometry data using an inverse control method, Geophysical Research Letters, 32, doi:10.1029/2004GL021693, 2005.

Larour, E., Utke, J., Csatho, B., Schenk, A., Seroussi, H., Morlighem, M., Rignot, E., Schlegel, N., and Khazendar, A.: Inferred basal friction and surface mass balance of the Northeast Greenland Ice Stream using data assimilation of ICESat (Ice Cloud and land Elevation Satellite) surface altimetry and ISSM (Ice Sheet System Model), Cryosphere, 8, doi:10.5194/tc-8-2335-2014, 2014.

Lea, J. M., Mair, D. W., Nick, F. M., Rea, B. R., Weidick, A., Kjær, K. H., Morlighem, M., Van As, D., and Schofield, J. E.: Terminus-driven retreat of a major southwest Greenland tidewater glacier during the early 19th century: insights from glacier reconstructions and numerical modelling, Journal of Glaciology, 60, 333–344, doi:10.3189/2014JoG13J163, 2014.

Leclercq, P. W., Oerlemans, J., and Cogley, J. G.: Estimating the Glacier Contribution to Sea-Level Rise for the Period 1800-2005, Surveys in Geophysics, 32, 519–535, doi:10.1007/s10712-011-9121-7, 2011.

Lefeuvre, P.-M., Jackson, M., Lappegard, G., and Hagen, J. O.: Interannual variability of glacier basal pressure from a 20 year record, Annals of Glaciology, 56, 33–44, doi:10.3189/2015AoG70A019, 2015.

Lindbäck, K., Pettersson, R., Doyle, S., Helanow, C., Jansson, P., Kristensen, S. S., Stenseng, L., Forsberg, R., and Hubbard, A.: High-resolution ice thickness and bed topography of a land-terminating section of the Greenland Ice Sheet, Earth System Science Data, 6, 331–338, doi:10.5194/essd-6-331-2014, 2014.

Lliboutry, L.: Une théorie du frottement du glacier sur son lit, Annals of Géophysics, 15, 1959.

Lliboutry, L.: General theory of subglacial cavitation and sliding of temperate glaciers, Journal of Glaciology, 7, 21–58, doi:10.1017/S0022143000020396, 1968.

Lliboutry, L.: Local friction laws for glaciers: a critical review and new openings, Journal of Glaciology, 23, 67–95, doi:10.1017/S0022143000029750, 1979.

Luckman, A., Murray, T., de Lange, R., and Hanna, E.: Rapid and synchronous ice-dynamic changes in East Greenland, Geophysical Research Letters, 33, doi:10.1029/2005GL025428, 2006.

Luckman, A., Benn, D. I., Cottier, F., Bevan, S., Nilsen, F., and Inall, M.: Calving rates at tidewater glaciers vary strongly with ocean temperature, Nature communications, 6, doi:10.1038/ncomms9566, 2015.

MacAyeal, D. R.: The basal stress distribution of Ice Stream E, Antarctica, inferred by control methods, Journal of Geophysical Research: Solid Earth, 97, 595–603, doi:10.1029/91JB02454, 1992.

Mair, D., Nienow, P., Willis, I., and Sharp, M.: Spatial patterns of glacier motion during a high-velocity event: Haut Glacier d'Arolla, Switzerland, Journal of Glaciology, 47, 9–20, doi:10.3189/172756501781832412, 2001.

McNabb, R., Hock, R., and Huss, M.: Variations in Alaska tidewater glacier frontal ablation, 1985–2013, Journal of Geophysical Research: Earth Surface, 120, 120–136, doi:10.1002/2014JF003276, 2015.

Medrzycka, D., Benn, D. I., Box, J. E., Copland, L., and Balog, J.: Calving Behavior at Rink Isbræ, West Greenland, from Time-Lapse Photos, Arctic, Antarctic, and Alpine Research, 48, 263–277, doi:10.1657/AAAR0015-059, 2016.

Meyer, C. R., Fernandes, M. C., Creyts, T. T., and Rice, J. R.: Effects of ice deformation on Röthlisberger channels and implications for transitions in subglacial hydrology, Journal of Glaciology, 62, 750–762, doi:10.1017/jog.2016.65, 2016.

Michel-Griesser, L., Picasso, M., Farinotti, D., Funk, M., and Blatter, H.: Bedrock topography reconstruction of glaciers from surface topography and masse balance data, Computational Geosciences, 18, 969–988, doi:10.1007/s10596-014-9439-6, 2014.

Minchew, B., Simons, M., Björnsson, H., Pálsson, F., Morlighem, M., Seroussi, H., Larour, E., and Hensley, S.: Plastic bed beneath Hofsjökull Ice Cap, central Iceland, and the sensitivity of ice flow to surface meltwater flux, Journal of Glaciology, 62, 147–158, doi:10.1017/jog.2016.26, 2016.

Moon, T., Joughin, I., Smith, B., and Howat, I.: 21st-Century Evolution of Greenland Outlet Glacier Velocities, Science, 336, 576–578, doi:10.1126/science.1219985, 2012.

Moon, T., Joughin, I., Smith, B., van den Broeke, M. R., van de Berg, W. J., Noël, B., and Usher, M.: Distinct patterns of seasonal Greenland glacier velocity, Geophysical Research Letters, 41, 7209–7216, doi:10.1002/2014GL061836, 2014.

Moorman, B. J. and Michel, F. A.: Glacial hydrological system characterization using ground-penetrating radar, Hydrological Processes, 14, 2645–2667, doi:10.1002/1099-1085(20001030)14:15<2645::AID-HYP84>3.0.CO;2-2, 2000.

Morlighem, M., Rignot, E., Seroussi, H., Larour, E., Ben Dhia, H., and Aubry, D.: Spatial patterns of basal drag inferred using control methods from a full-Stokes and simpler models for Pine Island Glacier, West Antarctica, Geophysical Research Letters, 37, doi:10.1029/2010GL043853, l14502, 2010.

Morlighem, M., Rignot, E., Seroussi, H., Larour, E., Ben Dhia, H., and Aubry, D.: A mass conservation approach for mapping glacier ice thickness, Geophysical Research Letters, 38, doi:10.1029/2011GL048659, l19503, 2011.

Morlighem, M., Bondzio, J., Seroussi, H., Rignot, E., Larour, E., Humbert, A., and Rebuffi, S.: Modeling of Store Gletscher's calving dynamics, West Greenland, in response to ocean thermal forcing, Geophysical Research Letters, 43, 2659–2666, doi:10.1002/2016GL067695, 2016GL067695, 2016.

Motyka, R. J., Dryer, W. P., Amundson, J., Truffer, M., and Fahnestock, M.: Rapid submarine melting driven by subglacial discharge, LeConte Glacier, Alaska, Geophysical Research Letters, 40, 5153–5158, doi:10.1002/grl.51011, 2013.

Murray, T., Selmes, N., James, T. D., Edwards, S., Martin, I., O'Farrell, T., Aspey, R., Rutt, I., Nettles, M., and Baugé, T.: Dynamics of glacier calving at the ungrounded margin of Helheim Glacier, southeast Greenland, Journal of Geophysical Research: Earth Surface, 120, 964–982, doi:10.1002/2015JF003531, 2015JF003531, 2015.

Nahrgang, J., Varpe, Ø., Korshunova, E., Murzina, S., Hallanger, I. G., Vieweg, I., and Berge, J.: Gender specific reproductive strategies of an Arctic key species (Boreogadus saida) and implications of climate change, PLoS one, 9, e98 452, doi:10.1371/journal.pone.0098452, 2014.

Nick, F., Van der Veen, C. J., Vieli, A., and Benn, D.: A physically based calving model applied to marine outlet glaciers and implications for the glacier dynamics, Journal of Glaciology, 56, 781–794, doi:10.3189/002214310794457344, 2010.

Nick, F. M., Vieli, A., Howat, I. M., and Joughin, I.: Large-scale changes in Greenland outlet glacier dynamics triggered at the terminus, Nature Geoscience, 2, 110–114, doi:10.1038/ngeo394, 2009.

Nick, F. M., Vieli, A., Andersen, M. L., Joughin, I., Payne, A., Edwards, T. L., Pattyn, F., and van de Wal, R. S. W.: Future sea-level rise from Greenland's main outlet glaciers in a warming climate, Nature, 497, 235–238, doi:10.1038/nature12068, 2013.

Nienow, P., Sharp, M., and Willis, I.: Seasonal changes in the morphology of the subglacial drainage system, Haut Glacier d'Arolla, Switzerland, Earth Surface Processes and Landforms, 23, 825–843, doi:10.1002/(SICI)1096-9837(199809)23:9<825::AID-ESP893>3.0.CO;2-2, 1998.

Nuth, C., Schuler, T. V., Kohler, J., Altena, B., and Hagen, J. O.: Estimating the long-term calving flux of Kronebreen, Svalbard, from geodetic elevation changes and mass-balance modelling, Journal of Glaciology, 58, 119–133, doi:10.3189/2012JoG11J036, 2012.

Nuth, C., Kohler, J., König, M., von Deschwanden, A., Hagen, J. O., Kääb, A., Moholdt, G., and Pettersson, R.: Decadal changes from a multi-temporal glacier inventory of Svalbard, The Cryosphere, 7, 1603–1621, doi:10.5194/tc-7-1603-2013, 2013.

Nye, J.: A calculation on the sliding of ice over a wavy surface using a Newtonian viscous approximation, in: Proceedings of the Royal Society of London A: Mathematical, Physical and Engineering Sciences, vol. 311, pp. 445–467, The Royal Society, doi:10.1098/rspa.1969.0127, 1969.

Nye, J.: Water at the bed of a glacier, in: Symposium on the Hydrology of Glaciers, edited by Glen J, Adie R, J. D., pp. 189–194, International Association of Scientific Hydrology, 1973.

O'Leary, M. and Christoffersen, P.: Calving on tidewater glaciers amplified by submarine frontal melting, The Cryosphere, 7, 119–128, doi:10.5194/tc-7-119-2013, 2013.

O'Neel, S., Marshall, H. P., McNamara, D. E., and Pfeffer, W. T.: Seismic detection and analysis of icequakes at Columbia Glacier, Alaska, Journal of Geophysical Research: Earth Surface, 112, doi:10.1029/2006JF000595, f03S23, 2007.

Otero, J., Navarro, F. J., Martin, C., Cuadrado, M. L., and Corcuera, M. I.: A three-dimensional calving model: Numerical experiments on Johnsons Glacier, Livingston Island, Antarctica, Journal of Glaciology, 56, 200–214, doi:10.3189/002214310791968539, 2010.

Palmer, S., Shepherd, A., Nienow, P., and Joughin, I.: Seasonal speedup of the Greenland Ice Sheet linked to routing of surface water, Earth and Planetary Science Letters, 302, 423–428, doi:10.1016/j.epsl.2010.12.037, 2011.

Pimentel, S. and Flowers, G. E.: A numerical study of hydrologically driven glacier dynamics and subglacial flooding, Proceedings of the Royal Society of London A: Mathematical, Physical and Engineering Sciences, doi:10.1098/rspa.2010.0211, 2010.

Pollard, D., DeConto, R. M., and Alley, R. B.: Potential Antarctic Ice Sheet retreat driven by hydrofracturing and ice cliff failure, Earth and Planetary Science Letters, 412, 112–121, doi:10.1016/j.epsl.2014.12.035, 2015.

Raymond, C. F. and Harrison, W.: Fit of ice motion models to observations from Variegated Glacier, Alaska, IAHS Publ, 170, 153–166, 1987.

Raymond, M. J. and Gudmundsson, G. H.: Estimating basal properties of ice streams from surface measurements: a non-linear Bayesian inverse approach applied to synthetic data, Cryosphere, 3, 265–278, doi:10.5194/tc-3-265-2009, 2009.

Reeh, N.: On the calving of ice from floating glaciers and ice shelves, Journal of Glaciology, 7, 215–232, doi:10.1017/S0022143000031014, 1968.

Rignot, E., Fenty, I., Xu, Y., Cai, C., and Kemp, C.: Undercutting of marine-terminating glaciers in West Greenland, Geophysical Research Letters, 42, 5909–5917, doi:10.1002/2015GL064236, 2015GL064236, 2015.

Ritz, C., Edwards, T. L., Durand, G., Payne, A. J., Peyaud, V., and Hindmarsh, R. C.: Potential sea-level rise from Antarctic ice-sheet instability constrained by observations, Nature, 528, 115–118, doi:10.1038/nature16147, 2015.

Rommelaere, V. and Macayeal, D. R.: Large-scale rheology of the Ross Ice Shelf, Antarctica, computed by a control method, Annals of Glaciology, 24, 43–48, doi:10.1017/S0260305500011915, 1997.

Röösli, C., Walter, F., Husen, S., Andrews, L. C., Lüthi, M. P., Catania, G. A., and Kissling, E.: Sustained seismic tremors and icequakes detected in the ablation zone of the Greenland ice sheet, Journal of Glaciology, 60, 563–575, doi:10.3189/2014JoG13J210, 2014.

Röthlisberger, H.: Water pressure in intra- and subglacial channels, Journal of Glaciology, 11, 177–203, 1972.

Rousselot, M. and Fischer, U. H.: Evidence for excess pore-water pressure generated in subglacial sediment: Implications for clast ploughing, Geophysical Research Letters, 32, doi:10.1029/2005GL022642, l11501, 2005.

Rutter, N., Hodson, A., Irvine-Fynn, T., and Solås, M. K.: Hydrology and hydrochemistry of a deglaciating high-Arctic catchment, Svalbard, Journal of Hydrology, 410, 39–50, doi:10.1016/j.jhydrol.2011.09.001, 2011.

Scambos, T. A., Hulbe, C., Fahnestock, M., and Bohlander, J.: The link between climate warming and break-up of ice shelves in the Antarctic Peninsula, Journal of Glaciology, 46, 516–530, doi:10.3189/172756500781833043, 2000.

Schäfer, M., Zwinger, T., Christoffersen, P., Gillet-Chaulet, F., Laakso, K., Pettersson, R., Pohjola, V. A., Strozzi, T., and Moore, J. C.: Sensitivity of basal conditions in an inverse model: Vestfonna ice cap, Nordaustlandet/Svalbard, Cryosphere, 6, 771–783, doi:10.5194/tcd-6-427-2012, 2012.

Schellenberger, T., Dunse, T., Kääb, A., Kohler, J., and Reijmer, C. H.: Surface speed and frontal ablation of Kronebreen and Kongsbreen, NW Svalbard, from SAR offset tracking, The Cryosphere, 9, 2339–2355, doi:10.5194/tc-9-2339-2015, 2015.

Schild, K. M. and Hamilton, G. S.: Seasonal variations of outlet glacier terminus position in Greenland, Journal of Glaciology, 59, 759–770, doi:10.3189/

2013JoG12J238, 2013.

Schild, K. M., Hawley, R. L., Chipman, J. W., and Benn, D. I.: Quantifying suspended sediment concentration in subglacial sediment plumes discharging from two Svalbard tidewater glaciers using Landsat-8 and in situ measurements, International Journal of Remote Sensing, 38, 6865–6881, doi:10.1080/01431161.2017.1365388, 2017.

Scholz, C. H.: The mechanics of earthquakes and faulting, Cambridge University Press, 2002.

Schoof, C.: The effect of cavitation on glacier sliding, Proceedings of the Royal Society a-Mathematical Physical and Engineering Sciences, 461, 609–627, doi: 10.1098/rspa.2004.1350, 2005.

Schoof, C.: Ice-sheet acceleration driven by melt supply variability, Nature, 468, 803–806, doi:10.1038/nature09618, 2010.

Schoof, C., Rada, C. A., Wilson, N. J., Flowers, G. E., and Haseloff, M.: Oscillatory subglacial drainage in the absence of surface melt, The Cryosphere, 8, 959–976, doi:10.5194/tcd-7-5613-2013, 2014.

Sergienko, O. V. and Hindmarsh, R. C.: Regular patterns in frictional resistance of ice-stream beds seen by surface data inversion, Science, 342, 1086–1089, doi:10.1126/science.1243903, 2013.

Shapero, D. R., Joughin, I. R., Poinar, K., Morlighem, M., and Gillet-Chaulet, F.: Basal resistance for three of the largest Greenland outlet glaciers, Journal of Geophysical Research: Earth Surface, 121, 168–180, doi:10.1002/2015JF003643, 2016.

Shepherd, A., Hubbard, A., Nienow, P., King, M., McMillan, M., and Joughin, I.: Greenland ice sheet motion coupled with daily melting in late summer, Geophysical Research Letters, 36, doi:10.1029/2008GL035758, 2009.

Shoemaker, E. M.: Subglacial hydrology for an ice sheet resting on a deformable aquifer, Journal of Glaciology, 32, 20–30, doi:10.1029/JB092iB06p04935, 1986.

Shreve, R.: Movement of water in glaciers, Journal of Glaciology, 11, 205–214, doi: 10.1017/S002214300002219X, 1972.

Slater, D., Nienow, P., Goldberg, D., Cowton, T., and Sole, A.: A model for tidewater glacier undercutting by submarine melting, Geophysical Research Letters, 44, 2360–2368, doi:10.1002/2016GL072374, 2017a.

Slater, D., Nienow, P., Sole, A., Cowton, T., Mottram, R., Langen, P., and Mair, D.: Spatially distributed runoff at the grounding line of a large Greenlandic tidewater glacier inferred from plume modelling, Journal of Glaciology, 63, 309–323, doi: 10.1017/jog.2016.139, 2017b.

Slater, D. A., Nienow, P. W., Cowton, T. R., Goldberg, D. N., and Sole, A. J.: Effect of near-terminus subglacial hydrology on tidewater glacier submarine melt rates, Geophysical Research Letters, 42, 2861–2868, doi:10.1002/2014GL062494, 2014GL062494, 2015.

Slater, D. A., Goldberg, D. N., Nienow, P. W., and Cowton, T. R.: Scalings for submarine melting at tidewater glaciers from buoyant plume theory, Journal of Physical Oceanography, 46, 1839–1855, doi:10.1175/JPO-D-15-0132.1, 2016.

Sole, A., Nienow, P., Bartholomew, I., Mair, D., Cowton, T., Tedstone, A., and King, M. A.: Winter motion mediates dynamic response of the Greenland Ice Sheet to warmer summers, Geophysical Research Letters, 40, 3940–3944, doi:10.1002/grl.50764, 2013.

Sole, A. J., Mair, D. W. F., Nienow, P. W., Bartholomew, I. D., King, M. A., Burke, M. J., and Joughin, I.: Seasonal speedup of a Greenland marine-terminating outlet glacier forced by surface melt-induced changes in subglacial hydrology, Journal of Geophysical Research-Earth Surface, 116, doi:10.1029/2010JF001948, 2011.

Spring, U. and Hutter, K.: Numerical studies of Jökulhlaups, Cold Regions Science and Technology, 4, 227–244, doi:10.1016/0165-232X(81)90006-9, 1981.

Steen-Larsen, H. C., Waddington, E. D., and Koutnik, M. R.: Formulating an inverse problem to infer the accumulation-rate pattern from deep internal layering in an ice sheet using a Monte Carlo approach, Journal of Glaciology, 56, 318–332, doi:10.3189/002214310791968476, 2010.

Stevens, L. A., Straneo, F., Das, S. B., Plueddemann, A. J., Kukulya, A. L., and Morlighem, M.: Linking glacially modified waters to catchment-scale subglacial discharge using autonomous underwater vehicle observations, The Cryosphere, 10, 417–432, doi:10.5194/tc-10-417-2016, 2016.

Stone, D. B. and Clarke, G. K. C.: In-situ measurements of basal water quality and pressure as an indicator of the character of subglacial drainage systems, Hydrological Processes, 10, 615–628, doi:10.1002/(SICI)1099-1085(199604)10:4<615::AID-HYP395>3.0.CO;2-M, 1996.

Straneo, F. and Heimbach, P.: North Atlantic warming and the retreat of Greenland's outlet glaciers, Nature, 504, 36–43, doi:10.1038/nature12854, 2013.

Streit, A., Bala, P., and Beck-Ratzka: UNICORE 6 - Recent and Future Advancements, Annals of Telecommunications, 65, 757–762, doi:10.1007/s12243-010-0195-x, 2010.

Sundal, A. V., Shepherd, A., Nienow, P., Hanna, E., Palmer, S., and Huybrechts, P.: Melt-induced speed-up of Greenland ice sheet offset by efficient subglacial drainage, Nature, 469, 521–524, doi:10.1038/nature09740, 2011.

Tedstone, A. J., Nienow, P. W., Gourmelen, N., Dehecq, A., Goldberg, D., and Hanna, E.: Decadal slowdown of a land-terminating sector of the Greenland Ice Sheet despite warming, Nature, 526, 692–695, doi:10.1038/nature15722, 2015.

Thomason, J. F. and Iverson, N. R.: A laboratory study of particle ploughing and pore-pressure feedback: a velocity-weakening mechanism for soft glacier beds, Journal of Glaciology, 54, doi:doi:10.3189/002214308784409008, 2008.

Thorsteinsson, T., Raymond, C. F., Gudmundsson, G. H., Bindschadler, R. A., Vornberger, P., and Joughin, I.: Bed topography and lubrication inferred from surface measurements on fast-flowing ice streams, Journal of Glaciology, 49, 481–490, doi:10.3189/172756503781830502, 2003.

Todd, J. and Christoffersen, P.: Are seasonal calving dynamics forced by buttressing from ice mélange or undercutting by melting? Outcomes from full-Stokes simulations of Store Glacier, West Greenland, The Cryosphere, 8, 2353–2365, doi:10.5194/tc-8-2353-2014, 2014.

Tranter, M., Brown, G. H., Hodson, A. J., and Gurnell, A. M.: Hydrochemistry as an indicator of subglacial drainage system structure: a comparison of alpine and sub-polar environments, Hydrological Processes, 10, 541–556, doi:10.1002/(SICI)1099-1085(199604)10:4<541::AID-HYP391>3.0.CO;2-9, 1996.

Truffer, M. and Motyka, R. J.: Where glaciers meet water: Subaqueous melt and its relevance to glaciers in various settings, Reviews of Geophysics, 54, 220–239, doi:10.1002/2015RG000494, 2015RG000494, 2016.

Trusel, L. D., Powell, R., Cumpston, R., and Brigham-Grette, J.: Modern glacimarine processes and potential future behaviour of Kronebreen and Kongsvegen polythermal tidewater glaciers, Kongsfjorden, Svalbard, Geological Society, London, Special Publications, 344, 89–102, doi:10.1144/SP344.9, 2010.

Tsai, V. C., Stewart, A. L., and Thompson, A. F.: Marine ice-sheet profiles and stability under Coulomb basal conditions, Journal of Glaciology, 61, 205–215, doi:10.3189/2015JoG14J22, 2015.

Tulaczyk, S.: Scale independence of till rheology, Journal of Glaciology, 52, 377–380, doi:10.3189/172756506781828601, 2006.

Tulaczyk, S., Kamb, W. B., and Engelhardt, H. F.: Basal mechanics of Ice Stream B, west Antarctica: 1. Till mechanics, Journal of Geophysical Research: Solid Earth, 105, 463–481, doi:10.1029/1999JB900329, 2000a.

Tulaczyk, S., Kamb, W. B., and Engelhardt, H. F.: Basal mechanics of Ice Stream B, west Antarctica: 2. Undrained plastic bed model, Journal of Geophysical Research: Solid Earth, 105, 483–494, doi:10.1029/1999JB900328, 2000b.

van de Wal, R. S. W., Smeets, C. J. P. P., Boot, W., Stoffelen, M., van Kampen, R., Doyle, S. H., Wilhelms, F., van den Broeke, M. R., Reijmer, C. H., Oerlemans, J., and Hubbard, A.: Self-regulation of ice flow varies across the ablation area in south-west Greenland, The Cryosphere, 9, 603–611, doi:10.5194/tc-9-603-2015, 2015.

van der Veen, C. J.: Calving glaciers, Progress in Physical Geography, 26, 96–122, doi:10.1191/0309133302pp327ra, 2002.

van der Veen, C. J.: Fracture propagation as means of rapidly transferring surface meltwater to the base of glaciers, Geophysical Research Letters, 34, doi:10.1029/2006GL028385, 2007.

Van Pelt, W. J., Pettersson, R., Pohjola, V. A., Marchenko, S., Claremar, B., and Oerlemans, J.: Inverse estimation of snow accumulation along a radar transect on Nordenskiödbreen, Svalbard, Journal of Geophysical Research: Earth Surface, 119, 816–835, doi:10.1002/2013JF003040, 2014.

Van Pelt, W. J. J. and Kohler, J.: Modelling the long-term mass balance and firn evolution of glaciers around Kongsfjorden, Svalbard, Journal of Glaciology, 61, 731–744, doi:10.3189/2015JoG14J223, 2015.

Van Pelt, W. J. J., Oerlemans, J., Reijmer, C. H., Pohjola, V. A., Pettersson, R., and van Angelen, J. H.: Simulating melt, runoff and refreezing on Nordenskiöldbreen, Svalbard, using a coupled snow and energy balance model, The Cryosphere, 6, 641–659, doi:10.5194/tc-6-641-2012, 2012.

Van Pelt, W. J. J., Oerlemans, J., Reijmer, C. H., Pettersson, R., Pohjola, V. A., Isaksson, E., and Divine, D.: An iterative inverse method to estimate basal topography and initialize ice flow models, doi:10.5194/tc-7-987-2013, 2013.

Vieli, A. and Nick, F. M.: Understanding and Modelling Rapid Dynamic Changes of Tidewater Outlet Glaciers: Issues and Implications, Surveys in Geophysics, 32, 437–458, doi:10.1007/s10712-011-9132-4, 2011.

Vieli, A., Funk, M., and Blatter, H.: Flow dynamics of tidewater glaciers: a numerical modelling approach, Journal of Glaciology, 47, 595–606, doi:10.3189/172756501781831747, 2001.

Vieli, A., Jania, J., Blatter, H., and Funk, M.: Short-term velocity variations on Hansbreen, a tidewater glacier in Spitsbergen, Journal of Glaciology, 50, 389–398, doi:10.3189/172756504781829963, 2004.

Waddington, E. D., Neumann, T. A., Koutnik, M. R., Marshall, H.-P., and Morse, D. L.: Inference of accumulation-rate patterns from deep layers in glaciers and ice sheets, Journal of Glaciology, 53, 694–712, doi:10.1007/978-90-481-2642-2_336, 2007.

Wainwright, D.: Calving front dynamics : External forces that lead to specific sized calving events, Master's thesis, Uppsala University, Department of Earth Sciences, 2014.

Walder, J.: Hydraulics of subglacial cavities, Journal of Glaciology, 32, doi:10.1017/S0022143000012156, 1986.

Walder, J. and Hallet, B.: Geometry of former subglacial water channels and cavities, Journal of Glaciology, 23, 335–346, doi:10.1017/S0022143000029944, 1979.

Walder, J. S.: Stability of sheet flow of water beneath temperate glaciers and implications for glacier surging, Journal of Glaciology, 28, 273–293, doi:10.1017/S0022143000011631, 1982.

Walder, J. S. and Fowler, A.: Channelized subglacial drainage over a deformable bed, Journal of Glaciology, 40, doi:10.1017/S0022143000003750, 1994.

Walter, F., Deichmann, N., and Funk, M.: Basal icequakes during changing subglacial water pressures beneath Gornergletscher, Switzerland, Journal of Glaciology, 54, 511–521, doi:10.3189/002214308785837110, 2008.

Walter, F., O'Neel, S., McNamara, D., Pfeffer, W. T., Bassis, J. N., and Fricker, H. A.: Iceberg calving during transition from grounded to floating ice: Columbia Glacier, Alaska, Geophysical Research Letters, 37, doi:10.1029/2010GL043201, l15501, 2010.

Warren, C. R.: Iceberg calving and the glacioclimatic record, Progress in Physical Geography, 16, 253–282, doi:10.1177/030913339201600301, 1992.

Weertman, J.: On the sliding of glaciers, Journal of Glaciology, doi:10.1017/S0022143000024709, 1957.

Weertman, J.: Catastrophic glacier advances, US Army Cold Regions Research and Engineering Laboratory, Corps of Engineers, 1962.

Weertman, J.: Glacier sliding, Tech. rep., DTIC Document, 1964.

Weertman, J.: General theory of water flow at the base of a glacier or ice sheet, Reviews of Geophysics, 10, 287–333, doi:10.1029/RG010i001p00287, 1972.

Werder, M. A., Hewitt, I. J., Schoof, C. G., and Flowers, G. E.: Modeling channelized and distributed subglacial drainage in two dimensions, Journal of Geophysical Research: Earth Surface, 118, 2140–2158, doi:10.1002/jgrf.20146, 2013.

Westrin, P.: External Conditions Effects on the Self-Organised Criticality of the Calving Glacier Front of Tunabreen, Svalbard, Master's thesis, Uppsala University, Department of Earth Sciences, 2015.

Zhang, Z. F. and Eckert, J.: Unified Tensile Fracture Criterion, Physical Review Letters, 94, 094301, doi:10.1103/PhysRevLett.94.094301, 2005.

Zoet, L. K. and Iverson, N. R.: Rate-weakening drag during glacier sliding, Journal of Geophysical Research: Earth Surface, 121, 1206–1217, doi:10.1002/2016JF003909, 2016.

Zwally, H. J., Abdalati, W., Herring, T., Larson, K., Saba, J., and Steffen, K.: Surface melt-induced acceleration of Greenland ice-sheet flow, Science, 297, 218–222, doi:10.1126/science.1072708, 2002.

Acta Universitatis Upsaliensis

Digital Comprehensive Summaries of Uppsala Dissertations from the Faculty of Science and Technology 1606

Editor: The Dean of the Faculty of Science and Technology

A doctoral dissertation from the Faculty of Science and Technology, Uppsala University, is usually a summary of a number of papers. A few copies of the complete dissertation are kept at major Swedish research libraries, while the summary alone is distributed internationally through the series Digital Comprehensive Summaries of Uppsala Dissertations from the Faculty of Science and Technology. (Prior to January, 2005, the series was published under the title "Comprehensive Summaries of Uppsala Dissertations from the Faculty of Science and Technology".)

Distribution: publications.uu.se
urn:nbn:se:uu:diva-334787

ACTA
UNIVERSITATIS
UPSALIENSIS
UPPSALA
2017